Imaging Food Quality

Møller, Flemming

Publication date:
2012

Document Version
Publisher's PDF, also known as Version of record

Imaging Food Quality

Flemming Møller

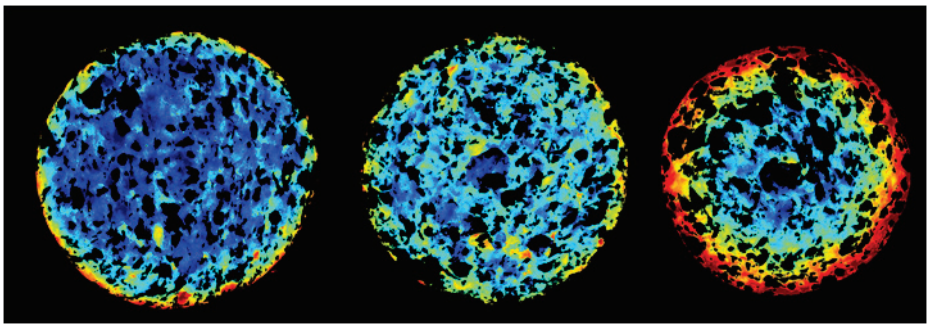

Kongens Lyngby 2012

IMM-PHD-2012-288

Technical University of Denmark

Informatics and Mathematical Modelling

Building 321, DK-2800 Kongens Lyngby, Denmark

Phone +45 45253351, Fax +45 45882673

reception@imm.dtu.dk

www.imm.dtu.dk

IMM-PHD: ISSN 0909-3192

Summary

Imaging and spectroscopy have long been established methods for food quality control both in the laboratories and online. An ever increasing number of analytical techniques are being developed into imaging methods and existing imaging methods to contain spectral information. Images and especially spectral images contain large amounts of data which should be analysed appropriately by techniques combining structure and spectral information.

This dissertation deals with how different types of food quality can be measured by imaging techniques, analysed with appropriate image analysis techniques and finally use the image data to predict or visualise food quality.

A range of different food quality parameters was addressed, i.e. water distribution in bread throughout storage, time series analysis of chocolate milk stability, yoghurt glossiness, graininess and dullness and finally structure and meat colour of dry fermented sausages. The imaging techniques ranged from single wavelength images, multispectral to hyperspectral images. The effect of different light geometries were utilised in measuring the light reflection of yoghurt surfaces.

What the best imaging technique for a given problem is, should be addressed by visual evaluation of a detectable difference between known samples. While doing image analysis, it was found to be advantageous to combine several small models. The combined model was used for extraction of object relevant information, i.e. spectral, texture or size. The data extracted was used for explorative or predictive data analysis.

RESUMÉ

Billedanalyse og spektroskopi er velkendte metoder til kontrol af fødevarekvalitet både i laboratorier og online. Et stadig stigende antal analyseteknikker videre udvikles til billede dannende metoder, og eksisterende metoder udvikles til også at måle spektral information, f.eks. temperatur, NIR og masse spektrofotometri. Billeder og særligt spektralbilleder indeholder store mængder data som skal analyseres hensigtsmæssigt ved hjælp af teknikker som kombinerer struktur og spektral information.

Denne afhandling behandler hvordan forskellige former for fødevarekvalitet kan vurderes med billedbehandlingsteknikker, analyseres med egnede billedanalyseteknikker og endelig hvordan billed-data kan bruges til at måle eller visualisere fødevarekvalitet.

En række forskellige parametre for fødevarekvalitet bliver behandlet, såsom fordelingen af vand i brød under lagring; stabilitet i kakaomælk over tid; blankhed, grynethed og mathed i yoghurt og endelig struktur og kødfarve i spegepølse. Billedbehandlingsteknikkerne strækker sig fra enkelt-bølgelængde billeder, over multispektrale til hyperspektrale billeder. Effekten af forskellige typer lysgeometri bliver anvendt ved måling af lysets refleksion på overfladen af yoghurt.

Hvad der er den bedste billede teknik til et givet problem, kan ofte afgøres ved en visuel bedømmelse af den synlige forskel mellem kendte prøver – kan billederne vise en prøve forskel, så kan denne også måles. Under arbejde med billedbehandlings teknikker blev det indset, at det kan være fordelagtigt at kombinere flere mindre modeller. Den kombinerede model blev brugt til at uddrage objekt-relevant information, f.eks. spektra, tekstur eller størrelse. De data, som blev trukket ud, blev brugt eksplorativ eller til forudsigende modeller.

PREFACE

This thesis was prepared at the Department of Informatics and Mathematical Modelling, the Technical University of Denmark (DTU) and DuPont Nutrition Biosciences ApS, in Brabrand, Denmark in partial fulfilment of the requirements for acquiring the Ph.D. degree in engineering.

This Ph.D. project was financed by DuPont Nutrition Biosciences ApS. The project was a part of "Center for Imaging Food Quality" partly funded by The Danish Council for Strategic Research.

The thesis deals with imaging, image analysis and prediction of food quality. The main focus is the combination of imaging techniques combined with image analysis strategies for objective measurement of food quality. This thesis represents a summary of my research with detailed descriptions provided in the back of the thesis.

The project was supervised by Professor Rasmus Larsen (DTU), Associate Professor Jens Michael Carstensen (DTU) and Development Director Susanne Kjærgaard Olesen (DuPont).

The thesis consists of a summary report and a collection of research papers written during the period 2008–2012, and elsewhere published.

Skanderborg, november 2012

Flemming Møller

LIST OF PUBLICATIONS

Paper I

Møller, F., D. Nilsson, and S.W. Lindström, Visualization of water distribution in bread by NIR imaging. Near Infrared Spectroscopy: proceedings NIR-2009 14th International conference, ed. S.K. S.Saranwong, W.Thanapase, P.Williams 2010, Bangkok.

Paper II

Møller, F., Barcode Technique to Visualize and Quantify Chocolate Milk Stability. Journal of Imaging Science and Technology, 2012. 56: p. 020402.

Paper III

Møller, F., Kragh, H., Laugand, D. and Carstensen, J.M. Measuring light reflection from yoghurt surfaces: Glossiness, graininess and dullness of yoghurt. Submitted to Food Hydrocolloids

Paper IV

Møller, F., Vogel, C. and Carstensen, J.M. Spectral imaging for monitoring structure and colour development of dry fermented sausages. Submitted to Meat Science

CO AUTHORED PAPERS

Christiansen, A.N., Carstensen, J.M., Møller, F. and Nielsen, A.A. Monitoring the change in colour of meat: A comparison of traditional and kernelbased orthogonal transformations. Journal of Spectral Imaging 3, 12 (2012)

Skytte, J.L., Nielsen, O., Andersen, U., Møller, F., Dahl, A.L. and Larsen, R. Monitoring Structure Formation during Milk Acidification using Hyperspectral Diffuse Reflectance Images. Submitted to Journal of Food Engineering

Nielsen, O.H.A., Dahl, A.L., Larsen, R., Møller, F., Nielsen F.D., Thomsen, C.L., Aanæs, H. and Carstensen, J.M. In Depth Analysis of Food Structures. Proceedings, Scandinavian Workshop on Imaging Food Quality 2011, pages: 29-34, 2011

Nielsen, O. H. A., Dahl, A. L., Larsen, R., Møller, F., Donbæk, F., Thomsen, C. L., Aanæs, H., Carstensen, J. M. Supercontinuum Light Sources for Hyperspectral Subsurface Laser Scattering. Proceedings, 17th Scandinavian Conference on Image Analysis (SCIA), pages: 327-337, 2011, Springer

Liu, Z., Møller, F. Bread Water Content Measurement Based on Hyperspectral Imaging. Proceedings, Scandinavian Workshop on Imaging Food Quality 2011, pages: 93-98, 2011.

ACKNOWLEDGEMENTS

It would not have been possible to write this thesis without the help, support and inspiration of the kind people around me, only some of whom it is possible to thank here.

I am grateful for the possibility to write this thesis. It has been a fantastic journey of learning new methods and technologies and having a laboratory full of images to play with. My colleagues at DuPont deserves acknowledgement for an inspiring environment. I am thankful that Development Director Susanne Kjærgaard Olesen found the time and money to finance this project – the best course I have ever taken! I am thankful for the many helpful colleagues, who helped with experiments, planning, explaining and just being interested in what I learned and how they could use this.

I appreciate the interest and support I have received from my supervisor Rasmus Larsen. I am impressed by how fast he has developed a food group at IMM. I am thankful for all the inspiring talks, I've had with my co-supervisor Jens Michael Carstensen and all of his fantastic colleagues at Videometer. A fantastic group of inspiring people. I have learned a lot from them and I truly enjoyed pulling on their expertise. I would also like to thank everyone involved with the spectral imaging discussion group at IMM – a good example of how one can learn a lot by discussing only half-finished projects.

You often hear movie stars saying "I could not have done it without….", well this one is true: I could not have done it without Birgitte, a joy to be around, accurate, productive and always with good ideas of how we can do things. She has a great "can do" attitude towards new techniques and is not afraid of all the data that comes with it. As many people I work very well up toward a deadline – this could be a problem for a secretary, who is a perfectionist like my secretary Linda, but I really appreciate all the help and making time for me that Linda gave me. I appreciate what she did to my texts and her beautiful graphics. As for my collages Henrik and Stine, I've always enjoyed the good office talks with them. It has been great how the two of them have helped to motivate and push me during this project. I am truly indebted and thankful to everyone, who has commented or participated in my writing, especially Henrik for all of his constructive suggestions.

Finally I would like to express my appreciation and love for family and friends – their interest and motivation throughout the project have been great. Thank you to Jan and Christian for lending me a bed in Copenhagen. Last but not least, my appreciation goes to Gitte, Kristine, Sofie and Nikoline for… everything!

Flemming Møller, Skanderborg, November 2012

LIST OF ABBREVIATIONS

AC	Auto Correlation
CDA	Canonical Discriminant Analysis
CLSM	Confocal Laser Scanning Microscope
CV	Cross Validation
GLCM	Gray-Level Co-occurrence Matrix
iPLS	Interval Partial Least Squares
LED	Light Emitting Diode
MAF	Maximum Autocorrelation Factors
MNF	Minimum Noise Fraction
nCDA	Normalized Canonical Discriminant Analysis
NIR	Near Infra Red
PC	Principle Component
PCA	Principle Component Analysis
PLS	Partial Least Squares
RGB	Red Green Blue
RMSECV	Root Mean Square Error of Cross Validation
RMSEP	Root Mean Square Error of Prediction
ROI	Region of interest
RT	Regression tree
SLS	Subsurface Laser Scattering

TABLE OF CONTENTS

CONTENTS

INTRODUCTION

Quality is an indefinite term and many terms have been suggested. What quality is depends on the perspective of the viewer. Food quality comprises both sensory attributes that are readily perceived by the human senses and hidden attributes such as safety, stability and nutrition that require instrumentation to be measured. Quality is often defined from either a product or a consumer perspective [Abbott, 1999; Shewfelt, 1999; Tamime and Robinson, 1999].

During the past decades, a number of different techniques have evolved into imaging techniques. What have proven to be valuable methods for single point properties is being developed into imaging methods [Abdullah et al., 2004; Becker and Salber, 2010]. An incomplete list of examples is: thermal imaging, EDX for element mapping, mass spectrometric imaging, NMR also known as MRI, UV - VIS – NIR and Raman imaging and atomic force microscopy for rheology imaging.

Using images for measurement of food quality is a multidisciplinary task which bridges the technologies of spectral imaging and image processing, as well as machine vision, see Figure 1. The first step is often to define a quality measure, next to select an appropriate imaging technique, quantifying relevant image structures and finally relating image data to food quality. This thesis touches upon all the aspects of using images for measuring food quality.

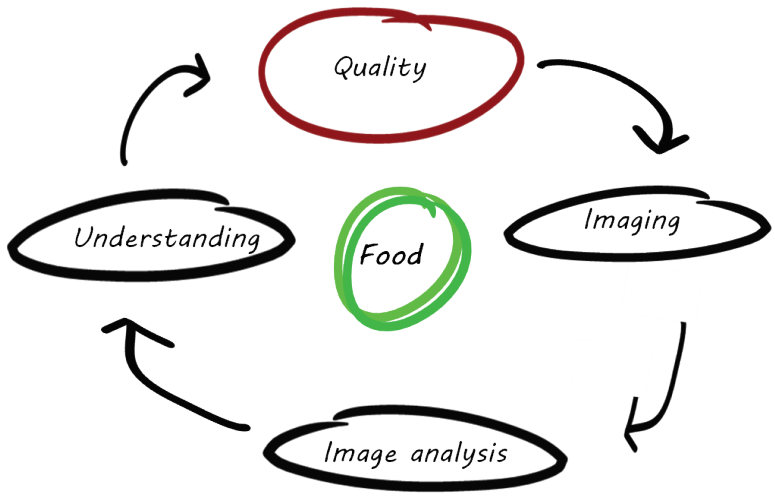

FIGURE 1 STEPS TO ADDRESS WHEN MEASURING FOOD QUALITY BY IMAGES. AN ITERATIVE PROCESS WHERE SEVERAL IMAGING(P. 15, 45), IMAGE ANALYSIS(P. 23) AND UNDERSTANDING METHODS(P. 41) SHOULD BE COMPARED COMBINED AND OPTIMISED.

OBJECTIVE

The objective of this thesis is to quantify food quality. It is the objective to detect and quantify different types of food quality, thereby using different imaging techniques, different methods of image analysis and lastly use different methods for predicting food quality.

The number of new chemical and physical imaging systems is rapidly increasing. A great deal of these instruments only comes with very basic visualisation tools. This thesis is based on the need for the food scientist himself being able to making more advanced image analysis and data interpretation – one would say: putting more tools into the toolbox.

OUTLINE OF THESIS

- Chapter 2 is a general introduction to food quality. There is a short introduction to bread, chocolate milk, dry fermented sausages and yoghurt making. Describing structure formation and some quality parameters.
- Chapter 3 describes imaging systems. Some illumination techniques to consider when defining how to measure food quality. The different acquisition types for spectral images are described.
- Chapter 4 is about image analysis. Describes the looping flow in analysing images, where several small models are combined into a final robust model. Deriving information from images.
- Chapter 5 introduces some techniques for relating the extracted image data to food quality.
- Chapter 6 contains examples of different instruments and image analysis approaches which have been used or developed during the project.
- Chapter 7 is conclusion and discussion.

FOOD QUALITY

How to define “food quality” depends on who you ask: food manufacturers, retailers and consumers might have different views on the term. There are many ways to define food quality, see Figure 2[Steenkamp, 1990; Shewfelt, 1999; Grunert et al., 2000; Brunsø et al., 2002].

Product-oriented quality is measured by means of the physical/chemical properties of a food product, factors such as fat percentage, alcohol content in beer, shelf life, etc.

Brand-oriented quality covers the way the food product has been produced, e.g. without pesticides, by organic production, according to regulations concerning animal welfare, etc.

Quality Control(QC) is quality parameters that can be brand-specific or follow some well-defined standard, e.g. ISO 9001. Quality control is about ensuring a stable and uniform quality.

Finally, *consumer-oriented quality* is the subjective quality perception of a consumer, and this may be the end consumer or a retailer. Since product- and brand-oriented quality are objective quality measures, they are measurable on the product by scientific methods. Consumer-oriented quality is subjective-quality since it can only be sensed by the consumer and can differ between consumers [Lawless and Heymann, 2010].

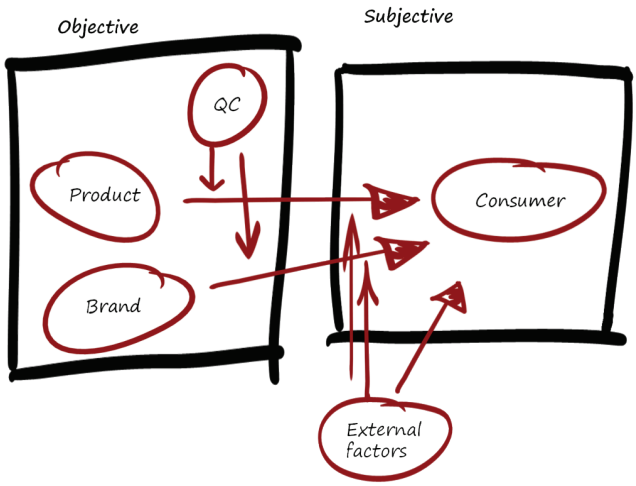

FIGURE 2 DIFFERENT VIEWS ON FOOD QUALITY, MODIFIED FROM [BRUNSØ ET AL., 2002]. PRODUCT DEVELOPMENT AND ANALYSIS WITHIN THE FOOD INDUSTRY IS FOCUSED ON OBJECTIVE PRODUCT FEATURES, E.G. VISCOSITY, PARTICLE SIZE, COLOUR, FLAVOUR OR TEXTURE.

Figure 2 illustrates how different types of quality are related. Consumer-oriented quality will be affected by brand and product quality [Brunsø et al., 2002]. But consumer-oriented quality can also be influenced by external factors like the purchase situation, the type of retail outlet, the price etc. Consumers often buy products the first time under influence of quality parameters for instance appearance, but repeated purchases are motivated by expected quality factors determined by flavour and texture experienced from previous purchase [Rico et al., 2007; Varela and Fiszman, 2013]. Quality parameters like organic grown or importance of a brand name can be difficult to measure [Brunsø et al., 2002].

Most quality development in the food industry is focused on product-, brand- and QC-oriented quality [Martens and Martens, 2001]. The challenge for food manufactures is to create a competitive advantage through quality improvements and to understand, how objective product characteristics affect subjective quality [Brunsø et al., 2002].

Most food innovation and development is based on a fundamental understanding of the technology going into a given product and how to link product quality and perceived quality. It is of vital importance to be able to rigorously and accurately measure food quality if one is to change or optimise quality. In this thesis the quality parameters of four very different food products have been evaluated: chocolate milk -stability, yoghurt – surface properties, bread - water distribution and finally dry fermented sausages - colour and structure development. Understanding the technology going into a product is important when defining quality and how it can be optimised, e.g. better stability, faster fermentation or a more homogeneous product etc. The next four sections give a short introduction to the technology behind the products evaluated.

CHOCOLATE MILK STABILISATION

Chocolate milk contains 1-3% cocoa powder. Cocoa particles are generally insoluble. If no special measures are taken, these particles will settle at the bottom of the container developing a firm sediment, which is difficult to disperse. If cocoa powder sedimentation is not desirable, it is necessary to form a thixotropic network which can keep the cocoa particles suspended while the chocolate milk is in storage. The principle of a thixotropic system is that it forms a very weak gel when the product is left to stand [Barnes, 1999]. Breaking down the gel by stirring, pumping or drinking will make the product change from a gel to a thin liquid. A thixotropic system is by definition a system that reforms its network structure – its gel – when left undisturbed, resulting in a permanently stable and homogeneous system. In order to develop a thixotropic system in chocolate milk; an emulsifier + stabiliser system is normally used. For chocolate milk, these are typically emulsifiers (monodiglycerides), carrageenan and guar gum [Danisco A/S, 2011]. The emulsifier ensures fat dispersion in the chocolate milk inhibiting fat separation adding creaminess and texture. Together with the carrageenan, the guar gum gives chocolate milk a further boost to the rich, creamy texture. However, it is only the carrageenan that has thixotropic properties.

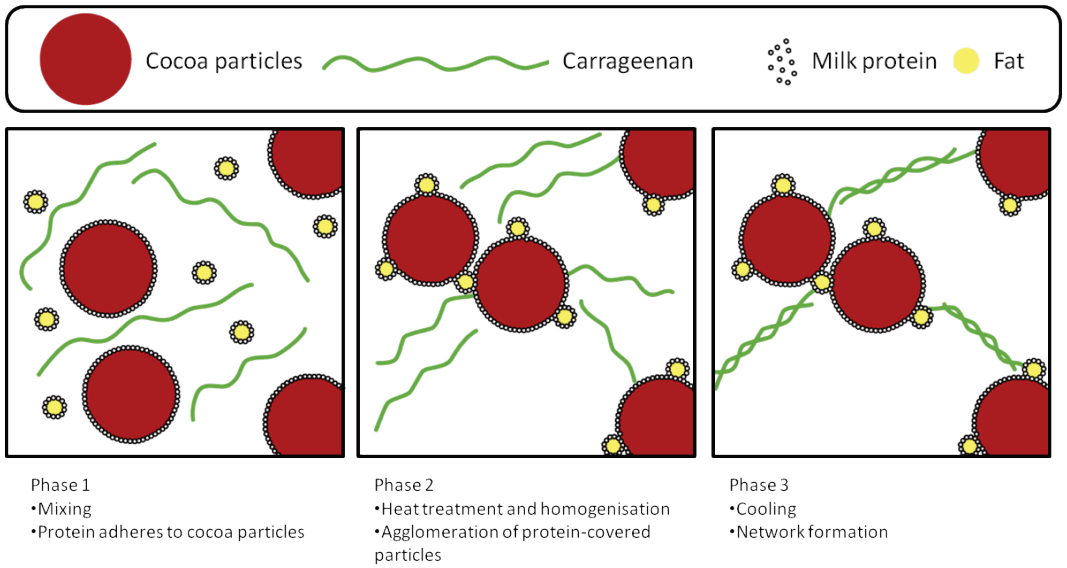

FIGURE 3 NETWORK FORMATION IN CHOCOLATE MILK. THE 3 FIGURES ILLUSTRATES HOW CHOCOLATE MILK CONSTITUANTS ARE DISPERSED IN MILK, PHASE 1. COCOA PARTICLES AND FAT IS COVERED WITH MILK PROTEIN AFTER HOMOGENISATION. PHASE 2: HEAT TREATMENT DISSOLVES AND UNFOLDS THE CARRAGEENAN AND DENATURATE WHEY PROTEIN, WHICH INTERACT AND SURSPEND THE CASEIN COVERED COCOA PARTICLES. PHASE 3: DURING COOLING THE CARRAGEENAN FORMS A WEAK GEL WHICH SURSPEND THE COCOA PARTICLES.

Figure 3 illustrates how cocoa particles are suspended in milk. Phase 1: the cocoa powder, sugar and stabiliser system are mixed with the milk and heated. The casein adsorbs to the cocoa particles. During homogenisation the fat particles are finely divided, and the casein adsorbs to the

surface of the fat particles as a kind of emulsifier. This new protein membrane around the fat globules will also react with the cocoa particles. Phase 2: the chocolate milk is then heat-treated. Situated on the surface of a carrageenan molecule are several reactive sites which are able to react with casein micelles [Snoeren, 1976]. Above 60°C, the carrageenan molecules dissolve and interact with casein micelles; casein covered cocoa particles and fat globules. The negatively charged groups on the carrageenan interact with the positively charged amino acid residue of the kappa-casein and αS2-casein present in the milk [Snoeren, 1976; Bourriot et al., 1999]. During the heat treatment, the whey proteins denature and bind to the casein micelles. This causes an agglomeration of casein micelles and, as a result, an agglomeration of the casein-covered cocoa and fat particles. Phase 3: finally, the chocolate milk is cooled to below 35°C. The carrageenan molecules form double helixes, and a solution-gelation transition occurs. This interlinks the cocoa particles, casein, denatured whey proteins, fat globules and carrageenan in a 3D network which keep the cocoa particles in suspension [Snoeren, 1976; Langendorff et al., 1997; Bourriot et al., 1999]. This explains why the stability of the chocolate milk depends on the quantity and quality of all parts of the network: cocoa particles, casein, denatured whey proteins, fat globules and carrageenan. The network prevents the separation of cocoa particles, stabilises the fat emulsion and prevents protein sedimentation. The thixotropic gel is so weak that it is hardly noticed when consuming the chocolate milk. Although a slight force can break the gel, it reforms once the force is removed. Carrageenan is the most commonly used hydrocolloid in chocolate milk as it fulfils the product's needs very well [Van Den Boomgaard et al., 1987]. It is the only hydrocolloid that can suspend cocoa in milk permanently by trapping it within a network. Other thickeners only suspend cocoa in milk temporarily due to their viscosity effect which delays but does not prevent sedimentation. Local gelation or complete separation can occur if the chemical balance of the system is changed too much, e.g. pH of system, changed cocoa, milk or carrageenan type [Snoeren, 1976; Van Den Boomgaard et al., 1987; Langendorff et al., 1997; Bourriot et al., 1999]. Some consumers may look at cocoa sedimentation as a sign of quality, others as the opposite.

YOGHURT

In yoghurt manufacture, the pH of the milk is lowered by the action of lactic acid bacteria, which produce lactic acid from lactose. Several production steps are involved in the production of stirred yoghurt (most common type in Denmark) : standardisation (protein, fat, stabilisers and sugar), pre-warming (60-65°C), homogenisation 200 bar, heat treatment 90-95°C for 5 minutes, cooling to fermentation temperature (42-43°C), fermentation until pH 4.6, stirring and cooling (optimally 20-25°C, but often down to 10-12°C for fast distribution after filling [Tamime and Robinson, 1999].

The aggregation of casein into a network during the acidification of milk is a much more complex process than simply aggregation of the casein micelles [Heertje et al., 1985; Famelart et al., 2004; Sodini et al., 2004; McMahon et al., 2009]. It involves the disaggregation of the casein micelles and

the release of β-casein and bound calcium phosphate [Walstra and Jenness, 1984; Heertje et al., 1985; McMahon et al., 2009]. As pH decreases, the β-casein re-absorbs onto the casein skeleton and forms new particles completely different in structure and composition from the native casein micelles. The structure development for acid milk gels is schematic shown in Figure 4 [Heertje et al., 1985; McMahon et al., 2009]. In Figure 4b the casein micelles are seen as dark particles and the released of β-casein as gray. At neutral pH is the dense casein particles held together by hydrophobic interactions and calcium-phosphate interactions. As the pH drops, calcium-phosphate is released and mainly the hydrophobic interactions are responsible for the structure of the casein particles [McMahon et al., 2009].

The model seen in Figure 4 was based only on casein, which accounts for 80% of the protein in cow's milk. The remaining 20% is whey protein, which is denatured by the pasteurisation of yoghurt milk. Only when denatured, the whey protein takes part in the yoghurt network formation, and then greatly enhances the strength of the resulting network [Tamime and Robinson, 1999; Famelart et al., 2004].

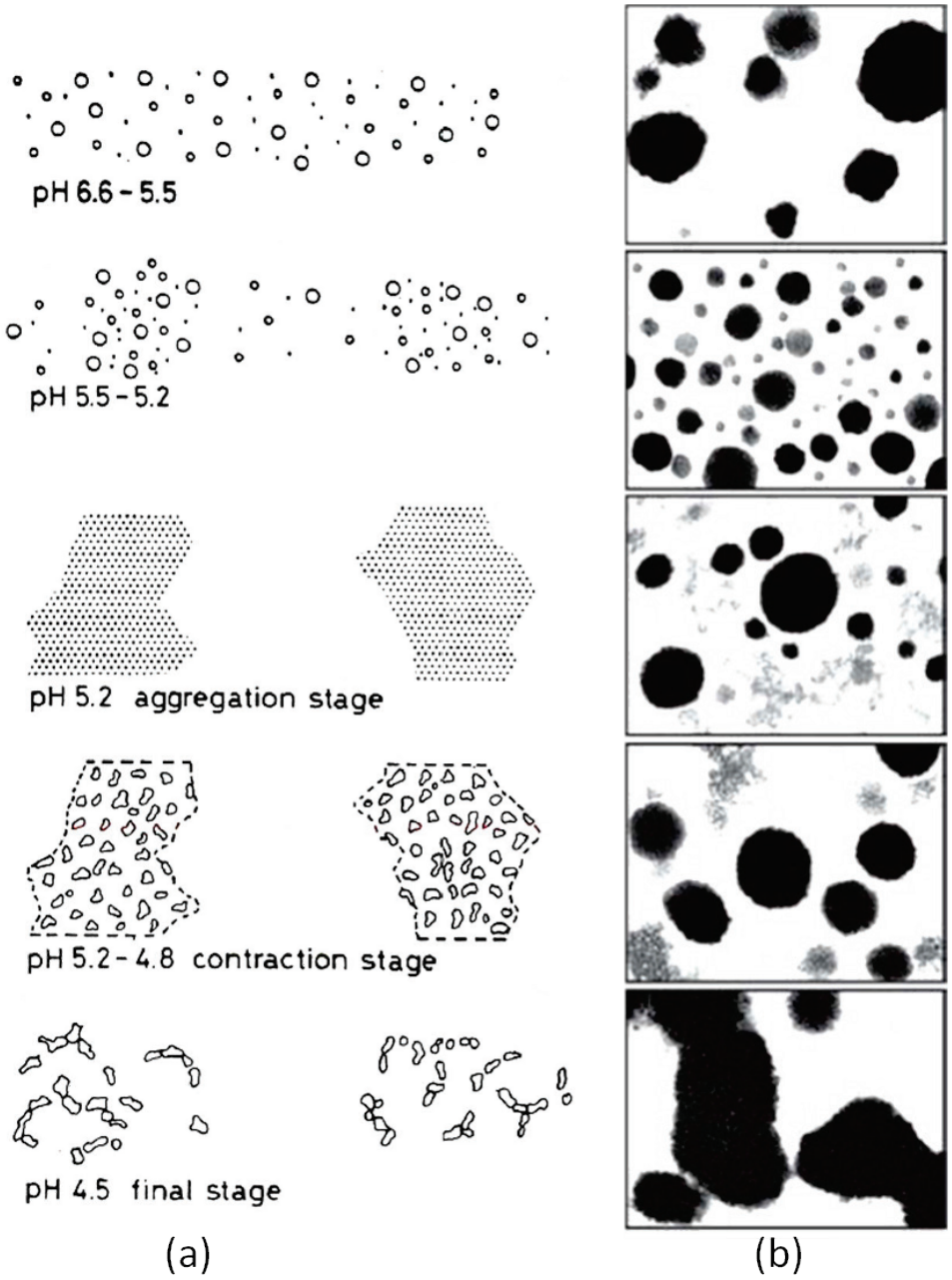

FIGURE 4 CHANGE IN CASEIN STATE DURING ACIDIFICATION, (A) SCHEMATIC DRAWING OF MICROSTRUCTURE, (B) IMAGES DERIVED FROM TRANSMISSION ELECTRON MICROGRAPHS, WITH COLLOIDAL CASEIN MICELLES DEPICTED IN BLACK AND LOOSELY ENTANGLED PROTEIN AGGREGATES DEPICTED IN GRAY, MODIFIED FROM HEERTJE ET AL. AND MCMAHON ET AL. [HEERTJE ET AL., 1985; MCMAHON ET AL., 2009].

The main ingredient in yoghurt is milk. Dairy ingredients are often added to adjust the composition, such as cream to adjust the fat content, and non-fat dry milk to adjust the solids content[Sodini et al., 2004]. Homogenised fat has a synergistic interaction with the protein network. Stabilisers may also be used in yoghurt to improve the body and texture by increasing firmness, preventing separation of the whey (syneresis). The main function of the starter cultures is to ferment lactose to produce lactic acid. A secondary effect of the cultures, are probiotic effects, inhibition of yeast or fungi or the production of exopolysaccharides, which is a type of stabiliser[Tamime and Robinson, 1999; Viljoen, 2001].

The most common sensory attributes relating to yoghurt texture are thickness (or viscosity), smoothness (opposite to lumpiness, graininess, grittiness), sliminess (or ropiness) and whey separation (or syneresis) [Sodini et al., 2004].

BREAD

Bread is one of the oldest prepared basic foods. Bread is made from flour, water, yeast, and salt. In many cultures bread is a substantial amount of the daily food intake.

Optimization of dough properties and the quality improvement of the finished product is of primary interest for the baking industry. The main interest for the consumers is the sensory appeal and stability during storage. After baking, the freshness of bread deteriorates very fast (staling) and therefore 'old bread' cannot be sold. It is therefore a challenge for the baking industry to improve dough properties and to understand and retard staling to keep bread quality high for as long time as possible.

The main functionality desired by most industrial bread producers, when adding bread improving ingredients to industrially produced breads, is dough stability, high volume soft bread, and fresh-keeping [Mondal and Datta, 2008; Kohajdová et al., 2009]. Fresh bread usually presents an appealing brownish and crunchy crust, a pleasant aroma, fine slicing characteristics, a soft and elastic crumb texture, and a moist mouthfeel. The challenge for bread manufacturers is to keep the characteristics of the fresh bread as long as possible [Mondal and Datta, 2008].

Several ingredients are used in bread manufacture, the list of ingredients can be long, some ingredients have multiple and synergistic effects and influence different parts of the baking process [Stampfli and Nersten, 1995; Caballero et al., 2007; Mondal and Datta, 2008; Kohajdová et al., 2009]. Emulsifiers, enzymes and hydrocolloids are examples of ingredients commonly used in bread. The ingredients have an effect on dough handling, crumb structure, slice-ability, fresh-keeping, crust colour and taste etc.

The quality of flour, fat and other ingredients added influence structural transformation of dough to bread. Some ingredients are used with a focus on the protein+starch network, while others influence the stability of gas cell wall, some ingredients 'work' during the proofing others during the baking, see Figure 5. After mixing, the dough contains small gas cells dispersed in a continuous starch-protein matrix. Each discrete gas cell expands in response to CO_2 production during fermentation, and the foam structure is maintained by thin membranes separating adjacent cells at the end of proofing. During baking, starch gelatinisation induces a dramatic increase in dough viscosity, resulting in a gas cell membrane rupture, converting the foam into a sponge [Gan et al., 1995].

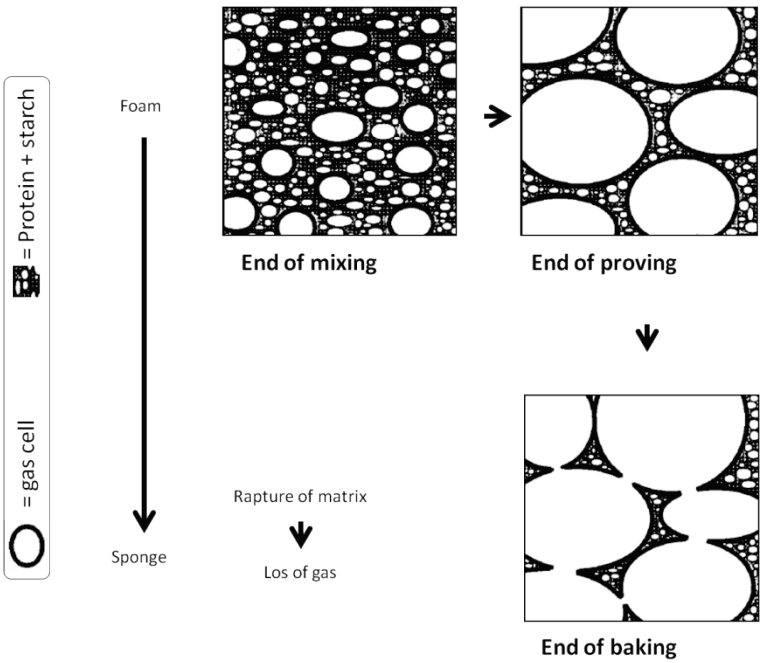

FIGURE 5 THE STRUCTURAL TRANSFORMATION OF DOUGH INTO BREAD – FROM FOAM TO SPONGE, MODIFIED FROM [GAN ET AL., 1995].

Several quality parameters are measured on the dough and bread, some of them are: dough rheology, specific bread volume, freshness/moistness throughout shelf-life, crumb structure and colour, crust structure and colour and shock stability [Gray and Bemiller, 2006; Caballero et al., 2007; Mondal and Datta, 2008].

SALAMI

The manufacture of dry-fermented sausages is done in three steps: formulation, fermentation, and ripening/drying [Marianski and Mariański, 2009].

Beef and pork are the main meat sausage materials. A number of non-meat ingredients, such as curing salts, sugar, spices and lactic acid bacteria, are commonly used in sausage production.

Salt is the main flavouring agent used in making sausages and it contributes to the basic taste characteristics of the final product, see Figure 6. Salt is also important for reducing the water activity, thereby also inhibiting several unwanted microorganisms. Nitrite and nitrate influence the colour development in the fermented sausage, and plays an important role in the protein structure development. Phosphates are added primarily for a better meat binding. The appearance of the characteristic pink-red colour in sausages is a sign that a good structure development has occurred. The absence of the pink colour or development of brown or grey discoloration indicate that a spoilage is under way or will soon occur [Mancini and Hunt, 2005; Feiner, 2006; Nanke et al., 2006].

Sugar is added to fermented sausages primarily to serve as a substrate for bacterial acid production in dry and semidry sausages.

The quality of fermented sausages is closely related to the ripening process that gives colour, flavour, aroma, and firmness to the product which are developed by a complex interaction of chemical and physical reactions associated with the fermentative action of the microbiological flora present in the sausage [de Macedo et al., 2012].

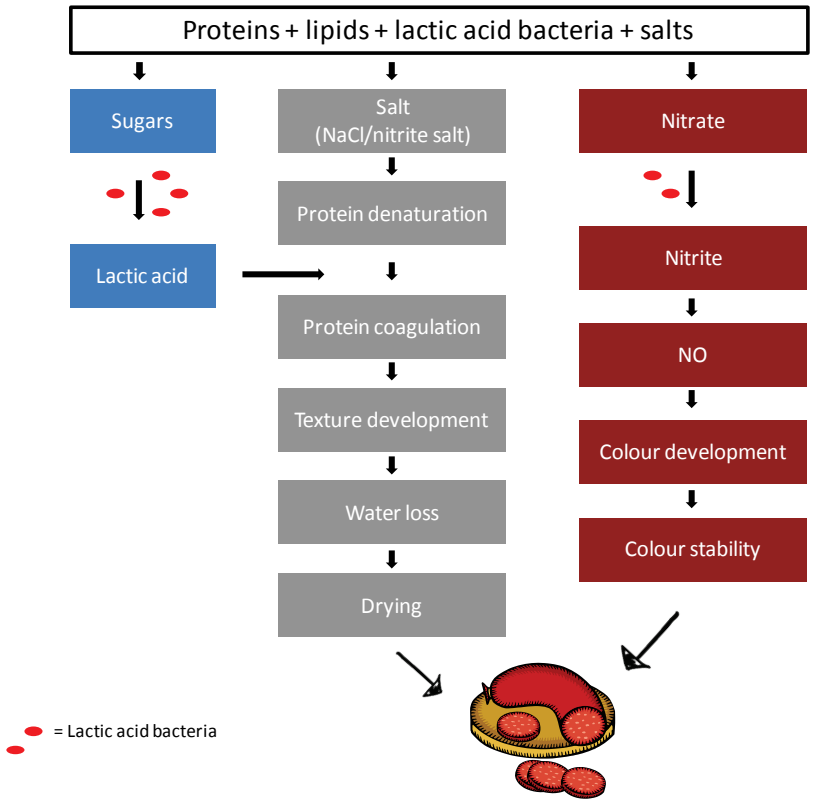

FIGURE 6 KEY TRANSFORMATION PROCESSES. SALT IS IMPORTANT FOR THE PROTEIN DENATURATION AND TEXTURE DEVELOPMENT. FERMENTATION BY LACTIC ACID BACTERIA INFLUENCES TASTE AND STRUCTURE. THE BACTERIA ALSO INFLUENCES THE COLOUR DEVELOPMENT THROUGH CONVERSION OF NITRATE TO NITRITE.

During fermentation, two basic microbiological reactions proceed simultaneously and influence each other: the formation of nitric oxide by nitrate and nitrite-reducing bacteria and the reduction of pH via the production of lactic acid from the added sugar, see Figure 6. The nitrite which is converted into nitrite oxide is important for colour development and stability. The Lactic acid is essential for protein coagulation, texture development and homogeneous drying. During storage the flavour, aroma and texture gradually changes. The sausages become firmer as a result of ripening and drying (water evaporation)[Ordóñez et al., 1999].

During the purchase, the visual product quality is very important, meaning that products with cured meat colour and low in visual fat are mostly preferred [Grunert et al., 2004]. Health concerns can also influence consumers when buying meat products. In general, products with low levels of animal fat and sodium are preferred [Vandendriessche, 2008].

IMAGING SYSTEMS

A vision system consists of many more parts than a camera! The lighting is as important as the optics, because it carries the primary information. To perform image quantification, the pixel values of the object and the background have to differ. Contrast, brightness, darkness, shadows, textures, or reflections are necessary. And it is all made with light. Different light geometries may result in different images using the same camera. A well-designed illumination system can improve the accuracy, reduce the time and complexity of the image analysis steps, lead to success of image analysis, and decrease the cost of an image processing system [Gunasekaran, 1996; Folm-Hansen, 1999; Jahr, 2007].

ILLUMINATION

Examples of different illumination techniques are presented in Figure 7 and Figure 8 and application of different techniques in Figure 10.

Diffuse illumination is commonly used on shiny or mixed reflectivity samples where a uniform illumination is needed. There are several implementations of diffuse lighting available, some common types is seen in Figure 7. Diffuse light produces a shadow free illumination like on a cloudy day.

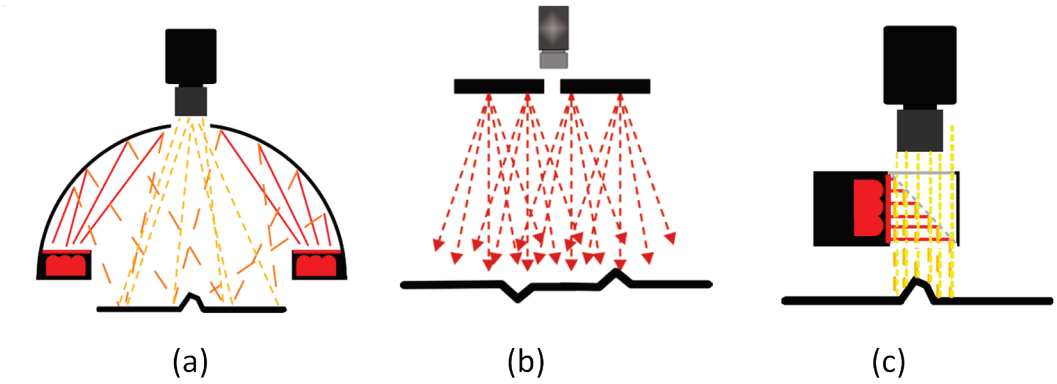

FIGURE 7 DIFFUSE LIGHT. (A) DIFFUSE DOME, (B) FLAT DIFFUSE AND (C) ON-AXIS DIFFUSE [41].

Bright field lighting is directional (Figure 8a), typically from a point source, and because of its directional nature, it is a well-suited for generating contrast and enhancing topographic detail. For shiny samples, bright field light produces a hot spot in the image, e.g. like sunlight reflection in a lake. With dark field illumination, most light reflects away from the camera and only light scattered by surface particles will be detected, see Figure 8b. Back lighting generates contrast as it creates dark silhouettes against a bright background, see Figure 8c.

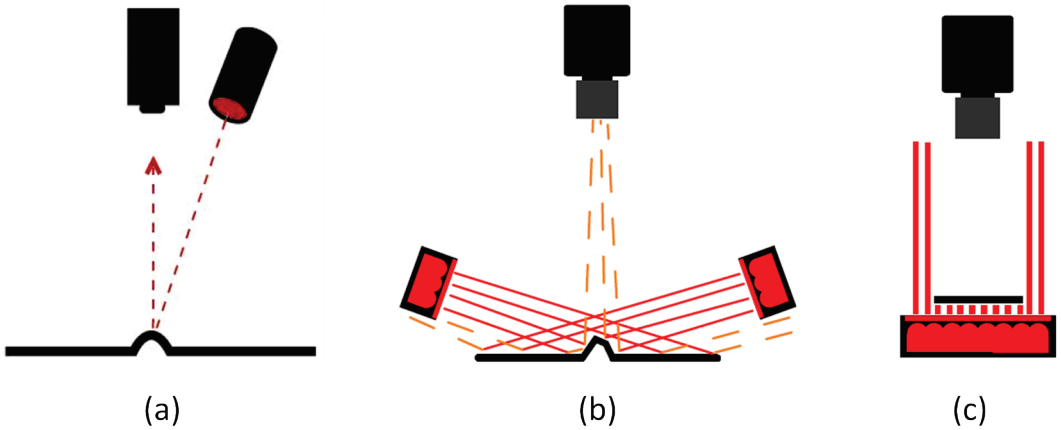

FIGURE 8 EXAMPLES OF DIFFERENT LIGHT GEOMETRY. (A) BRIGHT FIELD, (B) DARK FIELD, (C) BACK LIGHT [MARTIN, 2011].

Some illumination techniques can only be made by using a specific light and geometry, or relative placement of the camera, sample, and light; others do not. For example, a standard bright field light can also be used as a dark field illuminant; whereas a diffuse dome is used exclusively as such. For several applications, can the best results are obtained by combining multiple light types [Jahr, 2007; Martin, 2011].

Light interacts with the object it is illuminating. Some light is reflected from the surface (specular reflection), some is absorbed inside the object, some is scattered inside the object and reemitted and some is transmitted through the sample, see Figure 9. The chemistry of the object will determine which principle is the dominating or if some of the light is reemitted as fluorescent light.

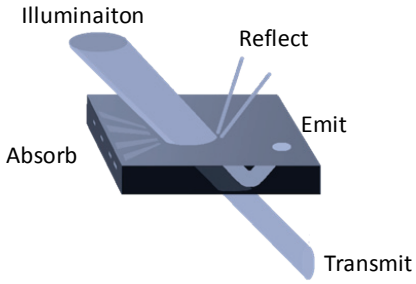

FIGURE 9 ILLUSTRATION OF HOW LIGHT INTERACTS WITH AN OBJECT. LIGHT CAN BE ABSORBED, REFLECTED, EMITED AND TRANSMITTED (MODIFIED FROM [MARTIN, 2011]). SURFACE AND SUBSURFACE PROPERTIES DETERMINES HOW AND HOW MUCH LIGHT IS REFLECTED [SALEH, 2011].

An example of simultaneously applying and evaluating multiple illumination techniques is seen in Figure 10. The experiment was made to find the best set-up for imaging glossiness, dullness and graininess of fermented milk products. Three classes of samples were evaluated: a shinny, a dull and a grainy fermented milk product. Six different illuminations were evaluated: a dome (VideometerLab), Diffuse light parallel with object surface[Johansen et al., 2008], Co-axial, bright field LED, a darkfield ringlight and a diffuse backlight. As it can be seen in Figure 10, threre are several light geometries that are able to discriminate between the different types of surfaces. The graphs in Figure 10d illustrate how each illuminant discriminate between the three samples. Co-axial and bright field illumination give a good separation between glossy and dull products (products a and b), whereas dark field and back lighting are best for visualizing larger surface particles. Surface reflection was quantified in paper III with a set-up of six bright field LEDs.

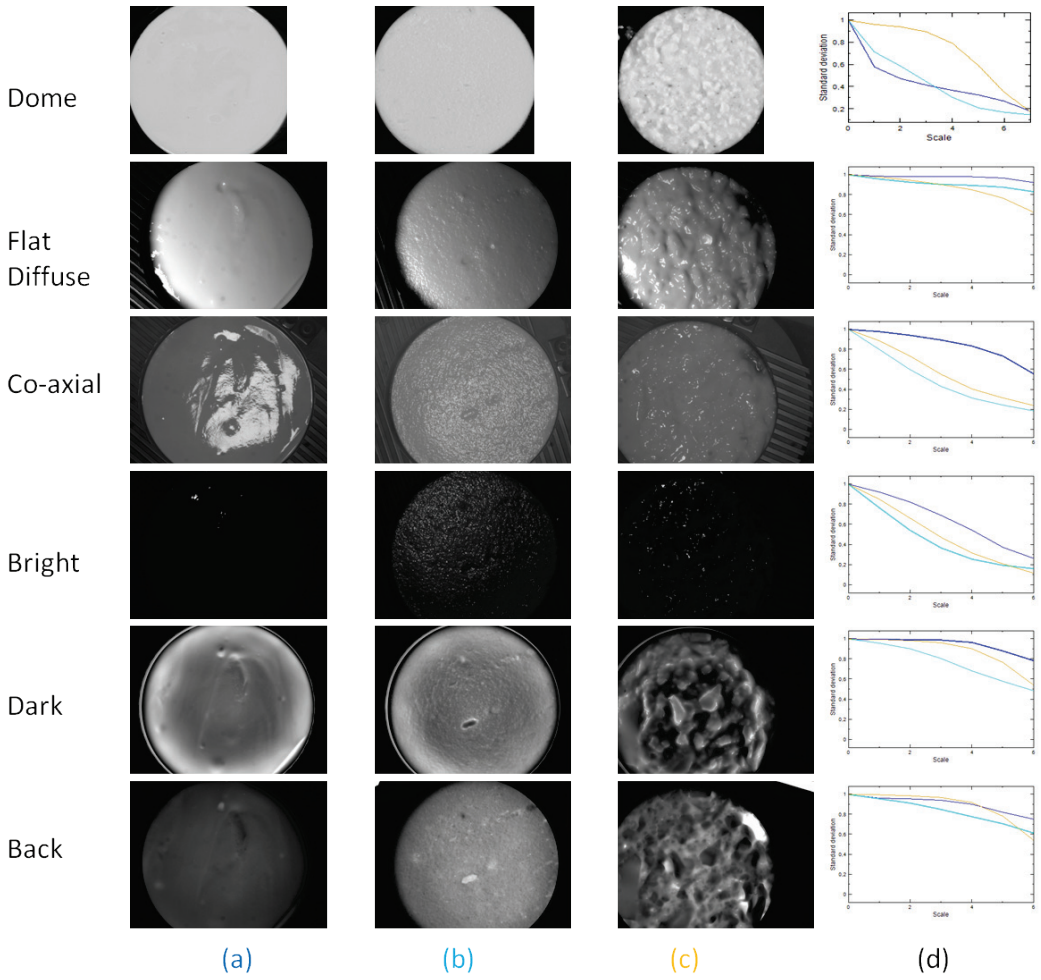

FIGURE 10 THREE FREMENTED PRODUCTS EVALUATED USING SIX DIFFERENT ILLUMINATIONS. (COLOUMN A) A SHINY CREME FRAICHE (18% FAT), (COLOUMN B) A DULL HIGH PROTEIN YOGHURT (7% PROTEIN), (COLOUMN C) STIRRED SET-YOGHURT WITH LUMPS, (D) IMAGE TEXTURE EXPRESSED AS STANDARD DEVIATION AS A FUNCTION OF SCALE (NORMALIZED GAUSSIAN PYRAMID, SEE PAGE 31). IMAGES AND DATA IS USED TO SELECT A ONE OR A COMBINATION OF ILLUMINATION TECHNIQUES WHICH BEST DISCRIMINATE BETWEEN SAMPLES, SEE PAGE 56.

LIGHT AND DETECTORS

While a black and white photo typically show the light intensity over the electromagnetic spectrum in a single image or band, a colour image can reflect the intensity over red, green, and blue bands of the spectrum. Increasing the number of bands can greatly increase the amount of information from an image. Ideally, a spectral image would cover all wavelengths, but in practice it is only a fraction of well-defined wavelength regions that are measured. Spectral imaging systems are often

categorized as *panchromatic, multispectral ,* or *hyperspectral,* as shown in Figure 11. Spectral imaging typically measures scattered light (Rayleigh and Mie scattering), i.e. the scattered light has wavelength as an incandescent light source. Fluorescence and Raman scattering are examples of inelastic scattering where the wavelength is altered by the scattering process [Grahn and Geladi, 2007].

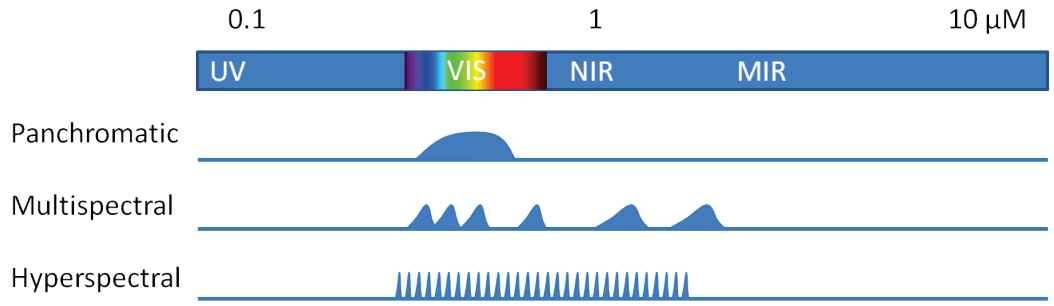

FIGURE 11 TYPES OF SPECTRAL IMAGING. IN PANCHROMATIC SENSING, A SINGLE BAND IMAGE IS MEASURED; IN MULTISPECTRAL, MULTIPLE SAMPLES OF THE SPECTRUM ARE MEASURED AT SELECTED WAVELENGTH RANGES SPACED AT DIFFERENT INTERVALS; IN HYPERSPECTRAL IMAGING, THE SPECTRUM IS SAMPLED UNIFORMLY AT NARROWLY SPACED WAVELENGTHS (MODIFIED FROM [SALEH, 2011]).

The spectral bands to use for a specific application depend on the application, the availability of light source and detectors. The signal to noise ratio is object and wavelength dependent; several molecules have wavelength-dependent chemical signatures.

Resolution is wavelength-dependent (both lateral and axial). Short wavelengths can generally detect finer details. Depth of penetration is related to the absorption and scattering of light, see Figure 9. Light absorption and scattering generally decrease with increasing wavelength. Above 900 nm, water absorption can interfere with signal-to-background ratio [Saleh, 2011]. An example of lights penetration depth as a function of wavelength info milk, is seen in Figure 12.

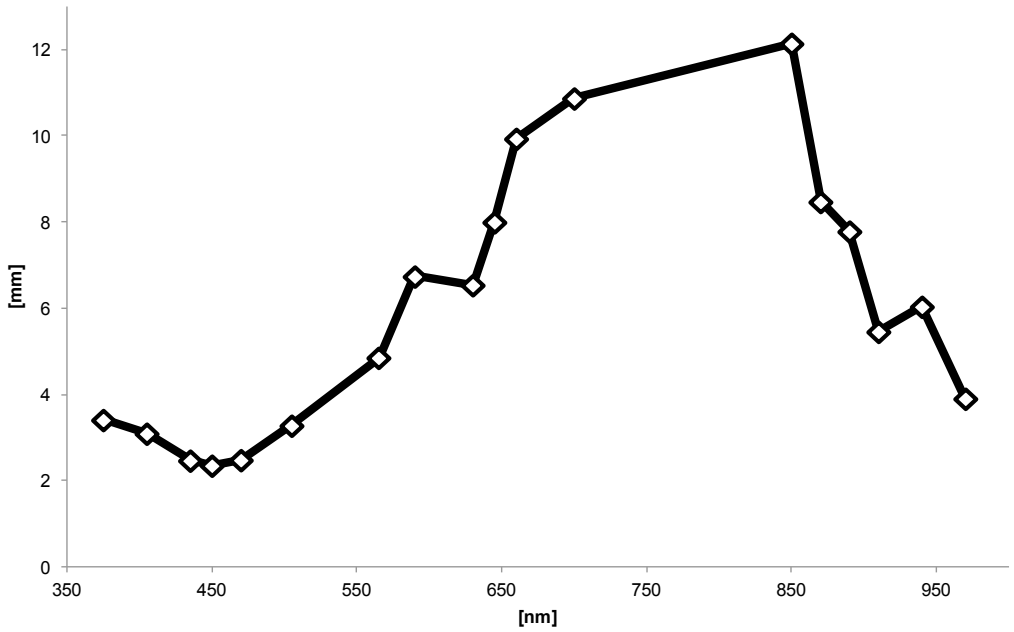

FIGURE 12 WAVELENGTH DEPENDENCE OF PENETRATION DEPTH INTO. PENETRATION DEPTH WAS MEASURED USING A VIDEOMETERLAB INSTRUMENT, SEE PAGE 52.

Spectral images are three-dimensional (3-D) in nature, two spatial and one wavelength (x, y, λ). There are four approaches used for acquiring 3-D spectral image cubes, see Figure 13. In the point-scanning method (also known as whisk broom), a single point is scanned along two spatial dimensions (x and y) by moving either the sample or the detector. A spectrophotometer equipped with a point detector is used to acquire a spectrum for each pixel in the scene. Examples of point scanning systems are: Confocal microscopes, Atomic Force Microscopes, TOF SIMS and X-ray Photoelectron Spectroscopy etc.

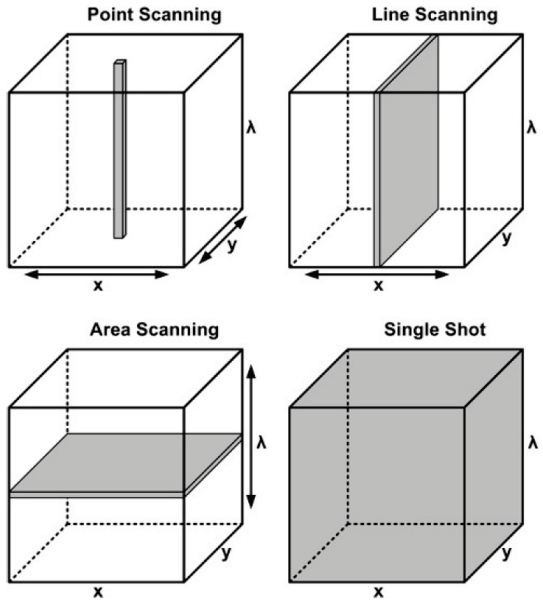

FIGURE 13 APPROACHES FOR CONSTRUCTING SPECTRAL IMAGE CUBES CONTAINING SPATIAL (X AND Y) AND SPECTRAL (λ) INFORMATION. ARROWS REPRESENT SCANNING DIRECTIONS, AND GRAY AREAS REPRESENT DATA ACQUIRED AT A TIME [SUN, 2010].

The line-scanning method (also known as push broom) simultaneously acquires a line of spatial information as well as spectral information corresponding to each spatial point in the line. A 2-D image (y, λ) with one spatial dimension (y) and one spectral dimension (λ) is taken at a time. A complete image cube is generated as the line is scanned over the product surface (x). Line-scanning instruments have typically been used in satellite imaging but also for food imaging [Møller et al., 2010]. The SisuCHEMA instrument is an example of a line scanning NIR camera [Specim Ltd, 2012].

The area-scanning method (also known as band sequential method), is a spectral-scanning method. The image cube contain a stack of single band images, that are built by scanning in the spectral domain through a number of wavelengths. No relative movement between the sample and the detector is required for this method. Area scan systems often use filters, either in front of the light source or the camera. The VideometerLab is an example of an area-scan system.

The single shot method record both spatial *and* spectral information with one exposure. No scanning is needed for obtaining a 3-D image cube, making it attractive for applications requiring fast spectral image acquisitions. Cubert GmbH (Ulm, Germany) has a single shot instrument, which can acquire 140 wavelengths with a speed of 25 frames per second.

QUANTIFICATION OF IMAGES

Image analysis can be seen as an attempt to find a link between images and models of the real world. The transition from image to the model reduces the information contained in the image to relevant information for the application. This transition is usually divided into several steps that have to be combined and repeated to make up the model.

Image analysis is expected to obtain similar results to those provided by human vision. Humans use a prior knowledge to interpret images, whereas a computer works with arrays of numbers. Figure 14 displays the same data in two different ways; on the left, the height on the vertical axis represents the brightness at a specific location – the right image contains the same information, only the representation has changed. For image analysis to be successful, knowledge about the problem can often help guide the analysis to a solution which extracts relevant features.

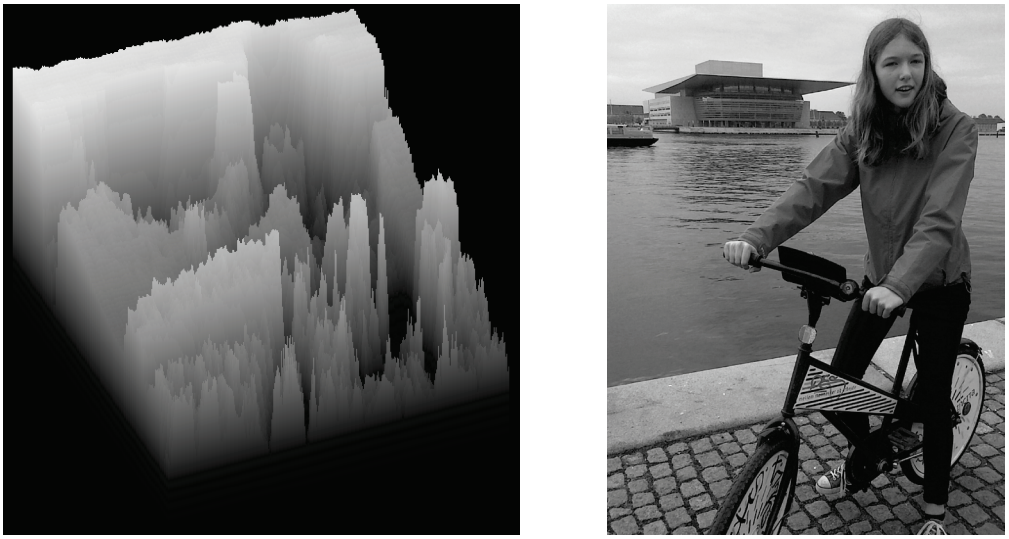

FIGURE 14 IMAGE DATA WITH AN UNUSUAL REPRESENTATION (LEFT) AND THE SAME DATA AS AN IMAGE.

In literature, several examples can be found of how image analysis has been done. It is commonly a series of tasks repeated and combined in a unique way. Figure 15 summarises some of the steps in image analysis. Most important is the image quality. Several metrics can be used for image quality, but most importantly, is that the desired difference can be seen in the image, i.e. a high contrast between the object of interest and the background [Gonzalez et al., 2004]. The image quality is decisive for the quality of results. Information lost during image acquisition cannot be reconstructed using software.

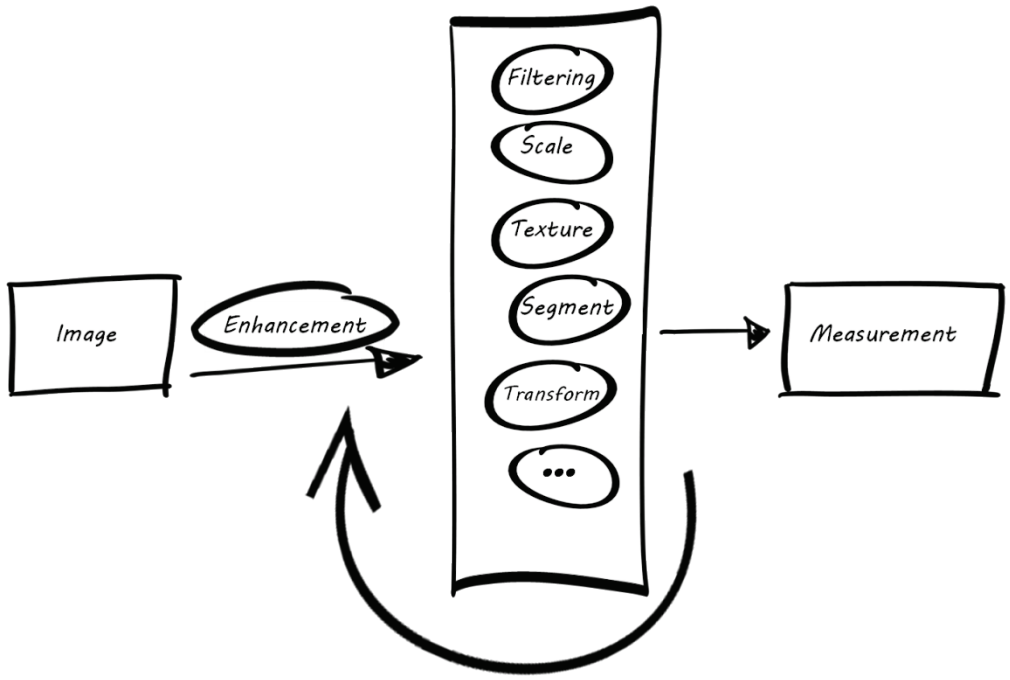

FIGURE 1 POSSIBLE STEPS IN IMAGE ANALYSIS. THE RAW IMAGE DATA IS OFTEN ENHANCED, E.G. FOR NOISE REDUCTION, CROPPING OR CALIBRATION. A TYPICAL IMAGE ANALYSIS NORMALLY COMBINES SEVERAL STEPS OF ANALYSIS, E.G. SEVERAL SEGMENTATIONS CAN BE COMBINED INTO ONE SEGMENTATION. BASED ON ONE OR SEVERAL SEGMENTATIONS CAN RELEVANT IMAGE FEATURES BE MEASURED, E.G. NUMBER OF OBJECTS, TEXTURE, SPECTRAL OR SHAPE.

It is often advantageous to build image analysis models as a hierarchical model containing and merging several simple models [Carstensen, 2011]. The list of methods used for image analysis is extensive, and the methods are often used in combination and in a recurring manner. There are several good text books and tools available to build all the small sub-models which go into building a robust image analysis algorithm [Gonzalez et al., 2004; Hastie et al., 2009].

A typical image analysis is seen in paper IV where processing steps are shown in a flowchart. In paper IV, the salami is separated from the background using a transformation (nCDA) followed by a segmentation, then a new transformation (nCDA) and segmentation to separate meat and fat is done. Then a third transformation (nCDA) to define a colour scale is performed. Finally, the scale is used to extract colour at specific positions in the salami.

PRE-PROCESSING AND FILTERING

Pre-processing or enhancement steps are applied to remove artefacts occurring during image acquisition or applied during the image analysis to enhance or suppress features. Pre-processing steps are typically performed systematically on all images, e.g. noise reduction, contrast enhancement, image smoothing, colour correction or cropping. Image filters can be used both to reduce noise and enhance features (edges, lines or circles etc). Spatial filtering refers to the convolution of an image with a specific filter mask. The process simply moves a filter mask from point to point in an image. At each point, the response of the filter is the weighted average of neighbouring pixels which fall within the window of the mask. Table 1 shows some examples of filters commonly used; statistical filters such as mean, median and standard deviation can also be used. Fourier and wavelet transforms can be used for smoothing or sharpening in the frequency domain (sometimes better that then spatial filtering)[Randen and Husoy, 1999].

TABLE 1 EXAMPLES OF SPATIAL FILTERS FOR NOISE REDUCTION AND EDGE DETECTION.

Low-pass	High-pass	Laplacian	Roberts	Prewitt	Sobel
$\frac{1}{9}\times\begin{bmatrix}1&1&1\\1&1&1\\1&1&1\end{bmatrix}$	$\begin{bmatrix}-1&-1&-1\\-1&9&-1\\-1&-1&-1\end{bmatrix}$	$\begin{bmatrix}&-1&\\-1&4&-1\\&-1&\end{bmatrix}$	$\begin{bmatrix}1&0\\0&-1\end{bmatrix}$	$\begin{bmatrix}-1&0&1\\-1&0&1\\-1&0&1\end{bmatrix}$	$\begin{bmatrix}-1&0&1\\-2&0&2\\-1&0&1\end{bmatrix}$
			$\begin{bmatrix}0&1\\-1&0\end{bmatrix}$	$\begin{bmatrix}-1&-1&-1\\0&0&0\\1&1&1\end{bmatrix}$	$\begin{bmatrix}-1&-2&-1\\0&0&0\\1&2&1\end{bmatrix}$

Confocal laser scanning microscope (CLSM) images can show significant intensity heterogeneity, for example, due to photo-bleaching and fluorescent attenuation in depth [LEE and Bajcsy, 2006]. Figure 16 is an example of illumination correction of CLSM images, the original image (a) is filtered with a large Gauss filter mask (b) and the corrected images is obtained by dividing the original with the filtered image (c=a/b).

FIGURE 16 CORRECTION OF UNEAVEN ILLUMINATION OF MICROSCOPY IMAGES. (A) ORIGINAL IMAGE DARK AREAS DUE TO POOR STAIN DIFFUSION, (B) GAUSSIAN FILTER OF ORIGINAL IMAGE, (C) CORRECTED IMAGE(A/B). THE CONFOCAL IMAGE IS OF A YOGHURT, PROTEIN IS STAINED GREEN AND FAT IS RED.

SEGMENTATION

Segmentation refers to the process of segmenting or dividing an image into parts or objects. Proper segmentation is very important – a user selecting an area of interest can be seen as supervised and simple way of focusing on relevant areas in an image. Often, the first step in assuring successful segmentation is control of background uniformity. For monochrome images, segmentation is normally performed by looking at the gray scale histogram. Segmentation algorithms are based on the discontinuity or similarity of the gray level values. Discontinuities in image gray scale indicate sharp changes in image brightness such as between the background and the object. Thresholds are widely used for image segmentation since it is intuitive and simple to implement. There are a number of approaches for obtaining optimal thresholds. Generally, the pixels are said to belong to one of two classes or clusters, foreground or background, see Figure 17.

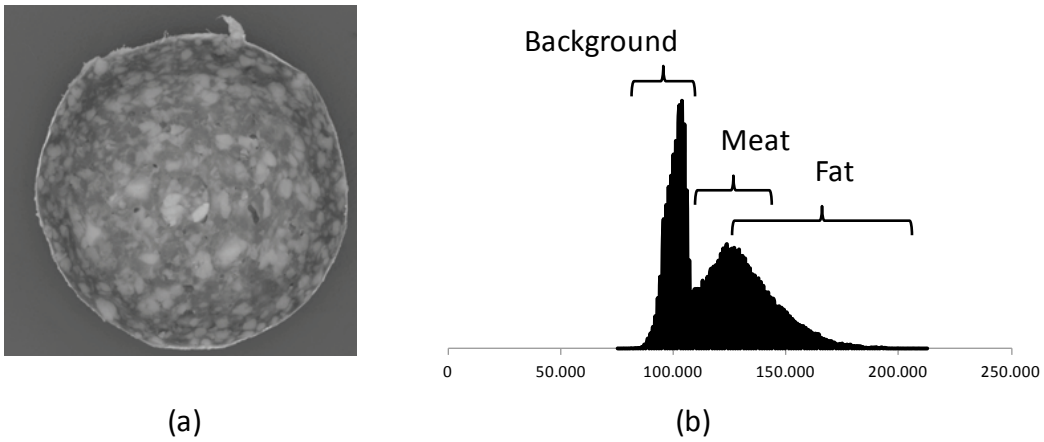

FIGURE 17 SALAMI IMAGE (A) AND CORRESPONDING HISTOGRAM OF GRAY LEVELS (B). MEAT AND FAT SEGMENTATION WITH A GLOBAL THRESHOLD IS NOT POSSIBLE DUE TO THE LARGE OVERLAP IN PIXEL INTENSITIES (DARK EDGE AND LIGHTER CENTER).

There are several methods for automatically selecting an optimal threshold [Tajima and Kato, 2011], see Figure 18. Thresholds work well if the background and object have a uniform and unequal gray level. If the object differs from the background by some property other than the gray level, such as texture, an operation (spatial filter) can enhance that property to a gray level. Then the gray level threshold can segment the processed image.

Spectral transformations or clustering algorithms can be used for segmentation using all data in a multivariate image. One example is the k-means algorithm [Hastie et al., 2009]. K-means is an unsupervised clustering algorithm that classifies the input data points into multiple classes based on their inherent distance from each other. The algorithm assumes that the data features form a vector space and tries to find natural clustering in them. The user defines how many classes k-means are to search for.

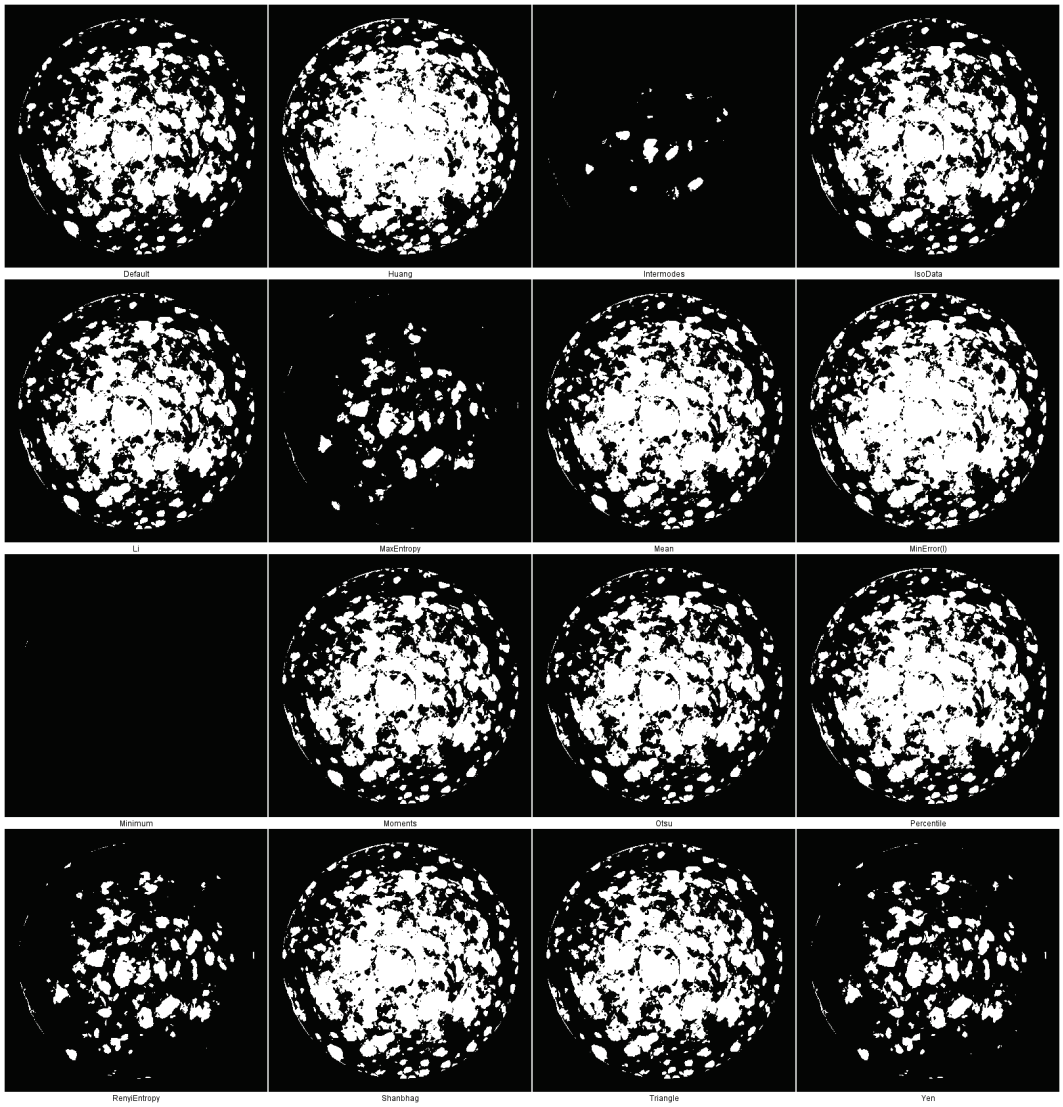

FIGURE 18 25 METHODS FOR AUTOMATIC THRESHOLDING OF GRAY SCALE IMAGES. THE METHODS ARE, *ROW 1:* DEFAULT(*ITERATIVE INTERMEANS,* HUANG, INTERMODES, ISODATA, *ROW 2:* LI, MAXENTROPY, MEAN, MINERROR(I), *ROW 3:* MINIMUM, MOMENTS, OTSU, PERCENTILE, *ROW 4:* RENYIENTROPY, SHANBHAG, TRIANGLE AND YEN.

SPECTRA EXTRACTION

For spectral images is it often relevant to extract first-order measures based on segmented objects or manually selected regions of interest (ROI). First-order measures are based on the gray level distribution, features which are commonly extracted: Mean, standard deviation, percentiles, skewness and kurtosis.

TEXTURE

Texture is, in image processing, an attribute representing the spatial arrangement of the gray levels of the pixels in a region[IEEE Computer Society., 1990]. Image texture can be defined as the spatial distribution of grey levels and be described as fine, smooth, coarse, grainy etc. Several methods are used for measuring image texture, here will only describe two: the gray level co-occurrence matrix and ganulometry.

GRAY LEVEL CO-OCCURRENCE MATRIX

The gray level co-occurrence matrix (GLCM) is an old and popular tool for texture analysis [Haralick et al., 1973] The GLCM approach is based on statistics of pixel intensity distributions. The N × N co-occurrence matrix describes the spatial dependency of the different gray levels, whereas N is the number of gray levels in the image. Figure 19a shows an example of a very small image for which GLCM is calculated for the neighbour pixel (spatial displacement of 1 (d=1)). Figure 19b shows the resulting GLCM. Haralick[Haralick et al., 1973] suggested 14 features which can extracted from the co-occurrence matrix and the can be used to describe image texture.

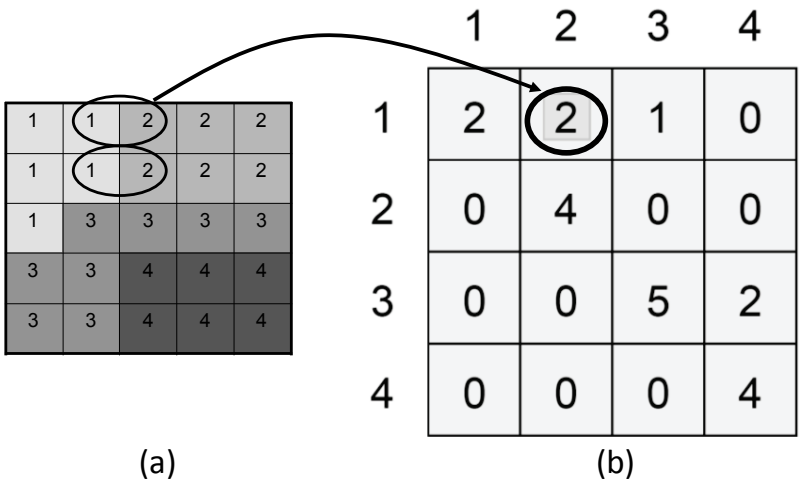

FIGURE 19 CO-OCCURRENCE MATRICES FOR A SMALL IMAGE, (A) SHOWS THE ORIGINAL IMAGE; (B) SHOWS THE RESULTING CO-OCCURRENCE MATRIX FOR D = (0,1).

Figure 20 shows confocal images of yoghurt for which the GLCM has been calculated. Since textures are often directional, GLCM is commonly calculated for different angles and averaged.

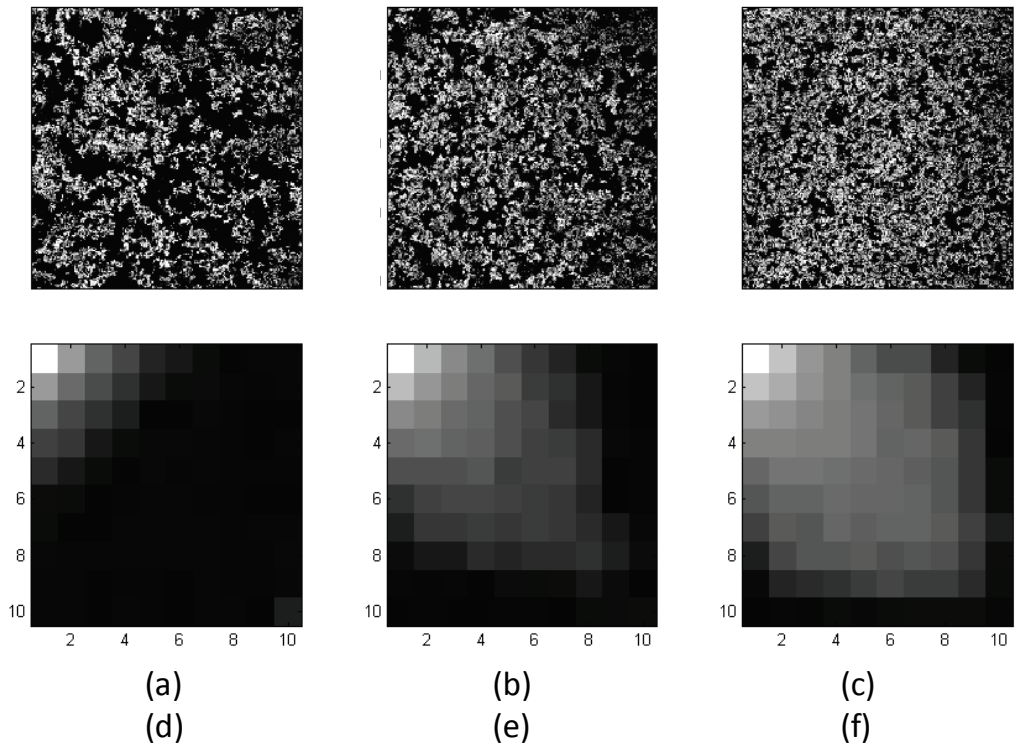

FIGURE 20 CLSM IMAGES OF YOGHURT AND CORRESPONDING GLCM. (A-C) THREE YOGHURTS WITH DIFFERENT TEXTURE, (D-F) SHOW THE RESULTING GLCM, 10 PIXEL LEVELS AND D=(0,1).

The scale dependency can be calculated by incrementally increasing the spatial displacement or by the use of a Gaussian Pyramid [Lindeberg, 1994]. The Gaussian Pyramid can be generated with logarithmic scaling which resembles the human perception of scale [Koenderink, 1984], the lower levels of the pyramid is used to extract fine spatial information and the higher level for larger objects like network structures in CLSM images. The incremental method generates many and highly correlated features, whereas pyramid methods are faster to calculate and can be used with most texture descriptors (fist and second order)[Schulerud et al., 1995; Siqueira F. R. de et al., 2013]. An example of a Gaussian Pyramid and a CLSM image of yoghurt at level 0 and level 3 are seen in Figure 21. In Figure 38 is seen an example where image texture has been calculated for 3 yoghurts in a multilevel Gaussian pyramid.

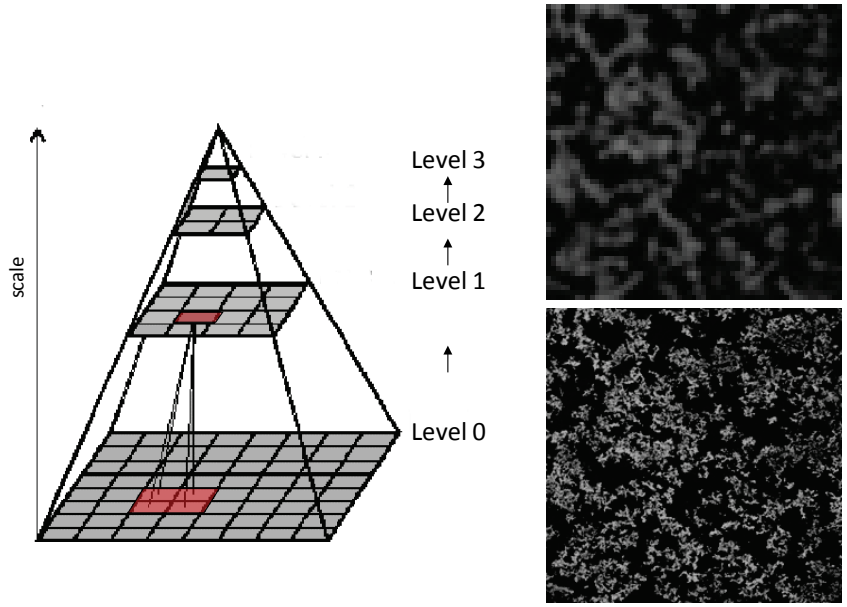

FIGURE 21 EXAMPLE OF GAUSSIAN PYRAMID. (A) A GAUSSIAN PYRAMID WITH 3 LEVELS, (B+C) EXAMPLE OF CONFOCAL IMAGE OF YOGHURT AT LEVEL 0 AND LEVEL 3.

GRANULOMETRY

The term granulometry is used in the field of materials science to characterize the granularity of materials by passing them through sieves of different sizes while measuring their mass retained by each sieve [Boschetto and Giordano, 2012]. This principle is also used in image processing, where the measure is the amount of image detail removed by applying morphological openings of increasing size. The mass is represented by the sum of the pixel values, known as image volume. The volumes of the opened images are plotted against opening size, producing a granulometry curve, see Figure 22. The idea of sieving the image often makes it easier for food scientist to understand and accept granulometry compared to GLCM [Lassoued et al., 2007; Rami-shojaei et al., 2009]. The sieving is done by a morphological opening operator and is preformed on the gray scaled image, no threshold is necessary [Gonzalez et al., 2004].

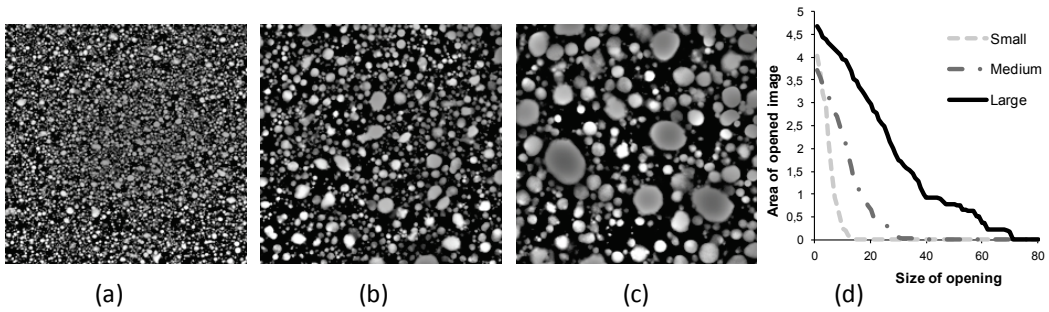

FIGURE 22 CONFOCAL IMAGES OF OIL EMULSIONS AND THEIR CORRESPONDING GRANULOMETIC CURVES. (A) EMULSION WITH SMALL OIL DROPS, (B) MEDIUM SIZED, (C) LARGE OIL AND (D) THE GRANULOMETRIC CURVE.

TRANSFORMATION

Spectral images often contain a lot of redundant data, therefore transformations are commonly used to enhance predominant structures in an image [Grahn and Geladi, 2007]. A range of linear and non-linear, supervised and non-supervised models, with different constraints and advantages exists. The unsupervised methods are good for explorative data analysis, whereas the supervised ones are often better for segmentation between object and background.

UNSUPERVISED METHODS

Principal component analysis (PCA) is probably the most commonly used linear transformation. It maximises the variance in the spectral information and disregards any spatial information [Geladi and Grahn, 1996; Hastie et al., 2009]. Switzer et al. introduced the Maximum Autocorrelation Factor (MAF) transform, which maximises the autocorrelation between neighbouring pixels based on spatial information [Switzer and Green, 1984]. A similar transform was presented by Green et al. as the Minimum Noise Fraction (MNF) transform, which maximises the signal-to-noise ratio in the image [Green et al., 1988].

The MAF and MNF transformations are not influenced by linear transformations, unlike PCA. All three methods are influenced by non-linear spectral transformations, e.g. SNV, normalization or logarithmic scaling.

PCA

PCA is defined as an orthogonal linear transformation that transforms data to a new coordinate system ensuring that the greatest variance of the data lies on the first coordinate (called the first principal component), the second greatest variance on the second coordinate etc. PCA describes the data in terms of the matrix factorization:

$$X = TP' + E$$

Where X is the original data matrix that is decomposed into a score matrix (T), which describes the samples, and a loading matrix (P), which describes the variables. The residual (E) should typically contain unsystematic variation. Principal components are constructed and ordered so that they serially maximize the variance in the data that they accounts for. Mean-centring, scaling or weighting of the variables are examples of pre-treatments commonly applied before PCA modelling [Wold et al., 1987; Rinnan et al., 2009].

MAF

The Minimum/Maximum autocorrelation factors (MAF) create a set of orthogonal vectors similar to PCA but instead of maximizing the variance, the MAF seeks to minimize the autocorrelation defined by the relationship between neighbouring pixels. By including the spatial structure into the transformation, MAF highlights spatially connected areas of with similar spectral shapes [Switzer and Green, 1984; Nielsen, 1999].

MNF

The MNF transform [Green et al., 1988] is a noise-adjusted principal components transform that estimates and equalizes the amount of noise in each image band. For MNF are the components ordered by image quality (signal to noise), rather than variance as in PCA.

MNF requires an estimate of the signal and noise dispersion matrices. Common noise filters are mean or median filters of different size. The MNF transformation is equivalent to a transformation of the data to a coordinate system in which the noise covariance matrix is the identity matrix (noise whitening) followed by a principal components' transformation. When noise is estimated as the difference between neighbouring pixels, the same eigenvectors as in the MAF analysis are obtained [Green et al., 1988; Nielsen, 1999].

EXAMPLE OF UNSUPERVISED TRANSFORMATION

When imaging food samples; shadows and changes in surface reflectance may result in spectra intensity shifts, e.g. cereal and baked products with a high level of topography/shadow and products meat, fish and dairy products with a dry/wet surface.

The sample, seen in Figure 23, is an image of three coloured papers: Red, Green and Blue (R, G and B). A metal cylinder is placed in the centre of the image, , which limits the light, resulting in a shadow version of red, green and blue, see Figure 23a. Representative areas outside and inside the cylinder are annotated, see Figure 23b. The mean spectra with standard deviation for the six annotated areas are seen in Figure 23c. The shadowed areas (inside the metal ring) have a lower reflection than areas outside.

(a) (b) (c)

FIGURE 23 RED-GREEN-BLUE PAPER WITH SHADOW IN THE CENTER CAUSED BY METAL CYLINDER: (A) PHOTO OF SET-UP; (B) ANNOTATED VIDEOMETERLAB IMAGE, TWO AREAS FOR EACH COLOUR ARE SELECTED, I.E. INSIDE AND OUTSIDE THE METAL CYLINDER; (C) SPECTRA WITH STANDARD DEVIATION FOR THE 6 ANNOTATED AREAS.

Figure 24 shows how PCA, MAF and MNF transform the image seen in Figure 23. For the PCA (Figure 24 a+b) the first PC separates the perfect illuminated from the shadowed colours, while the second PC separate the three colours. MAF and MNF have a better separation of the three colours and especially the MNF shows very little influence by shadowed area. Spectral pre-processing [Rinnan et al., 2009] could have removed most of the shadow effect and would therefore have resulted in better class separation(R, G and B).

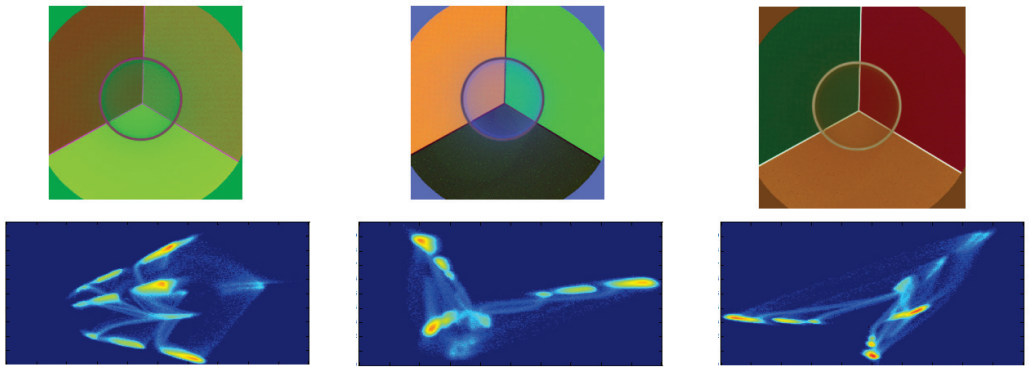

(a) (c) (e)
(b) (d) (f)

FIGURE 24 PCA, MAF AND MNF TRANSFORMATIONS OF THE SPECTRAL IMAGE SEEN IN FIGURE 23B. TOP ROW SHOWS AN RGB IMAGE OF THE FIRST 3 PCS, BOTTOM ROW PC2 VS. PC1. (A+B) PCA , (C+D) MAF AND (E+F) MNF.

SUPERVISED METHODS

A supervised method is made from known training samples belonging to different classes. Having enough and representative training samples is important for supervised methods. Selecting samples for model building is done by annotation (Figure 23b), as for all data analysis, is it important to include all relevant variation in the training of the model.

CANONICAL DISCRIMINANT ANALYSIS

Canonical discriminant analysis (CDA) separates classes into a lower dimensional discriminant space. This is done by finding linear combinations of variables to achieve maximum separation of the classes while minimizing the within group scatter, see Figure 25. CDA is also known as Fisher discriminant analysis which is again similar to Linear Discriminant Analysis [Guang and Maclean, 2000; Hastie et al., 2009].

CDA derives canonical variables that summarize between-class variation in much the same way that PCA summarizes total image band variation. Canonical components are not necessarily orthogonal. A single principal component cannot discriminate better than the first canonical function [Guang and Maclean, 2000; Franc and Hlavác, 2004].

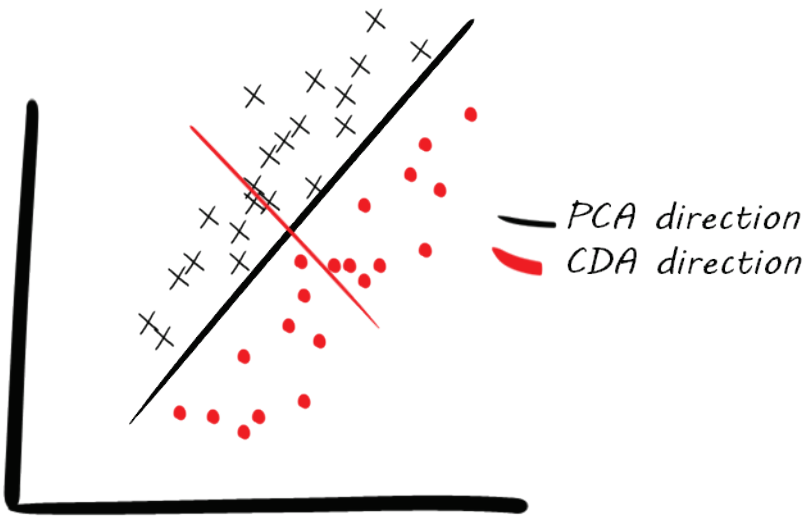

FIGURE 25 AN ILLUSTRATION OF THE FIRST PRINCIPAL COMPONANT AND CANONICAL DIRECTION IN A SIMPLE DATA SET WITH TWO CLASSES OF OBJECTS (X AND •). THE PCA MAXIMISES THE DATA VARIATION THE PCA MAXIMISES THE CLASS SEPARATION.

Normalized Canonical Discriminant Analysis (nCDA) is very similar to CDA. With nCDA, the mean is set to the mean of classes instead of the overall mean, and all nCDFs are scaled to a numerical

deviation of one for the max class mean [Carstensen, 2011]. Two classes will therefore respectively have a mean of 1 and -1.

For the three coloured paper were the separation or segmentation done one colour at the time, i.e. first model separated red from blue+green, second model separated green from red+blue etc. Figure 26 show CDA used to separate the shadowed areas from the rest of the image. nCDA gives the same result as CDA but scales the result differently, as seen in the two histograms in Figure 26d+e. The advantage of nCDA is that the result is centred on zero, which always results in a threshold value of zero, seen in Figure 26e.

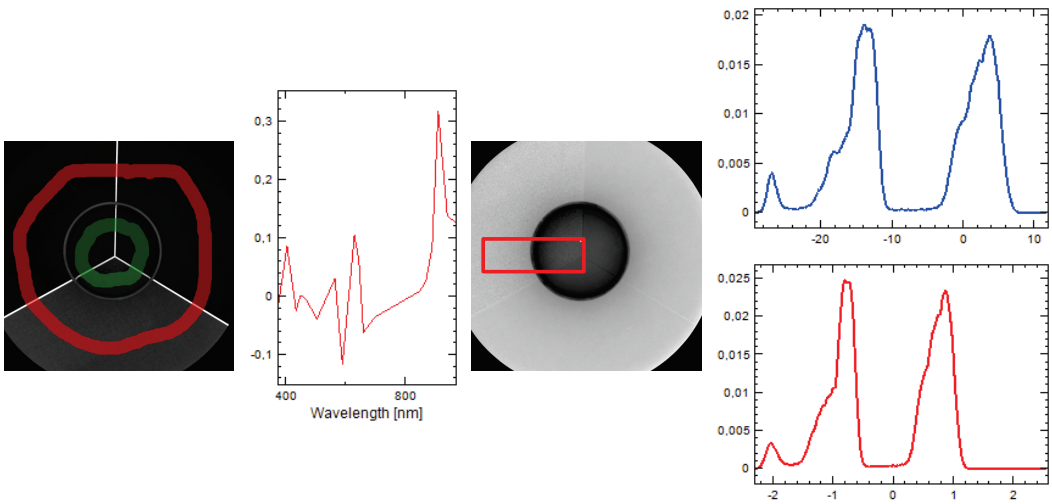

FIGURE 26 CDA AND nCDA TRANSFORMATIONS USED TO SEPARATE SHADOW FROM PERFECTLY ILLUMINATED AREAS. (A) PAINTED AREAS FOR MODELLING, (B) LOADING VECTOR, (C) SCORE IMAGE - RED AREA USED FOR HISTOGRAM (D+E), (D) HISTOGRAM FROM SELECTED AREA (CDA), AND (E) HISTOGRAM FROM SELECTED AREA WHEN USING nCDA.

DECISION TREES

All of the previously described unmixing models were based on linear transformations of the input variables. Decision trees is a supervised *non-linear* method based on variable selection and splitting [Hastie et al., 2009].

Decision trees used to be constructed on the basis of prior human understanding of the underlying processes or data. Well-defined methods of building them are a recent innovation [Breiman et al., 1984]. Small decision trees are often easy to understand and explain.

Figure 27 shows how a tree model looks for separating the 3-coloured paper. The first split separates the perfectly illuminated parts from the shadowed centre (split at 850 nm). Next split of

both leaves selects the red colour (split at 630 and 700 nm). The last split is to separate blue and green paper (split at 405 nm).

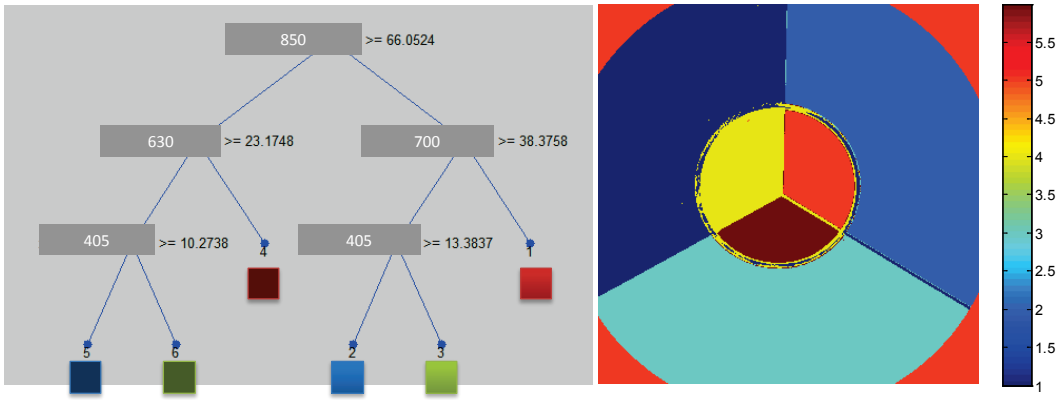

FIGURE 27 DECISION TREE FOR SEPARATING 6 CLASSES OF COLOURED PAPER. (A) TREE MODEL, NUMBER IN DARK BOX SHOWS WHICH WAVELENGTHS TO SPLIT AND AT WHICH VALUE, SEE WAVELENGTHS IN FIGURE 23C, (B) THE RESULTING CLASSIFICATION.

Figure 28 shows how linear and non-linear, unsupervised and supervised transformations can be used to separate meat and fat in salami. The salami has a dark edge which makes meat/fat segmentation difficult. The PCA gives some separation of meat/fat but not enough to make segmentation based on the score images. The wavelength normalisation removes some of the colour gradient and improves the supervised nCDA segmentation. The non-linear tree model gives a good segmentation between meat/fat and in very little influence by the wavelength normalisation.

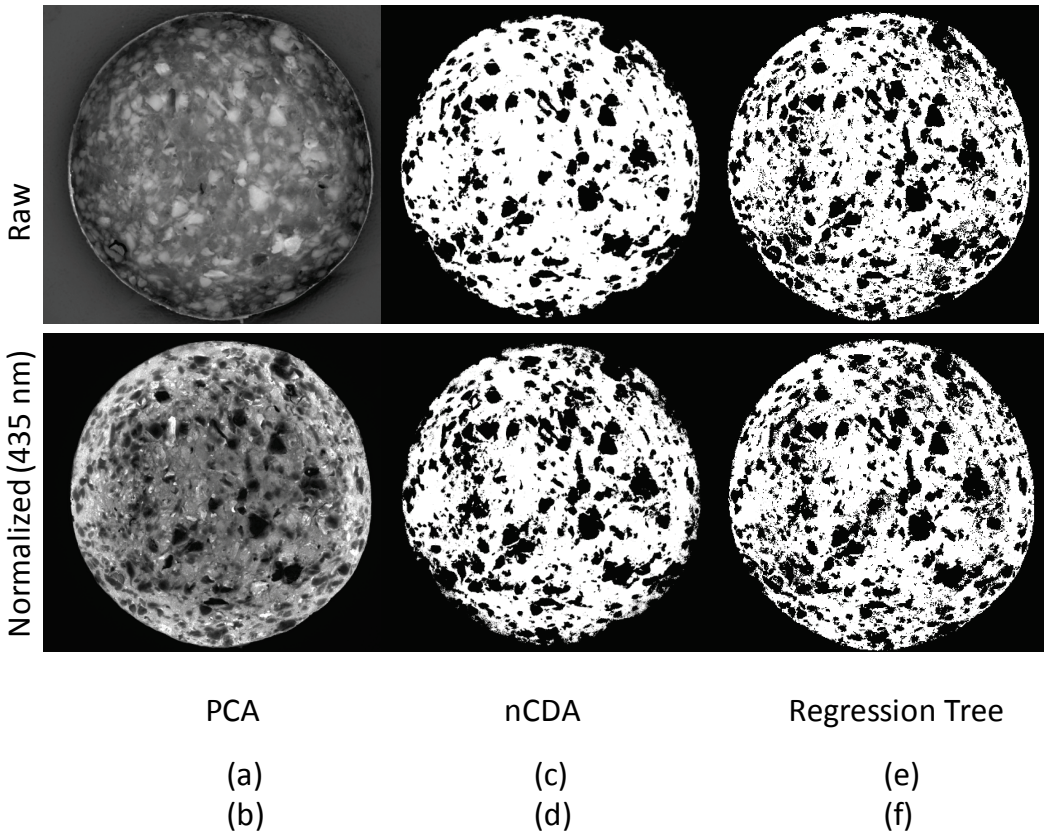

FIGURE 28 SEGMENTATION OF MEAT AND FAT IN SALAMI. THE TOP ROW IS BASED ON RAW INSTRUMENT DATA, IN THE BOTTOM ROW BASED ON NORMALIZED SPECTRA (DIVIDED BY 435 NM). NORMALIZATION IMPROVES SEGMENTATION FOR THE LINEAR METHODS (PCA AND nCDA). REGRESSION TREES IS ONLY SLIGHTLY INFLUENCED BY THE SPECTRAL NORMALIZATION.

IMAGE ANALYSIS USED IN ARTICLES

WATER IN BREAD

A PLS model was generated based on a large number of small bread pieces. The bread pieces were separated from the background (segmented) by thresholding a single wavelength image. The median spectra were extracted from all bread pieces. Based on the extracted spectra and corresponding measured water content were a PLS model of water build. The PLS model was applied to complete slices of bread.

CHOCOLATE MILK

Pre-processing of these images included removal of dead pixels and extraction of a region of interest – some flask structure had to be removed. In this paper was the focus to develop a

method which could detect the development of fine surface structures. The wavelength with the highest signal to noise ratio was used for all structure quantification. Three types of image filters were used to generate stability barcodes, i.e. median, standard deviation and H-domes [Vincent, 1993]. To remove edge effects and colour differences were all stability barcodes centred by subtracting the first barcode. The stability barcodes were used to visual summarise each chocolate milk formulations stability. Kinetic curves were derived in the top, middle and bottom of the stability barcodes/flasks. This was done by plotting the intensity in the pre-defined zones as a function of time. The kinetic curves were used to compare destabilisation between samples.

SALAMI

Image texture measured using a Gaussian pyramid was used to quantify how the structure/slice ability/homogeneity of salami changes during ripening. To segment meat from fat was a serie of nCDAs used. The spectra were normalised to remove a colour gradient from centre toward the edge of the salami. A meat colour scale was made using nCDA. This new meat colour scale was used to visualise the colour distribution in different salamis. A distance map was used to calculate the average meat colour as a function of salami radius.

YOGHURT

The image texture was measured using multiple levels in a Gaussian pyramid – especially useful for dull grainy yoghurts. The six most reflecting hot spots were found by filtering the image with a Gaussian filter and then extracting the six spots that had the highest light reflection (ensuring that they did not overlap). The total amount of light reflected were measured, the ratio of light reflecting from the six hot spots and in a zone around the hot spot were derived. H-domes were used to measure the number of small speckles in the hot spot and the zone around it.

SUMMARY ON IMAGE ANALYSIS

Images with a high signal-to-noise ratio are essential for a good and robust image analysis. It is often advantageous to combine several small models into one large robust model. Often image data have to be averaged from several images (repetitions), in such cases can it be an advantage to work with medians.

UNDERSTANDING AND PREDICTING FOOD QUALITY

The field of machine learning and statistics is the foundation for modelling the vast amounts of data generated modern instruments. A good introduction and coverage of the field is found in [Hastie et al., 2009].

EXPLORATIVE

Data extracted from images can be used to describe differences among samples or to predict quality parameters such as sensory characteristics, stability, appearance ect. The Principal Component Analysis (PCA) is probably the most commonly used method for explorative data analysis [Wold et al., 1987]. PCA is an unsupervised method where data is linearly transformed or rotated, to maximise sample variation. The rotated samples can be visualised in a score plot and variables in a loadings plot (the weight by which each variable should be multiplied to get the component score). By applying non-linear transformation to the variables, a non-linear PCA can be performed. There are several other unsupervised linear and non-linear methods such as hierarchical clustering, kernel methods, k-means and self-organising maps etc. [Hastie et al., 2009; Christiansen et al., 2012]. In this report the PCA has been the main method for unsupervised data visualisation.

FACTOR ANALYSIS

Often groups of samples can be seen in a PCA score plot, groups that can be related to experimental differences, e.g. yoghurt produced with different ingredients or concentrations. 50-50 MANOVA [Langsrud, 2002; Bjerke et al., 2008] is a form of multivariate ANOVA which can test for significant effects of the design factors. 50-50 MANOVA handles co-linearity of data by first reducing the data by PCA followed by variance testing using an ordinary MANOVA. The method also calculates the explained variance of each factor, which is the sum-of-squares for each response variable divided by the total sum-of-squares.

PREDICTION

Predictive models generally relate data variables (X) with a quality parameter (Y). Prediction of food quality can either be done using one or many variables (univariate or multivariate), with a linear or non-linear model. Generally, the simplest model should be preferred. Simple models with only a few variables are often easier to interpret, whereas larger models use extra variables for better prediction and to be less influenced by variable noise. To find the best model and fine-tune the variable selection, some types of model validation are recommended, e.g. test set, cross validation or bootstrapping [Hastie et al., 2009].

In chemometrics, the Partial Least Squares regression (PLS) is probably the most popular multivariate regression method. PLS can be seen as two linked PCAs, i.e. a PCA on the measured variables and one on the variables to predict [Geladi and Kowalski, 1986]. The decomposition of Y

influences the decomposition of X and the opposite way around. This is done by estimating PLS components that capture and maximise the variance and correlation between X and Y. PLS predicts one or more variables simultaneously. All variables are usually included in the model.

Removing noisy and non-informative variables can influence both the predictive ability and interpretability of a model. The simplest type of variable selection is manual variable selection where variables with small loadings are removed. Interval PLS (iPLS) is a stepwise search for the best sub-set of variables (forward or backward) [Norgaard et al., 2000]. Ridge and Lasso are also linear regression methods which have a form of variable selection inherent [Hastie et al., 2009]. Ridge method shrinks the non-important variables (but keeps them), whereas the Lasso find representative variables and drops the rest. Elastic Net regression is a combination of Lasso and Ridge regression [Hastie et al., 2009].

Regression trees (RT) is an example of a method for non-linear prediction. Tree models are easy to understand and can handle both continuous and discreet variables [Breiman et al., 1984]. Building RTs is done by recursively splitting the input variables. To avoid overfitting, the RT is pruned by cross validation. Random forest is an extension of RT, where several trees are built (a forest) using bootstrapping [Breiman, 2001]. Random forest models are more robust but not as readable as RT. An example of a RT is seen in Figure 29. Two variables from a rheology flow curve of freshly produced yoghurt (up curve: 135 s^{-1} and down curve: 1 s^{-1}) were used to predict syneresis (%) of yoghurt after a stress test (r^2=0,82 and RMSEP=3,3). The model were optimised using 10-fold cross validation and pruning [Hastie et al., 2009]. Figure 29a show the resulting RT, at each node is the right leave chosen when the equation is correct. The RT can also be visualised by dividing lines in a scatter plot, see Figure 29b.

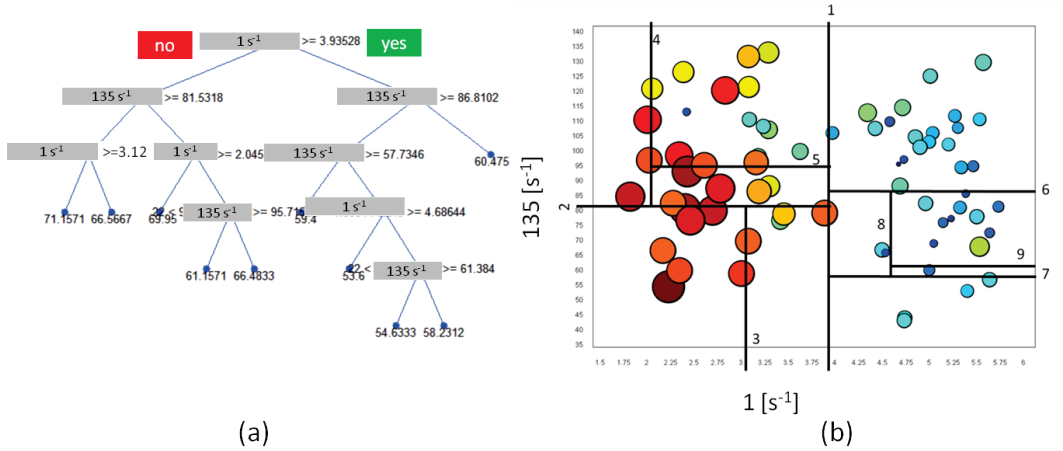

FIGURE 29 YOGHURT SYNERESIS (%) PREDICTED USING TWO VARIABLES (SHEAR STRESS AT 1 AND 135 S^{-1} MEASURED BY RHEOLOGY FLOW CURVES). (A) THE REGRESSION TREE – THE PREDICTED VALUE IS SEEN AT THE BOTTOM OF THE LEAVES, (B) SCATTER PLOT OF THE TWO MODEL VARIABLES, THE TREE NODES ARE SHOWN WITH NUMBERED LINES. THE SIZE COLOUR OF SCATTER PLOT POINTS INDICATES LEVEL OF SYNERESIS (%).

CROSS VALIDATION

Proper cross validation (CV) is the key to developing good regression models [Geladi and Kowalski, 1986; Kohavi, 1995; Hastie et al., 2009]. An un-validated model is likely to fit training data but predict new data poorly. The validation step is to avoid false/chance correlations, determine the optimal model parameters and to ensure that the estimated model reflects reality. All CV is about how good a model is at predicting new samples. The quality of a CV model can be measured by the correlation coefficient and prediction error, i.e. Root Mean Square Error of Cross Validation (RMSECV).

For CV, is a set of new and independent samples preferred, known as a test set. The test set should be large enough to reflect all variation to be covered by the model. If a test set is not available, internal validation is needed, known as Leave-One-Out, k-folds, Random Subsets or bootstrapping [Kohavi, 1995; Miller, 2005; Hastie et al., 2009].

With small data sets or when generating a test-data-set is too costly, “leave-one-out” or “bootstrapping” can be the best or only CV option. With “leave-one-out” CV is one observation is left out for testing at each step. Bootstrapping is a resampling technique with replacement. The true error is estimated as the average error of test data, see Figure 30 for a graphical example of bootstrapping [Kohavi, 1995].

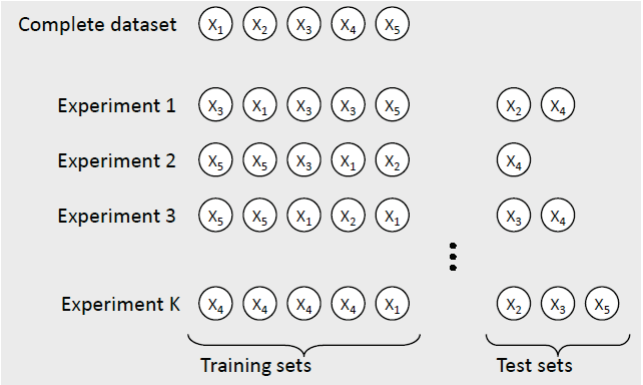

FIGURE 30 GRAPHICAL EXAMPLE OF BOOTSTRAPPING. THE NUMBER OF BOOTSTRAPS (K) IS TYPICALLY SET TO 500.

CONCLUSION ON PREDICTING

Cross validation is probably the most important step to remember when doing data modelling. For explorative data analysis is the PCA, and in combination with a k-means clustering a good and well accepted method. Variable selection is always recommendable when building predictive models. The PLS models are based a linear combination of variables. Regression Trees models are nonlinear and often easy to intrepid.

IMAGING TECHNIQUES

"If all you have is a hammer, everything looks like a nail" Abraham Maslow, 1966

The focus should be the nail or a robust answer and not of a preferred method. The same is valid for imaging and food science- use the best method – the best answer might come from a simpler method.

With an optimal combination of sample preparation, wavelengths, detector and light geometries is it possible to build very powerful dedicated instruments. In most dedicated imaging applications, is it only necessary to separate 2-5 different classes or components.

Some questions to ask when selecting the ideal set-up:

- Chemical differences?
    - UV, VIS, NIR, fluorescent or Raman
- Structure differences
    - Can light geometries enhance Signal to noise Ratio (SNR)?
    - Size of object
- Sample handling
    - Preparation
    - Imaging speed
- Image analysis
- Price

This chapter demonstrates examples of different imaging techniques explain why the set-up was chosen and show examples of results.

SUBSURFACE LASER SCATTERING

The development of this method for food analysis was initially inspired by the measurements and modelling being used in computer vision [Jensen et al., 2001]. The method is non-contact, fast, inexpensive and it measures physical properties of translucent materials, all features that in themselves make an interesting method.

FIGURE 31 SCHEMATIC EXAMPLE OF AN ANALYTICAL SET-UP FOR SUBSURFACE LASER SCATTERING. LASER LIGHT IS FOCUSED ONTO A SAMPLE AND RESULTS IN A HALO ON THE SAMPLE SURFACE DUE TO SUB-SURFACE PARTICLE SCATTERING. A PHOTO OF THE HALO IS USED FOR DATA ANALYSIS.

The set-up is simple; a laser is focused on a product surface and an image of the surface is recorded, see Figure 31. The system setup is very flexible, it works directly on a surface or through a transparent material, the object can be flowing or standing still, the angle and distance between laser, sample and camera can be changed.

The laser light interacts with food product in several ways but what is imaged is primarily a halo developing around the laser incident point. The size, decay and texture of this halo are influenced by particle size, number of light scatters and the refractive index [Nicolai and McClements, 2007], i.e. properties very much related to the underlying structure. Figure 32 shows two halo examples obtained from dairy desserts with different air bubble sizes (illustrated by circle size).

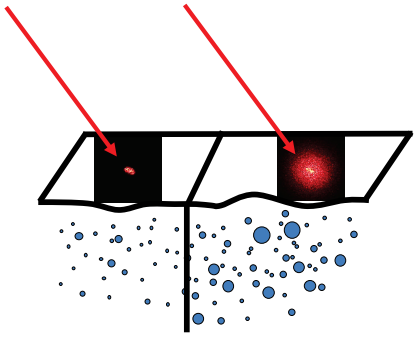

FIGURE 32 EXAMPLES OF RESULTING IMAGES OF TWO DAIRY DESSERTS. ONE WITH SMALL AIR BUBBLES AND ONE WITH LARGE AIR BUBBLES.

For homogeneous food products such as milk and emulsions, the halo is 'smooth' and the pixel decay has been calculated as a metric [Carstensen and Møller, 2009]. Pixel intensities along a line through centre of the halo can be modelled by linear regression,

$$\log(\log(i+1)+1) = a + bx$$

With *i* being the pixel intensity and x the position along the line through the halo. The halo is now described by two values, an offset (*a*) and the slope *b*. The slope is sample and composition dependent whereas the offset is mainly camera and laser dependent. Figure 33 describes how the line through the halo is placed, pixel intensities along the line is plotted and transformed, before calculating the slope (SLS=Subsurface Laser Scattering). For more heterogeneous products can structures or elongation be seen in the halo, see Figure 34. For such products can it be relevant to calculate texture or shape of the halo [Møller, 2006].

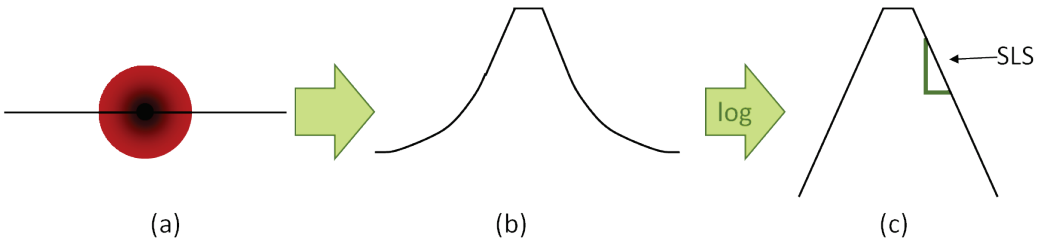

FIGURE 33 QUANTIFICATION OF LASER HALO. (A) EXTRACT A LINE OF PIXEL VALUES THROUGH HALO CENTER, (B) PIXEL INTENSITY AS A FUNCTION OF DISTANCE, (C) A LOG-LOG TRANSFORMATION OF PIXEL VALUES RESULT IN TWO LINES, THE SLOPE(SLS) IS CALCULATED.

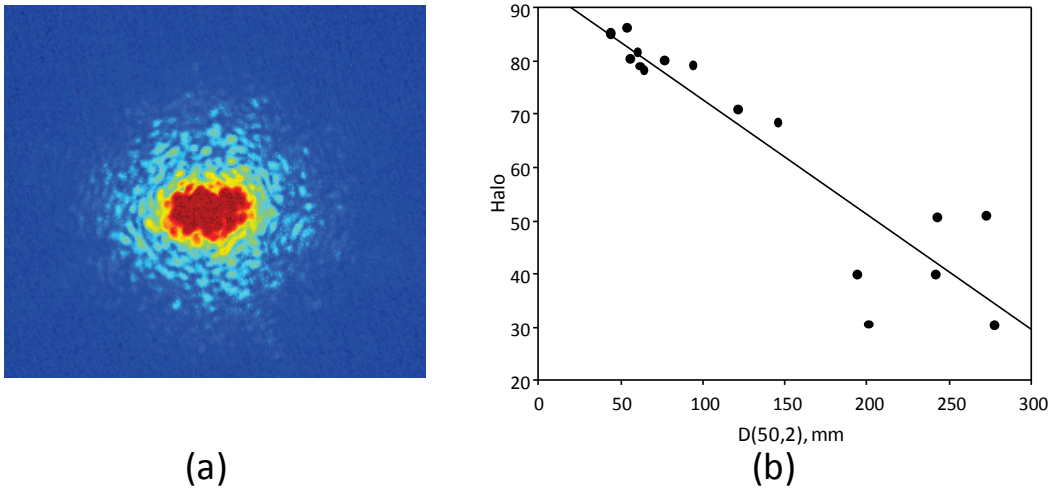

FIGURE 34 ANALYSIS OF FOAM. (A) LARGE AIR BUBBLES CAN BE IN THE HALO, (B) HALO INTENSITY RELATED TO AIR BUBBLE SIZE, MEASURED USING CLSM.

Experiments have shown the relationship to particle size, concentration and refractive index but the method has also been used to predict air bubble size in foam and sensory parameters of drinking yoghurt and stirred yoghurt, Figure 34 presents examples of air bubbles. The method has a large potential in process monitoring, etc. for monitoring particle size changes. Figure 35 shows two examples of process monitoring using SLS. Figure 35a illustrates how rheology and the SLS parameter change during milk acidification. Both SLS and rheology can measure a structure development, but where rheology measures the visco-elastic properties and network formation, SLS measures the particles changing size and formation of the yoghurt network. During the acidification, the viscosity increases to a maximum followed by a slight decrease [Horne, 2003], the SLS method shows a similar but time shifted curve. The SLS values start by decreasing, followed by an increase till a maximum which is reached later than the rheology curve – the initial decrease in SLS value can be related to a slight increase in particle size and the transition to the maximum SLS value for the gelled product. The ability and details obtained with SLS during acidification are very similar to what have been reported with Diffusing Wave Spectroscopy [Pine et al., 1988; Hemar et al., 2004].

Oil cooling and subsequent crystallisation are seen in Figure 35b. In this set-up, the laser illuminates through the side of a glass beaker, placed in a 20°C water bath (100 images per minute). SLS was measured during the cooling of 80°C oil to 20°C. A propeller was used to ensure a homogeneous temperature distribution in the sample and prevent the build-up of an oil crystal layer on the side of the glass beaker. Until crystallisation (10-11,5 minutes), the light scatter increases due to crystals dispersed in the oil phase, see pictures in Figure 36 (time: 5, 7, 9, 11, 13, 15, 17, 19, 21 and 23 minutes). While the oil is liquid, the halo disk is shaped (first 4 pictures in

Figure 36). When the oil crystallises (10-11.5 minutes), the halo decreases in size followed by increased reflection and halo size (11-25 minutes). The halo hot spot shifts location when the oil crystalises, this can be seen as a vertical position shift in Figure 36.

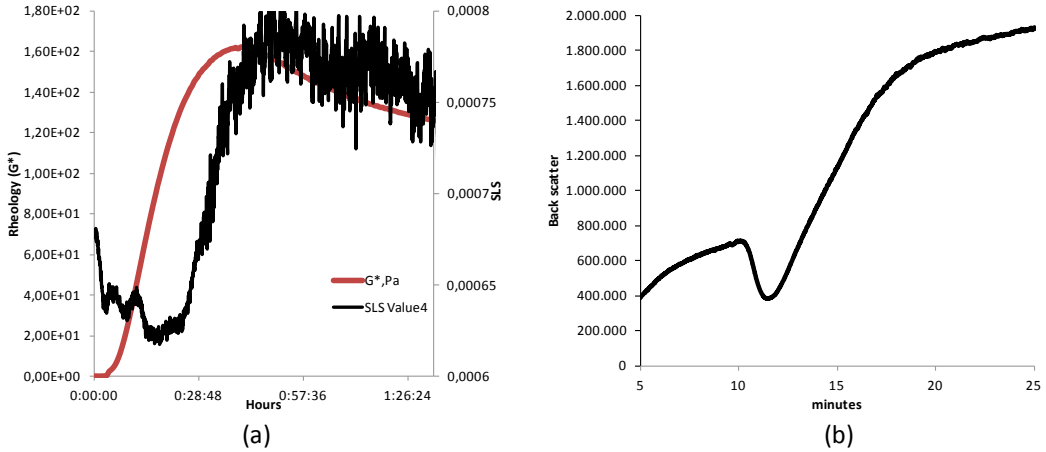

FIGURE 35 EXAMPLES OF PROCESS MONITORING USING SUBSURFACE LASER SCATTERING. (A) MILK ACIDIFICATION FOLLOWED BY RHEOLOGY AND SLS, (B) FAT CRYSTALLISATION (OCCOURING AROUND 10-11½ MINUTES).

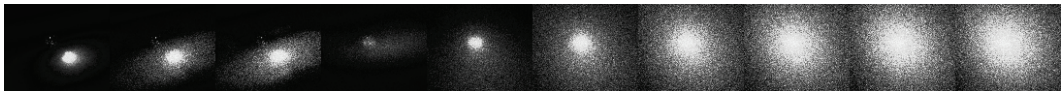

FIGURE 36 RAW IMAGES ACQUIRED DURING THE CRYSTALLISATION OF OIL, DATA SHOWN IN FIGURE 35B. THE IMAGES ARE WITH 2-MINUTE INTERVALS, STARTING AT 5 MINUTES (LEFT IMAGE).

In summary, these results show the great potential of this technique in studying the underlying mechanisms beyond aggregation and structuring of food systems. Currently CIFQ efforts are being made to develop a theoretical platform to quantitatively explain the differences obtained experimentally. The potential in SLS is less in measuring particle sizes as such, but rather in studying dynamic changes in colloidal systems. The potential of the method is two-fold:

- A simple non-invasive system that can measure physical changes multiple places in the production chain (from R&D, online to QC).
- Combined with a NIR or Raman detector could this method give valuable information about which and how food constituents interact and generate food microstructure.

There are, in literature and commercially, other instruments available which also measure light scattering from concentrated suspensions, e.g. Diffusing Wave Spectroscopy [Pine et al., 1988; Mezzenga et al., 2005], Steady Light Transport [Baravian et al., 2005], and Small Angle Light

Scattering [Herle et al., 2005]. They are all single wavelength and are all mainly focused on laboratory work.

CONFOCAL LASER SCANNING MICROSCOPY

Confocal Laser Scanning Microscopy (CLSM) is a technique to image inside the food microstructure with minimal sample preparation [Pawley, 2006]. Different ingredients can be visualized simultaneous by addition of fluorescent dyes. Dyes are readily available to identify protein, fat, and starch granules within the food microstructure. Specific ingredients can be visualized by using specialized antibodies[Arltoft et al., 2007].

The primary value of the CLSM to research, is its ability to produce optical sections and thereby produce either high contrast images inside a food product or by generating three-dimensional images. CLSM images are mostly produced using the point-scanning technique. Most CLSMs work in fluorescent or reflection mode using either filters or spectral detectors. The confocal technique is extended to label-free techniques by the use of other detector types, examples are spontaneous Raman microscopy and coherent anti-stokes Raman (CARS) microscopy [Romero et al., 2011; Yang and Ying, 2011]. Figure 37 is an example of label-free CLSM image made using a Raman detector.

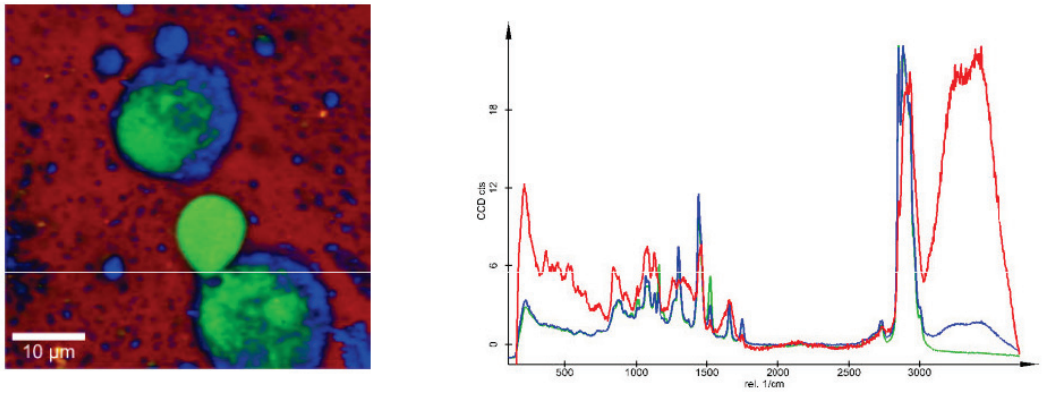

(a) (b)

FIGURE 37 CONFOCAL RAMAN IMAGE OF A DAIRY DESSERT, PROTEIN NETWORK IS RED, FAT IS BLUE AND AIR BUBBLE SURFACE IS GREEN. (A) COMPOSIT IMAGE OF DESSERT, (B) CORRESPONDING RAMAN SPECTRA.

CLSM is often used in food science to visualize and quantify how the microstructure changes as a function of composition, processing, stress and shelf life. The ability to differentiate between different food constituents is an important ability of CLSM, but often the size of the ingredients used is too small to be detected by CLSM, whereas a changed microstructure can be detected, i.e. most enzymes, hydrocolloids and emulsifiers are too small to be detected as individual particles.

Figure 38 is an example of low-fat yoghurt stabilized with pectin at low, medium and recommended pectin concentration. At the magnification applied pectin cannot be seen, but the effect of pectin on the protein network is clearly detectable. Images of the three yoghurts were evaluated using generating a 8-leveled Gaussian pyramid and calculating kurtosis of GLCM at each level, see Figure 38d. Depending upon the magnification, there may be large variations from location to location in food samples. It is common to acquire 5-20 pictures at different locations. It is recommended to calculate the median of resulting feature vectors. The use of the median is advisable since extreme feature values do not have as much influence as they could have in the mean calculation.

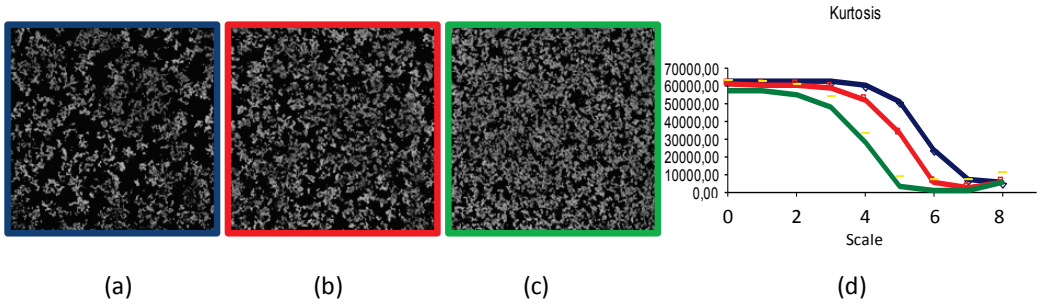

(a) (b) (c) (d)

FIGURE 38 CLSM OF YOGHURT PROTEIN WITH INCREASING AMOUNTS OF PECTIN, AND IMAGE ANALYSIS PERFORMED USING GLCM AS A FUNCTION OF SCALE. (A, B AND C) ARE NO, MEDIUM AND HIGH CONCENTRATION OF PECTIN, (D) KURTOSIS CALCULATED BASED ON GLCM AS A FUNCTION OF GAUSSIAN PYRAMID SCALE; BLUE, RED AND GREEN INDICATE THE PECTIN CONCENTRATION.

VIDEOMETERLAB

This instrument is used in paper IV, [Møller et al., 2013b].

The VideometerLab [Videometer A/S, 2012] acquires multi-spectral images of up to 20 different wavelengths ranging from 375 to 970 nm. The system uses LEDs and an integrating sphere to achieve a uniform and reproducible illumination, resulting in a good spectral and high spatial resolutions plus reproducibility over time. The instrument is NIST calibrated which enables easy conversion to different colour scales or the simulation of different illuminants, i.e. RGB, CieLab, D65 and D50 [Westland and Ripamonti, 2004].

Figure 39a shows a spectral VideometerLab image converted to a colour image. The image clearly illustrates how difficult it can be to measure the size of the yeast colonies. By a combination of wavelength selection and transformation (MNF), it is possible to make a good separation of yeast on yoghurt, see Figure 39b. Figure 39c shows reflectance spectra of yeast and yoghurt.

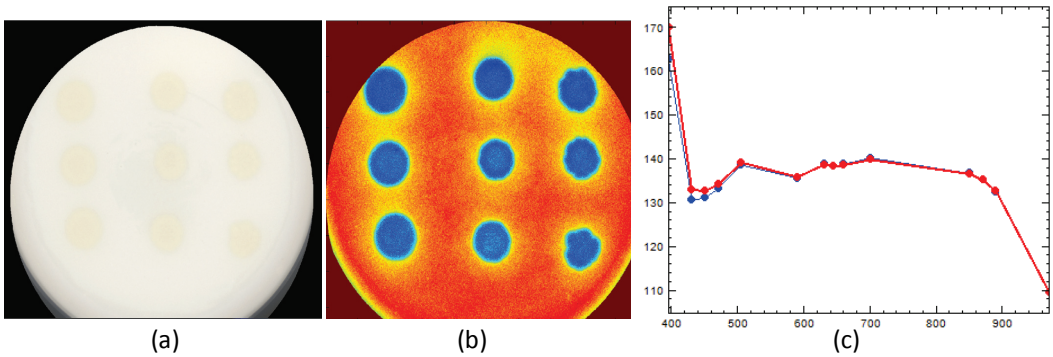

FIGURE 39 IMAGES FOR MEASUREMENT OF YEAST INHIBITION BY YOGHURT AGAR. (A) COLOUR IMAGE OF NINE YEAST SPOTS ON A YOGHURT AGAR, (B) NINE YEAST SPOTS ON YOGHURT VIWED AFTER MNF TRANFORMATION, (C) SPECTRA FROM YEAST (BLUE) AND YOGHURT.

Key quality parameter of a coffee whitener is the whiteness after blending with coffee, this can be measured using the average reflectance spectra, see Figure 40c. More important is the detection of unwanted defects occurring when blending the whitener with hot coffee, defects such as aggregated protein and difficult blending of the two (marbling), see Figure 40a+b. Whiteness of the blend was modelled using PLS, and the aggregation and marbling were quantified using image texture features (autocorrelation and standard deviation measured using a Gaussian Pyramid).

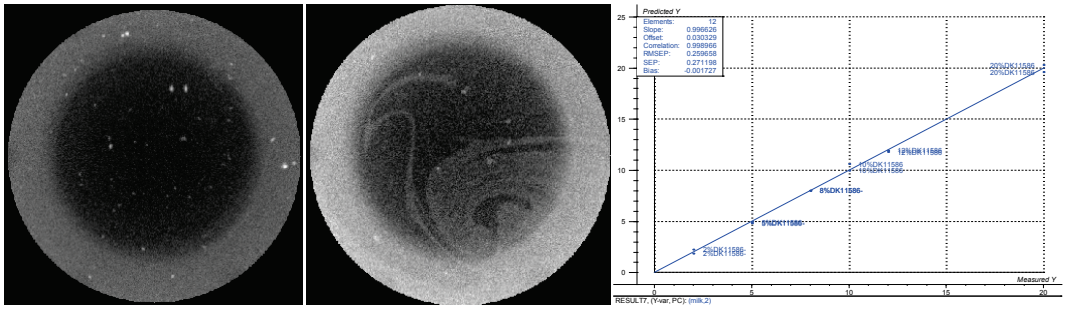

(a) (b) (c)

FIGURE 40 COFFEE WHITENER QUALITY AND DEFECTS. (A) FLOCULATED PROTEIN AGGREGATES, (B) FEATHERING, (C) CALIBRATION CURVE TO PREDICT % COFFEE WHITENER IN COFFEE.

Quantifying colours and relating human perception is a key ability of an instrument like VideometerLab. The conversion of a spectral image of a slice of 20-day-old salami is seen in Figure 41. Figure 41a-c show the conversion to RGB images simulating three different illuminants, D50 (horizon light), D65 (noon daylight) and D75 (north sky daylight)[Westland and Ripamonti, 2004; Videometer A/S, 2012]. Food scientists often like to measure food colours in the CieLab colour space, Figure 41d-f present the same salami image converted to L (luminance:0-100), a (red-green scale) and b (yellow-blue scale). In paper IV a meat colour scale is defined using the nCDA transformation, ranging from fresh to mature salami meat.

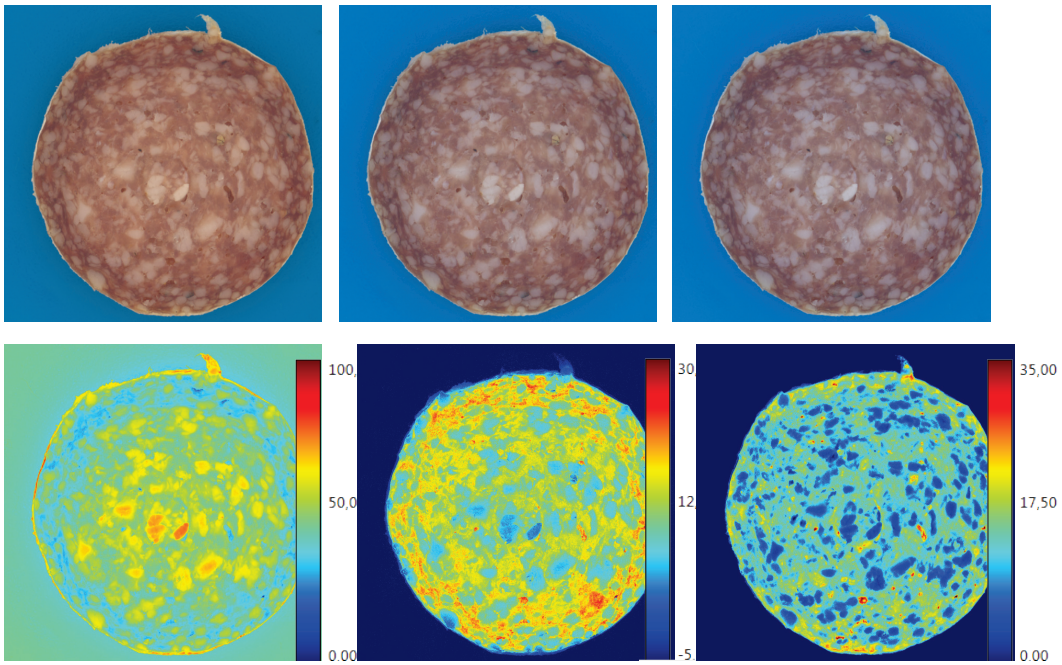

FIGURE 41 EXAMPLES OF CONVERTING A SPECTRAL IMAGE TO OTHER COLOUR SPACES. D50 (A), D65 (B) AND D75 (C), AND IN THE SECOND ROW: CieLab COLOUR SPACE, L (D), a (E) AND b (F).

VIDEOMETERLIQ

This instrument is used in paper II, [Møller, 2012].

This instrument was developed to visualize and quantify physical stability of liquid food samples. The instrument was developed as a natural extension of the VideometerLab work with Coffee Whiteners. And from a need to improve an existing measurement system [Formulaction, 2012]. The VideometerLiq is a downsized VideometerLab that takes time series of multispectral images of liquid products in a flask. The instrument acquires a 10-channelled reflectance image (405-850 nm) and one backlight illuminated image (850 nm). The time series of images are used to quantify physical or chemical stability of liquids, gels or foams. By measuring changes in the bottom or top of the product, it is possible to quantify changes in sediment, whey off or creaming. Physically stable products may change colour due to oxidation or particle size changes; this is typically measurable throughout the height of the flask.

It was a Turbiscan instrument [Formulaction, 2012] that was replaced by the VideometerLiq. The Turbiscan uses a 850 nm laser and measures the amount of backscattered and transmitted light as a function of height and time. The 850 nm is a good choice when a large penetration depth is needed, see Figure 12. For fine product structures and colour changes is the 850 nm not suitable.

Table 2 summarizes which chocolate milk defects that can be measured by humans, Turbiscan and the VideometerLiq instrument. It can be argued that only defects detectable by humans are relevant, but humans have a short memory and small product changes are often an indication of latent product instability. Instability can be detected by Turbiscan and VideometerLiq in days or weeks, instability which is only noticeable after weeks or months of storage [Grotenhuis et al., 2003; Lawless and Heymann, 2010].

TABLE 2 SUMMARY OF DEFECTS OCCURRING IN RECOMBINED MILK AND THE THREE METHODS' ABILITY TO DETECT DEFECTS.

	Human	Turbiscan	VideometerLiq
Layer formation	++	+++	+++
Marbling	+++	---	+++
Gelling	++	---	---
Colour change	+	---	+++
Sedimentation	+++	+++	+++
Stability kinetics	---	+++	+++

SURFACESCAN

This instrument is used in paper III, [Møller et al., 2013a].

This instrument was developed to visualise and quantify light reflection from food surfaces, e.g. how shiny and grainy a yoghurt appears. In literature, there was no method for the measurement of specular food gloss, but only methods for surface homogeneity and graininess, measured with diffuse light and after dilution, respectably [Johansen et al., 2008; Kücükcetin, 2008].

The SurfaceScan [Videometer A/S, 2012] uses a ringlight with six Brightfield LEDs. An image of a shinny product will have six shinny points, a mirror image of the six LEDs. In the centre of the six Brightfield hot spots, the specular reflection (gloss) can be measured. Away from the six specular spot, surface roughness (grains) can be measured. Paper III explains how the LED reflection points are found and quantified, and how the texture of the image is measured. Figure 42 shows six examples of reflection images; three shiny but still very different and three images of grainy or dull surfaces.

The instrument is a result of experiments with different light geometries, sample preparation methods and simulations of how humans evaluate food gloss [Baudet et al., 2012]. By building a dedicated instrument, it is possible to compare different formulations and compare samples when available.

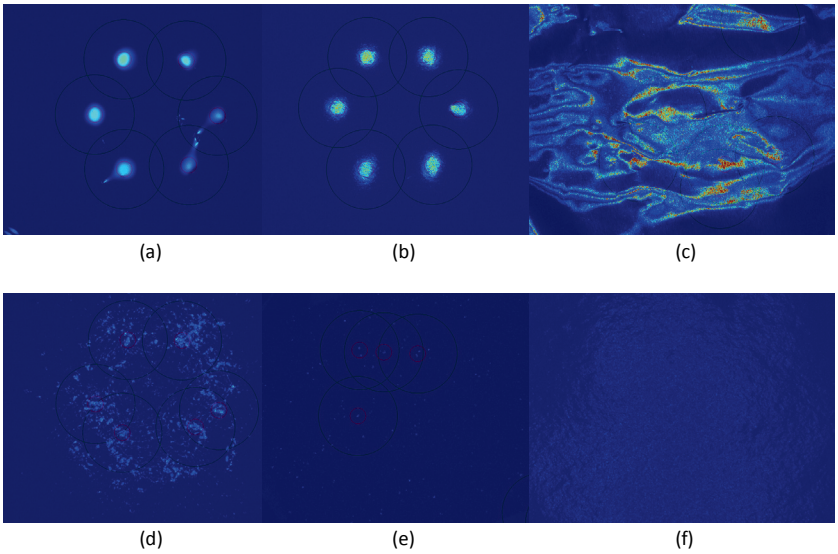

FIGURE 42 EXAMPLES FOR SURFACESCAN REFLECTION IMAGES. (A-C) SHINY SURFACES, MILK, YOGHURT AND METAL FOIL, (D) GRAINY YOGHURT, (E) DULL CHOCOLATE FOAM AND (F) A DULL AND SMOOTH YOGHURT SURFACE.

SISUCHEMA

This instrument is used in paper I, [Møller et al., 2010].

SisuCHEMA is a line-scanning system (pushbroom), it has a spectral range from 1000-2500 nm and a 320 pixel field of view[Specim Ltd, 2012]. The pixel size is between 30 and 600 µm and the instrument can acquire up to 100 lines per second. The instrument uses a diffuse light source and prism-grating-prism spectrograph [Sun, 2010].

The advantage of line-scanning instruments is the high number of wavelengths combined with speed. The line-scanning makes them easy to implement at conveyer belts. Main drawbacks could be price, low number of pixels and noise. Line-scanning instruments inherently have a problem with saturated pixels/absorption, i.e. the spectral resolution is low at the water *absorptions* peeks.

Series of white bread was followed throughout the shelf life while water content was measured concurrently. Figure 43a+b show a typical SisuCHEMA image of white bread, Figure 43c shows selected spectra extracted from the two pieces of white bread. Based on the analytically measured water, pixel-wise predictions of water in bread were made, seen in Figure 43d [Møller et al., 2010; Liu and Møller, 2011]. Figure 43e show a histogram of the predicted water concentrations - for fresh bread a bi-polar distribution is found(dry crust and humid centre) and after 11 days, the water was homogeneously distributed in the slice of bread. The total water content remains constant throughout the evaluation period, only the spatial distribution of the water changes.

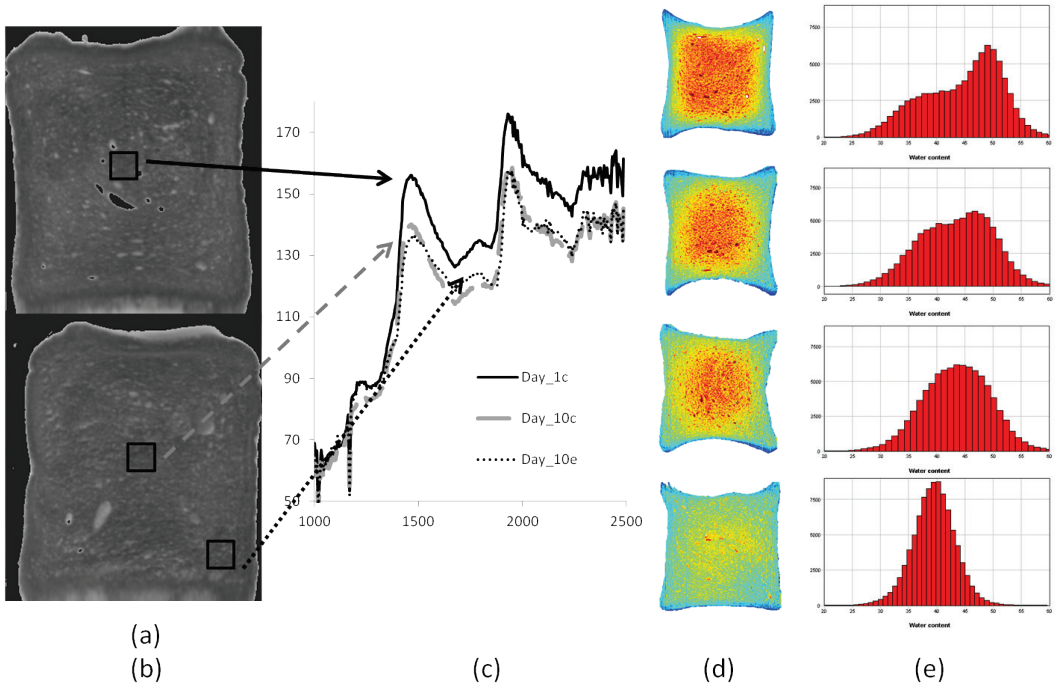

FIGURE 43 HYPERSPECTRAL IMAGES OF WHITE BREAD. (A) DAY 1 BREAD (1300 NM), (B) DAY 11 BREAD (1300 NM), (C) MEAN SPECTRA FROM CENTER OF DAYS 1+11 AND EDGE DAY 10, (D) PREDICTED WATER CONTENT, TOP-TO-BOTTOM: DAYS 1, 4, 7 AND 11, (E) HISTOGRAM OF WATER DISTRUBUTION OF BREAD ON DAYS 1, 4, 7 AND 11.

CONCLUSION & DISCUSSION

Imaging and especially spectral imaging is a complex, multidisciplinary field that may involve simultaneous acquisition of images in several light or spectral bands. Imaging is a very potent technique for characterising and analysing biological and food samples. The motivation behind the development of imaging systems in food is the desire for gaining information fast and non-destructively, for identification and visualisation of objects spatial distribution.

In paper I, a water prediction model was built before applying to different bread. The model was used to provide information about how the spatial distribution of water changed throughout storage. Paper II analyses chocolate milks with known differences of stability. Paper III measured different types of light reflection from yoghurt surfaces and correlated the data to sensory data. Paper IV segmented meat and fat in dry fermented sausages and applied a new meat colour scale.

The combined learning in papers I-IV is that imaging food quality is a multidisciplinary task. When setting up a new method, it is recommended to start in an explorative manner where a few selected samples are tested. These initial tests focus on sample handling and how to present the sample to an imaging set-up. An important part of setting up an imaging method is to find the best light geometry, wavelengths, magnification, and camera etc. In this explorative phase, focus is on finding a robust set-up which can discriminate between the samples selected.

Relevant samples are selected for the rest of the model building. A range of samples is selected which are representative of *all* the qualities that are relevant to measure in the future – not too extreme, but representative! If possible, there should be enough samples for cross-validation of the image analysis and predictive model.

The best advice for defining the steps involved in the image analysis is to combine several smaller models. A small model can apply special filtering or spectral pre-processing before separating two classes (foreground and background). Especially the supervised transformations are well-suited for building small models, e.g. nCDA which is easy to threshold, since classes are centred on zero. Combining several small models can make very advanced segmentations. Based on the combined models, it may be relevant to measure object size, mean spectra or texture etc. This multi-model approach was used in papers III and IV.

It is advisable for prediction of food quality to evaluate both linear and non linear models, two examples are partial least squares and regression trees. Variable selection and data pre-treatment can greatly improve predictability and model interpretability. In paper I, SNV pre-treatment was used to remove the shadow in the bread crumb, in paper III, variable selection was used to

improve the model and in paper IV, a spectral normalisation was applied to facilitate meat/fat segmentation.

An important part of predicting food quality using images is result visualisation. In papers I and IV, the predictive models were applied to spectral images which gave the food scientist a good visual tool for understanding the evaluated ingredient or process effects. In paper II, the results were either a new image or a curve. The barcode images in paper II gave the food scientist a fast visual tool for evaluation multiple types of food quality. In paper III, the raw images mainly served as documentation of the analytical data.

It has been seen that the imaging has a unique ability of capturing morphological and chemical information of food. Effective use of imaging systems requires an understanding of the nature and limitations of the data and of various strategies for processing and interpretation with the large amounts of data available. The application benefits with working with 2D spectral image instead of a 1D spectrum are almost without limit in monitoring, control, inspection, quantification, classification, and identification purposes. The fast development of new, better, faster and cheaper spectral imaging techniques can only be expected to continue, this means new possibilities and significant challenges to everyone working with food science, instrument development and data handling.

BIBLIOGRAPHY

Abbott JA (1999). Quality measurement of fruits and vegetables. *Postharvest Biology and Technology* 15: 207-225.

Abdullah MZ, Guan LC, Lim KC, Karim AA (2004). The applications of computer vision system and tomographic radar imaging for assessing physical properties of food. *Journal of Food Engineering* 61: 125-135.

Arltoft D, Madsen F, Ipsen R (2007). Screening of probes for specific localisation of polysaccharides. *Food Hydrocolloids* 21: 1062-1071.

Baravian C, Caton F, Dillet J, Mougel J (2005). Steady light transport under flow: Characterization of evolving dense random media. *Physical Review E* 71: 066603.

Barnes HA (1999). The yield stress—a review or 'παντα ρει'—everything flows? *Journal of Non-Newtonian Fluid Mechanics* 81: 133-178.

Baudet N, Maire JL, Pillet M (2012). The visual inspection of product surfaces. *Food Quality and Preference*.

Becker JS, Salber D (2010). New mass spectrometric tools in brain research. *TrAC Trends in Analytical Chemistry* 29: 966-979.

Bjerke F, Langsrud Ø, Aastveit AH (2008). Restricted randomization and multiple responses in industrial experiments. *Quality and Reliability Engineering International* 24: 167-181.

Boschetto A, Giordano V (2012). Powder sampling and characterization by digital image analysis. *Measurement*.

Bourriot S, Garnier C, Doublier JL (1999). Micellar-casein–κ-carrageenan mixtures. I. Phase separation and ultrastructure. *Carbohydrate polymers* 40: 145-157.

Breiman L (2001). Random forests. *Machine learning* 45: 5-32.

Breiman L, Friedman J, Stone CJ, Olshen RA (1984). *Classification and regression trees*, Chapman & Hall/CRC.

Brunsø K, Fjord TA, Grunert KG (2002). *Consumers' food choice and quality perception*, Aarhus School of Business, MAPP-Centre for Research on Customer Relations in the Food Sector.

Caballero PA, Gómez M, Rosell CM (2007). Improvement of dough rheology, bread quality and bread shelf-life by enzymes combination. *Journal of Food Engineering* 81: 42-53.

Carstensen JM (2011). Multispectral imaging with videometerlab. p 17. (c) Videometer A/S.

Carstensen JM, Møller F (2009). Online monitoring of food processes using subsurface laser scattering. *Advances in process analytics and control technologies APACT*: 5-7.

Christiansen AN, Nielsen AA, Møller F, Carstensen JM (2012). Monitoring the change in colour of meat: A comparison of traditional and kernelbased orthogonal transformations. *Journal of spectral Imaging* 3: 11.

Danisco A/S (2011). Chocolate milk. In *Technical Memorandum*. Danisco A/S.

de Macedo REF, Pflanzer SB, Gomes CL (2012). Probiotic meat products. In *Probiotic in animals* (Rigobelo EC ed.), p 272. InTech.

Famelart MH, Tomazewski J, Piot M, Pezennec S (2004). Comprehensive study of acid gelation of heated milk with model protein systems. *International Dairy Journal* 14: 313-321.

Feiner G (2006). Meat products handbook. *Practical Science*.

Folm-Hansen J (1999). On chromatic and geometrical calibration. In *IMM*, p 258. DTU.

Formulaction (2012). Www.Formulaction.Com. Web page.
Franc V, Hlavác V (2004). Statistical pattern recognition toolbox for matlab. *Prague, Czech: Center for Machine Perception, Czech Technical University*.
Gan Z, Ellis P, Schofield J (1995). Gas cell stabilisation and gas retention in wheat bread dough. *Journal of Cereal Science* 21: 215-230.
Geladi P, Grahn H (1996). *Multivariate image analysis*, Wiley Chichester, UK.
Geladi P, Kowalski BR (1986). Partial least-squares regression: A tutorial. *Analytica Chimica Acta* 185: 1-17.
Gonzalez RC, Woods RE, Eddins SL (2004). *Digital image processing using matlab*. Upper Saddle River, NJ, Pearson/Prentice Hall.
Grahn H, Geladi P (2007). *Techniques and applications of hyperspectral image analysis*, Wiley.
Gray J, Bemiller J (2006). Bread staling: Molecular basis and control. *Comprehensive reviews in food science and food safety* 2: 1-21.
Green AA, Berman M, Switzer P, Craig MD (1988). A transformation for ordering multispectral data in terms of image quality with implications for noise removal. *Geoscience and Remote Sensing, IEEE Transactions on* 26: 65-74.
Grotenhuis Et, Tuinier R, de Kruif CG (2003). Phase stability of concentrated dairy products. *Journal of dairy science* 86: 764-769.
Grunert KG, Bech-Larsen T, Bredahl L (2000). Three issues in consumer quality perception and acceptance of dairy products. *International Dairy Journal* 10: 575-584.
Grunert KG, Bredahl L, Brunsø K (2004). Consumer perception of meat quality and implications for product development in the meat sector—a review. *Meat science* 66: 259-272.
Guang Z, Maclean AL (2000). A comparison of canonical discriminant analysis and principal component analysis for spectral transformation. *PE&RS, Photogrammetric Engineering & Remote Sensing* 66: 841-847.
Gunasekaran S (1996). Computer vision technology for food quality assurance. *Trends in Food Science & Technology* 7: 245-256.
Haralick RM, Shanmugam K, Dinstein IH (1973). Textural features for image classification. *Systems, Man and Cybernetics, IEEE Transactions on*: 610-621.
Hastie T, Tibshirani R, Friedman JH (2009). *The elements of statistical learning : Data mining, inference, and prediction*. New York, NY, Springer.
Heertje I, Visser J, Smits P (1985). Structure formation in acid milk gels. *Food microstructure* 4: 10.
Hemar Y, Singh H, Horne D (2004). Determination of early stages of rennet-induced aggregation of casein micelles by diffusing wave spectroscopy and rheological measurements. *Current Applied Physics* 4: 362-365.
Herle V, Fischer P, Windhab EJ (2005). Stress driven shear bands and the effect of confinement on their structures a rheological, flow visualization, and rheo-sals study. *Langmuir* 21: 9051-9057.
Horne DS (2003). Casein micelles as hard spheres: Limitations of the model in acidified gel formation. *Colloids and Surfaces A: Physicochemical and Engineering Aspects* 213: 255-263.
IEEE Computer Society. (1990). Ieee standard glossary of image processing and pattern recognition terminology. Institute of Electrical and Electronic Engineers, Incorporated.
Jahr I (2007). Lighting in machine vision. *Handbook of Machine Vision*: 73-203.

Jensen HW, Marschner SR, Levoy M, Hanrahan P (2001). A practical model for subsurface light transport. In *Proceedings of the 28th annual conference on Computer graphics and interactive techniques*, pp 511-518. ACM.

Johansen SMB, Laugesen JL, Janhøj T, Ipsen R, Frøst MB (2008). Prediction of sensory properties of low-fat yoghurt and cream cheese from surface images. *Food Quality and Preference* 19: 232-246.

Koenderink JJ (1984). The structure of images. *Biological cybernetics* 50: 363-370.

Kohajdová Z, Karovičová J, Schmidt Š (2009). Significance of emulsifiers and hydrocolloids in bakery industry. *Acta Chimica Slovaca* 2: 46-61.

Kohavi R (1995). A study of cross-validation and bootstrap for accuracy estimation and model selection. In *International joint Conference on artificial intelligence*, pp 1137-1145. Lawrence Erlbaum Associates Ltd.

Kücükcetin A (2008). Effect of heat treatment and casein to whey protein ratio of skim milk on graininess and roughness of stirred yoghurt. *Food Research International* 41: 165-171.

Langendorff V, Cuvelier G, Launay B, Parker A (1997). Gelation and flocculation of casein micelle/carrageenan mixtures. *Food Hydrocolloids* 11: 35-40.

Langsrud Ø (2002). 50–50 multivariate analysis of variance for collinear responses. *Journal of the Royal Statistical Society: Series D (The Statistician)* 51: 305-317.

Lassoued N, Babin P, Della Valle G, Devaux MF, Réguerre AL (2007). Granulometry of bread crumb grain: Contributions of 2d and 3d image analysis at different scale. *Food Research International* 40: 1087-1097.

Lawless HT, Heymann H (2010). *Sensory evaluation of food: Principles and practices*, Springer.

LEE SC, Bajcsy P (2006). Intensity correction of fluorescent confocal laser scanning microscope images by mean‐weight filtering. *Journal of microscopy* 221: 122-136.

Lindeberg T (1994). Scale-space theory: A basic tool for analyzing structures at different scales. *Journal of applied statistics* 21: 225-270.

Liu Z, Møller F (2011). Bread water content measurement based on hyperspectral imaging. Scandinavian Workshop on Imaging Food Quality 2011, Ystad, May 27, part of.

Mancini R, Hunt MC (2005). Current research in meat color. *Meat science* 71: 100-121.

Marianski S, Mariański A (2009). *The art of making fermented sausages*, Bookmagic Llc.

Martens H, Martens M (2001). Multivariate analysis of quality. An introduction. *Measurement Science and Technology* 12: 1746.

Martin D (2011). Product sourcebook - led lightning & eletronics. (Illumination A, ed.). www.advancedillumination.com, Advanced Illumination.

McMahon DJ, Du H, McManus WR, Larsen KM (2009). Microstructural changes in casein supramolecules during acidification of skim milk. *Journal of dairy science* 92: 5854-5867.

Mezzenga R, Schurtenberger P, Burbidge A, Michel M (2005). Understanding foods as soft materials. *Nature materials* 4: 729-740.

Miller CE (2005). Chemometrics in process analytical chemistry. *Process Analytical Technology. Blackwell publishing, Oxford*: 226-227.

Mondal A, Datta AK (2008). Bread baking – a review. *Journal of Food Engineering* 86: 465-474.

Møller F (2006). Analysing a food sample by the use of light scattering. In *UK patent application* (Danisco A/S, ed.), p 52. Denmark.

Møller F (2012). Barcode technique to visualize and quantify chocolate milk stability. *Journal of Imaging Science and Technology* 56: 020402.

Møller F, Kragh H, Lugand D, Carstensen JM (2013a). Measuring light reflection from yoghurt surfaces: Glossiness, graininess and dullness of yoghurt. *Food Hydrocolloids* submitted.

Møller F, Nilsson D, Lindström SW (2010). *Visualization of water distribution in bread by nir imaging*. Bangkok.

Møller F, Voggel C, Carstensen JM (2013b). Spectral imaging for monitoring structure and colour development of dry fermented sausages. *Journal of meat Science* submitted.

Nanke K, Sebranek J, Olson D (2006). Color characteristics of irradiated vacuum ‐ packaged pork, beef, and turkey. *Journal of Food Science* 63: 1001-1006.

Nicolai T, McClements D (2007). Food characterisation using scattering methods. *Understanding and controlling the microstructure of complex foods*: 288-310.

Nielsen AA (1999). Orthogonal transformations. In *Available at* www.imm.dtu.dk/~aa, p 13.

Norgaard L, Saudland A, Wagner J, Nielsen JP, Munck L, Engelsen S (2000). Interval partial least-squares regression (ipls): A comparative chemometric study with an example from near-infrared spectroscopy. *Applied Spectroscopy* 54: 413-419.

Ordóñez JA, Hierro EM, Bruna JM, Hoz Ldl (1999). Changes in the components of dry-fermented sausages during ripening. *Critical reviews in food science and nutrition* 39: 329-367.

Pawley J (2006). *Handbook of biological confocal microscopy*, Springer.

Pine D, Weitz D, Chaikin P, Herbolzheimer E (1988). Diffusing wave spectroscopy. *Physical Review Letters* 60: 1134-1137.

Rami-shojaei S, Vachier C, Schmitt C (2009). Automatic analysis of 2d foam sequences: Application to the characterization of aqueous proteins foams stability. *Image and Vision Computing* 27: 609-622.

Randen T, Husoy JH (1999). Filtering for texture classification: A comparative study. *Pattern Analysis and Machine Intelligence, IEEE Transactions on* 21: 291-310.

Rico D, Martin-Diana AB, Barat J, Barry-Ryan C (2007). Extending and measuring the quality of fresh-cut fruit and vegetables: A review. *Trends in Food Science & Technology* 18: 373-386.

Rinnan Å, Berg F, Engelsen SB (2009). Review of the most common pre-processing techniques for near-infrared spectra. *TrAC Trends in Analytical Chemistry* 28: 1201-1222.

Romero G, Rojas E, Estrela-Lopis I, Donath E, Moya SE (2011). Spontaneous confocal raman microscopy--a tool to study the uptake of nanoparticles and carbon nanotubes into cells. *Nanoscale research letters* 6: 1-4.

Saleh B (2011). *Introduction to subsurface imaging*, Cambridge University Press.

Schulerud H, Danielsen H, Carstensen J (1995). Multiresolution texture analysis of four classes of mice liver cells using different cell cluster representations. In *PROCEEDINGS OF THE SCANDINAVIAN CONFERENCE ON IMAGE ANALYSIS*, pp 121-130. Citeseer.

Shewfelt R (1999). What is quality? *Postharvest Biology and Technology* 15: 197-200.

Siqueira F. R. de , Schwartz W. R. , H. P (2013). Multi-scale gray level co-occurrence matrices for texture description. *Neurocomputing*.

Snoeren THM (1976). Kappa-carrageenan: A study on its physico-chemical properties, sol-gel transition and interaction with milk proteins. H. Veenman and Zonen BV.

Sodini I, Remeuf F, Haddad S, Corrieu G (2004). The relative effect of milk base, starter, and process on yogurt texture: A review. *Critical reviews in food science and nutrition* 44: 113-137.

Specim Ltd (2012). Www.Specim.Fi.

Stampfli L, Nersten B (1995). Emulsifiers in bread making. *Food Chemistry* 52: 353-360.
Steenkamp JBEM (1990). Conceptual model of the quality perception process. *Journal of Business Research* 21: 309-333.
Sun DW (2010). *Hyperspectral imaging for food quality analysis and control*, Academic Press.
Switzer P, Green AA (1984). Min/max autocorrelation factors for multivariate spatial imagery. *Computer Science and Statistics: The Interface (L. Billard, Ed.)*: 16.
Tajima R, Kato Y (2011). Comparison of threshold algorithms for automatic image processing of rice roots using freeware imagej. *Field Crops Research* 121: 460-463.
Tamime AY, Robinson RK (1999). *Yoghurt: Science and technology*, Woodhead Publishing.
Van Den Boomgaard TH, Van Vliet T, Van Hooydonk ACM (1987). Physical stability of chocolate milk. *International Journal of Food Science & Technology* 22: 279-291.
Vandendriessche F (2008). Meat products in the past, today and in the future. *Meat science* 78: 104-113.
Varela P, Fiszman SM (2013). Exploring consumers' knowledge and perceptions of hydrocolloids used as food additives and ingredients. *Food Hydrocolloids* 30: 477-484.
Videometer A/S (2012). Www.Videometer.Com. pp Hørsholm, Denmark.
Viljoen BC (2001). The interaction between yeasts and bacteria in dairy environments. *International journal of food microbiology* 69: 37-44.
Vincent L (1993). Morphological grayscale reconstruction in image analysis: Applications and efficient algorithms. *Image Processing, IEEE Transactions on* 2: 176-201.
Walstra P, Jenness R (1984). *Dairy chemistry & physics*, John Wiley & Sons.
Westland S, Ripamonti C (2004). *Computational colour science using matlab*. Hoboken, NJ, J. Wiley.
Wold S, Esbensen K, Geladi P (1987). Principal component analysis. *Chemometrics and Intelligent Laboratory Systems* 2: 37-52.
Yang D, Ying Y (2011). Applications of raman spectroscopy in agricultural products and food analysis: A review. *Applied Spectroscopy Reviews* 46: 539-560.

Paper I

Møller, F., D. Nilsson, and S.W. Lindström, **Visualization of water distribution in bread by NIR imaging**. Near Infrared Spectroscopy: proceedings NIR-2009 14th International conference, ed. S.K. S.Saranwong, W.Thanapase, P.Williams 2010, Bangkok.

Visualisation of water distribution in bread by near infrared imaging

F. Moller,[a] D. Nilsson[b] and S. W. Lindstrom[b,c]

[a]*Danisco A/S, Edwin Rahrs Vej 38, 8220 Brabrand,Denmark*
[b]*UmBio AB, Tvistevägen 47, 907 19 Umeå, Sweden*
[c]*Umeå University, Energy Technology and Thermal Process Chemistry, SE-901 87 Umeå, Sweden*

Introduction

Objective and goal

Bread is probably one of the oldest prepared food types, dating back to the Neolithic era. Bread is prepared by baking or cooking a dough based on flour, water, yeast, salt, sugar, and other ingredients like. Fresh bread is valued for its taste, aroma, and texture. Bread that has stiffened or dried past its prime is said to be stale.

Ensuring and keeping bread fresh is important for both consumers and bread manufacturers. Preventing the bread from drying out and maintaining a uniform water distribution is important for bread to be perceived as being fresh. The bread composition, production process and storage conditions all play an important role in keeping bread fresh.

Traditional single point NIR techniques are commonly used to determine a variety of food properties. Sørensen[1] successfully used NIR to analyse bread, and predicted the content of protein, fat, dietary fibre, sugar, ash, saturated fatty acids, mono-unsaturated fatty acids, poly-unsaturated fatty acids and Na. There are numerous aspects of food and ingredient properties that result from heterogeneity in composition. Understanding and monitoring food ingredients, as well as final food properties, is of considerable importance for quality assurance within the food industry. If food ingredients are of an unacceptable quality or if contaminants are by accident added to the food, they could result in unforeseen consequences. Enormous amounts of food, already delivered to the distributor would be rejected, not to mention the bad reputation that the manufacturer would get with this type of accident. This is a consequence that the manufacturer cannot afford.

Hyperspectral NIR imaging is a state-of-the-art technique, as it has the potential to determine the spectral as well as the spatial information in the sample. By monitoring characteristic spectral features or by applying a calibration model to a spectral image, it is possible to generate a prediction image, visualising a specific spatial distribution e.g. the moisture distribution in bread.[2] In addition to the amount of information that can be extracted from the hyperspectral image, some other benefits compared to traditional single point NIR spectroscopy, should be mentioned. The hyperspectral imaging technique requires significantly less sample preparation and is likely to detect small material and chemical changes, which are a result of the spatial information plus non-invasive sample preparation.

The objective of this study was to investigate the possibility of developing a NIR imaging calibration model, suitable for monitoring the water distribution in different types of bread. A robust method would be of great importance for the research and development of commercially produced breads.

Materials and Methods

Sample preparation

Three types of bread were used in this study, two toasts (Toast 1 and Toast 2) and one free-standing bread (Kohberg trianon hvedetoast, toast made at Danisco and Schulstad Bondebrod). For each bread type, 3 or 4 replicates (loaves) were used in the study. Samples were collected over a period of 11 days including days 1, 4, 7 and 11, after the bread was baked. The sampling started on day one with slices collected from the middle of the loaf. Each slice was analysed with the spectral camera and then for the calibration model, the center and a near crust piece were cut from the bread. The cuts were analysed with the spectral camera, and water content determined by weight and oven drying, for 3 hours at 105°C. The water content was calculated as percentage of the total wet weight. In total 151 bread slices were measured over 11 days.

Hyperspectral imaging

The SisuChema workstation (Specim Imaging Ltd AB, Oulu, Finland) ranging from 1000-2500 nm, was used for NIR imaging measurements. Each measurement was performed using 1.7 ms exposure time, 31 mm lens and 100 mm field of view.

Data pre-treatment

Each NIR image (sample) is comprised of a three-dimensional data matrix, where each pixel is one spectrum. This matrix is referred to as $\mathbf{X}_{3D}$. The background exclusion was performed in the software Evince Image 2.3.9 (UmBio AB, Umeå, Sweden) using PCA to separate bread signals from background noise. The noise exclusion is done per sample, using no scaling or centering of the data. According to the background noise exclusion, the $\mathbf{X}_{3D}$ data were averaged in Matlab, creating a vector for each sample. All samples were put into one matrix, $\mathbf{X}$[N,K].

Table 1. Water variation of the different bread types and for the combined dataset, *n* = number of bread slices.

	N	Min	Max	Mean	*STDEV*
Free standing bread	64	41.8	48.1	45.0	1.7
Toast 1	46	35.3	44.4	39.5	2.6
Toast 2	41	37.8	48.9	43.5	3.9
All breads	151	35.3	48.9	42.9	3.6

Table 2. Model overview. Four models shown, three bread types and one global model combining data from the three bread types. Number of samples in models (n), number of loaves in test set (test set), number of slices in test set (test sets size), number of principal components in the model (PLS terms), average cross-validate explained variance (total Q2Y) and average root mean squared error of prediction (*RMSEP*).

	N	Test sets	Test set size	PLS terms	Total Q2Y	*RMSEP*
Free standing bread	48	4	16	4	0.82	0.72
Toast 1	30–31	3	15–16	4	0.86	0.87
Toast 2	25–29	3	12–16	4	0.98	0.69
All breads	104–107	3	44–47	4	0.94	0.87

Models

The **X**[N,K] data was evaluated for outliers by using PCA for each type of bread. Prior to PLS regression, the data matrix, **X**[N,K], was transformed and scaled using SNV (row-wise) and

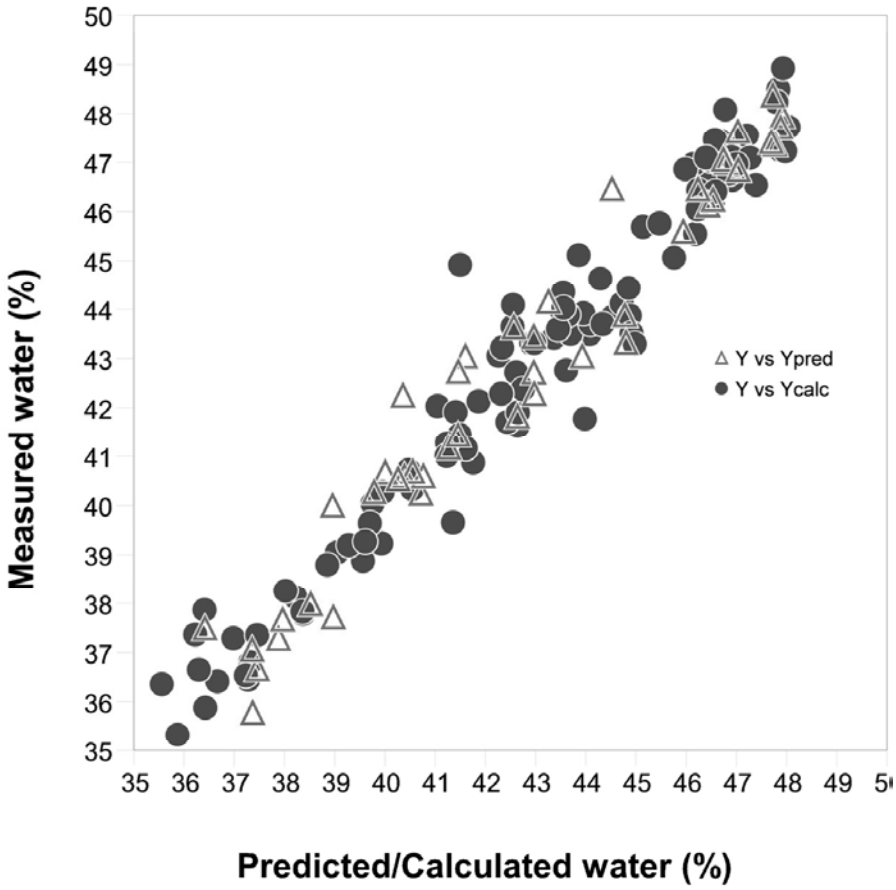

Figure 1. All 3 bread types used for modelling water content. Measured water content (%) vs. model calculated and predicted from test set.

centering (column-wise)[3–5]. PLS Models were built in the software Evince Image between the **X**[N,K] matrix and the moisture vector Y.

Results and discussion

Calibration development

Calibration by PLS regression was performed using center and near-crust cuts from the three bread types. A global model was developed combining data from all three bread types. The number of bread slices analysed and water variation of the sample sets are listed in table 1.

Individual models were made, one for each bread type and one global model containing all of the breads. Several calibration models were made for each bread type (one for each loaf). In each of these models one loaf (in turn) was excluded from the data and used as an external test set. For the global model one loaf of each bread type was used as a test set. Model validation was performed by calculating the root mean square error of predictions, RMSEP, for each model using

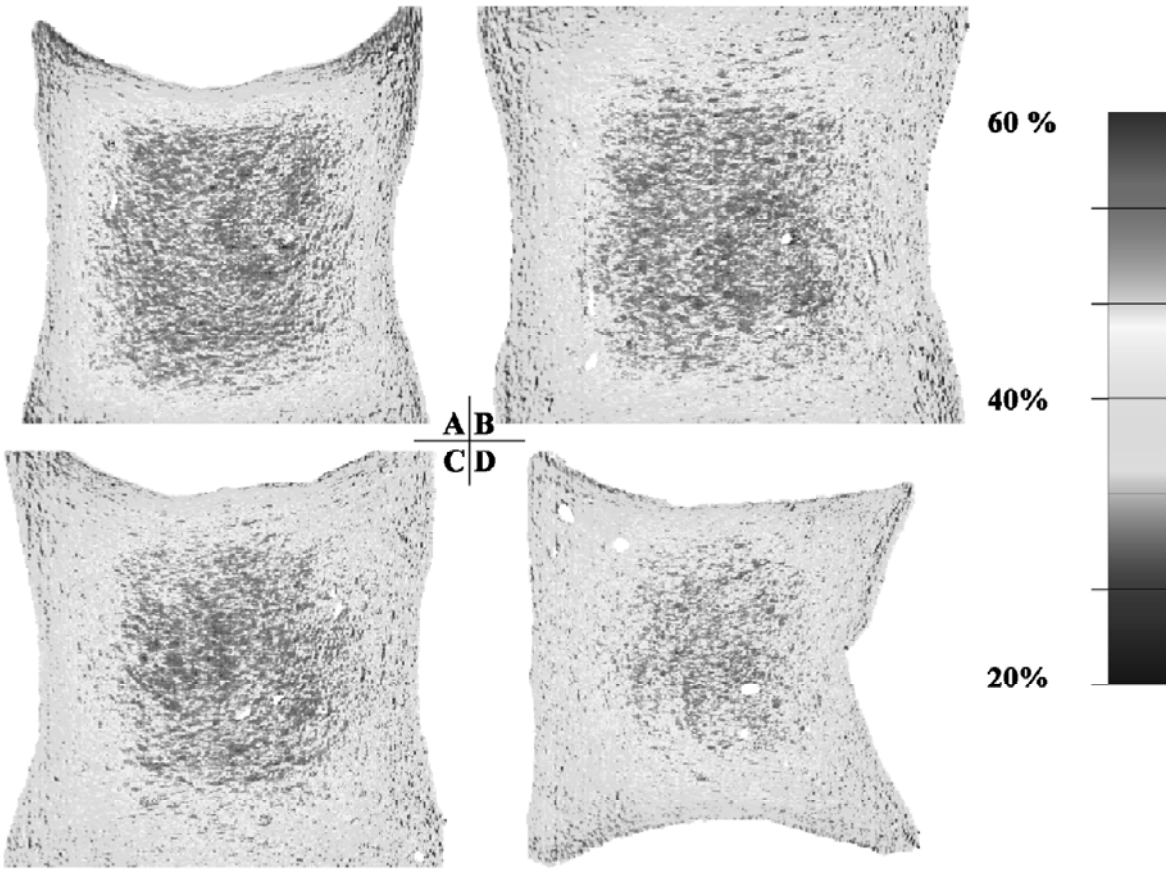

Figure 2. Predictions of water content and distribution in four slices of toast (Toast 2) as a function of storage time, day 1 (A), day 4 (B), day 7 (C) and day 11 (D).

the external test set[5]. Table 2 summarises the different models developed. Figure 1 shows the measured water content versus the calculated and test set predicted water content.

Spatial distribution of water in bread

By using the calibration model, water could be predicted in each pixel in the spectral image, thereby showing the spatial distribution of water in bread. Figure 2 shows how the global All bread model has been used to predict water in Toast bread.

The four different images in Figure 2 represent different ages of the toast bread (1, 4, 7 and 11 days). It is noticeable that fresh toast has both the lowest and highest water concentrations at the crust and centre of the slice. The water becomes more homogeneously distributed as the bread is stored.

Conclusion

This study demonstrated that it is possible to use hyperspectral NIR images to predict the water content in bread without any sample preparation, i.e. on whole slices of bread. The study also demonstrates that calculation of a calibration model can be used to visualise the spatial distribution of water in bread. This type of hyperspectral imaging application can easily be used in routine analysis in research and development of bread. The method can easily be extended to other ingredients in bread and thus become an even more valuable tool in bread research.

References

1. L.K. Sørensen, *Food Chem.* **113,** 1318 (2009).
2. F.H. Grahn and P. Geladi, *Techniques and Applications of Hyperspectral Image Analysis*, John Wiley & Sons Ltd, Chichester, UK (2007).
3. R.J. Barnes, M.S., Dhanoa and S.J. Lister. *Appl. Spectrosc*. **43,** 772 (1989).
4. P. Geladi and B. Kowalski, *Anal. Chim. Acta* **185,** 1 (1986).
5. Wiklund, D. Nilsson, L. Eriksson, M. Sjöström, S. Wold and K. Faber, *J. Chemometr.* **21,** 427 (2007).

Paper II

Møller, F., **Barcode Technique to Visualize and Quantify Chocolate Milk Stability.** Journal of Imaging Science and Technology, 2012. 56: p. 020402.

Journal of Imaging Science and Technology® 56(2): 020402-1–020402-6, 2012.

Barcode Technique to Visualize and Quantify Chocolate Milk Stability

Flemming Møller
DuPont Nutrition Biosciences ApS, Edwin Rahrs Vej 38, 8220 Brabrand, Denmark
E-mail: flemming.moller@danisco.com

Abstract. *Chocolate milk instability was monitored by time series of images. It is demonstrated how a time series of images can be summarized into a single image, named a stability barcode. The stability barcode is generated by collapsing time series frames to pixel columns and arranging the pixel columns to form the stability barcode. It is demonstrated how image filtering can be used in generation of different and more specific stability barcodes. Chocolate milk defects such as layers could be seen in barcodes generated using a median filter, curdling could be seen in barcodes generated using a standard deviation filter and marbling could be seen in barcodes made using an H-dome filter. Graphs for comparing the destabilization kinetics were deduced from the stability barcodes. The stability barcodes gave a visual summary of chocolate milk instability—the kinetic graphs a precise comparison of specific types of instability. © 2012 Society for Imaging Science and Technology.*
[DOI: 10.2352/J.ImagingSci.Technol.2012.56.2.020402]

INTRODUCTION

Chocolate milk is the most popular flavored milk product worldwide. It is also one of the most difficult flavored milk types to produce. Several factors should be controlled when producing chocolate milk. First, a good grade of cocoa powder should be selected with good flavor and good bacterial quality. As the cocoa particles are not soluble, large cocoa particles tend to sediment at the bottom during storage. Stabilizer compounds are added to chocolate milk to prevent sedimentation and enhancement of the perceived quality. Most stabilizers used in chocolate milk form a weak gel-like structure by interactions with milk proteins. This structure remains intact, while the milk is undisturbed, suspending the cocoa particles in its network, but breaks down as soon as the milk is gently shaken or disturbed during drinking.[1,2]

A stable chocolate milk is visually homogenous throughout the shelf life of the product. The most common types of instability seen in chocolate milk are sedimentation, fat creaming, top whey layer, marbling, or curdling. The formulation, processing, and storage conditions of the chocolate milk can greatly influence the instability type and kinetics of its development.[1]

Received Jun. 28, 2011; accepted for publication Mar. 28, 2012; published online May 22, 2012.
1062-3701/2012/56(2)/020402/6/$20.00.

This article focuses on visualizing chocolate milk defects and stability as a function of time. The aim of this study is to summarize a chocolate milk movie into one image, a stability barcode. Different types of chocolate milk defects can be detected using image filters and hence visualized in stability barcode images. From the stability barcodes can kinetic curves be deducted. Kinetic curves are a precise tool for comparing different chocolate milk formulations—the stability barcodes are for a fast overview of any instability in a chocolate milk.

STABILITY EVALUATION

Chocolate milk can develop instability as a function of storage time, conditions, and composition. The most common types of instability are listed in Table I.[3]

Defects are often due to poor raw materials or processing, i.e., alkalization or too large cocoa particles, too much or too little stabilizer blend, insufficient homogenization, or heat treatment conditions. Layer defects are typically seen in the top or bottom of the product container. Bulk defect are typically seen in large parts of the product—bulk defects are often easily removed by gentle product shaking, unlike layers which can be very difficult to remove by shaking. *Marbling* can be described as a variegated pattern in large parts of the product container. *Curdy* is seen as inhomogenity when pouring product out of a container. It is thought that the curdy inhomogenity is a local gelation taking place in the chocolate milk. A white haze is often associated with curdy products; the white haze is thought to be caused by the gel pressing out to be large protein particles. The *color* may change as a consequence of layer formation[1] or due to oxidation.

Quantification of chocolate milk stability can be done by consumers or better a trained sensory panel.[4] The Turbiscan instrument has for several years been the only instrument for an objective measurement of physical stability of dairy products.[2] The Turbiscan measures the turbidity of a product as function of the height of the emulsion in a vertical tube. Laser light (850 nm) is reflected by the product and increases with the concentration locally present in the product. Furthermore, the measurements can be performed as a function of time. This allows the monitoring of the time-dependent behavior of the chocolate milk.

Table I. Types of instability found in chocolate milk.

Layers	Bulk
Sedimentation	Marbling
Creaming	Color
Whey separation	Curdy (white haze)

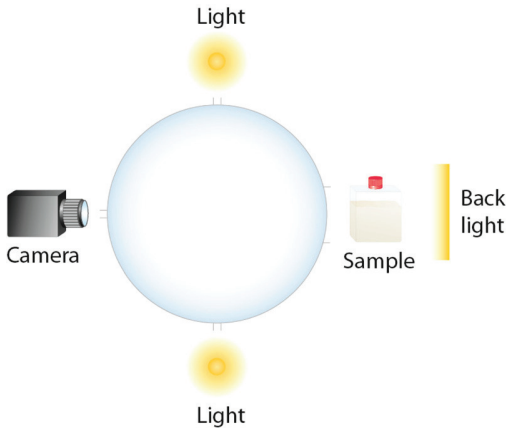

Figure 1. Illustration of instrument setup. A flask with sample is placed at an opening in an integrating sphere. The light source is ten diffuse LEDs and one LED backlight. A multiwavelength image is acquired with a gray tone camera by strobing one LED at a time.

Typical behaviors that can be observed are layers, which appear as a change of the turbidity as a function of height, and phase separation that is recognized by a clear and sharp interface between two phases.

The Turbiscan instrument is good for layer defect but it cannot detect bulk changes such as marbling, curdling, or color changes—The properties that can be seen in human beings, and this is the motivation for developing an image based method for detection of chocolate milk stability.

IMAGING DEVICE

The stability of the chocolate milk was evaluated using a VideometerLiq instrument (Videometer A/S, Hørsholm, Denmark). The instrument is composed of a camera, light emitting diodes (LED) placed in an integrating sphere and a backlight (405–850 nm). The equipment produces diffuse lighting, which ensures homogenous and reflection free images. The instrument generates multispectral images by strobing ten diffuse LEDs and a backlight one at a time. Figure 1 sketches the system setup. The wavelengths used were 405, 450, 470, 505, 525, 570, 630, 660, 700, and 850 nm diffuse LEDs and an 850 nm backlight. The resulting multispectral image is 460×1450 pixels, which correspond to 19×60 mm. Disposable sterile flasks with chocolate milk are placed in the VideometerLiq instrument. An auto sampler that can hold six samples which makes it easy to generate time series of images. Time series of images is necessary for visualization and quantification of any instability.

Table II. Composition of chocolate milk evaluated.

Composition	1	2	3	4	5	6
Total fat	1.48	1.48	1.48	1.48	1.48	1.48
Total MSNF*	2.56	5.48	5.99	5.48	5.48	8.01
Total dry matter	8.63	11.55	16.74	11.55	11.55	14.51
Total carbohydrate	5.58	7.1	12.05	7.1	7.1	8.6
Total protein	1.16	2.3	2.5	2.3	2.3	3.4

*MSNF = milk solid nonfat.

The light's penetration depth into soft materials like chocolate milk is wavelength dependent, i.e., long wavelengths penetrate further than short wavelengths. Long wavelengths are best for bulk properties and short wavelengths are best for measuring surface properties.[4]

CHOCOLATE MILK

To demonstrate different types of chocolate milk instability were six products produced by a standard dairy process (homogenization at 200 bar/70 °C and 137 °C/4 s) and varying the composition, see Table II.

A picture of the six chocolate milks 3 days after production is shown in Figure 2. Samples 1, 2, 4, and 5 appear stable. A closer look reveals that samples 2 and 5 show curdling (white haze/clouds). Sample 3 shows sedimentation and sample 6 marbling and creaming. In Fig. 2 does all samples seem to have a horizontal line one third down in the product—this is a camera artifact/light, since this could not be seen by human beings or the analytical setup.

All chocolate milks were evaluated for 3 days, and a total of 132 spectral images per sample were recorded. Figure 3 shows selected 505 nm images of sample throughout the evaluation period (505 nm had a high signal to noise ratio and was used for all work in this article). The first image from the time series (leftmost image in Fig. 3) shows stable chocolate milk with some air bubbles at the top. A bright top layer is forming soon after production which increases in thickness as a function of time. The same sample also develops marbling (bulk instability) seen as an inhomogeneous structure which forms after production.

STABILITY BARCODES

A time series of images can be converted into one image by collapsing each frame to a pixel column and let the width represent time—all pixel columns are then stacked to one 2D image. Conversion of movie frames to a 2D image is known as movie barcodes.[5] The conversion from a 2D image into a 1D column is done by applying standard image filters and then stacking the median pixel value in each 2D image row (from 2D to 1D). The width of the 1D column is scaled to reflect the period between two frames. All the scaled 1D columns are placed according to their order and together generate the stability barcode, see Figure 4.

In Figure 5, the median barcodes for the six evaluated chocolate milks of Fig. 2. The first measurement (first frame)

Figure 2. Picture of the chocolate milks evaluated at the end of analysis (3 days).

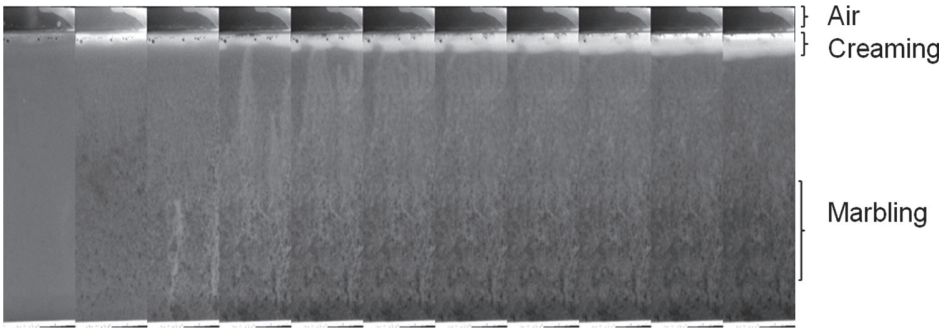

Figure 3. Selected images (11) at 505 nm of sample 6. Fat creaming and marbling defects are seen. The images are taken throughout the evaluation period. The freshly produced chocolate milk is seen to the left, the rightmost image is the same chocolate milk 3 days after production.

is subtracted from each barcode; thereby any intensity differences due to formulation (Table II) and processing removed. The subtraction of the first frame corresponds to centering of data, i.e., for a stable chocolate milk will the barcode remain constant at zero, a sample that becomes darker will have negative values and lightning of a sample will be seen as positive barcode values.

All samples show two very narrow and intense lines which can be explained by sunlight entering the instrument—the third evaluation day was cloudy.

Median barcodes can be used for detection of layers and color changes, see Fig. 5. Layers are seen as horizontal zones, i.e., samples 3 and 5 show sedimentation, sample 6 creaming, and samples 2 and 5 show a whey layer. Fat creaming and whey separation can both be seen as a top layer; the difference is that fat is seen as a white layer and whey as a transparent or black layer, seen, respectively, as a red and blue layers in Fig. 5. A chocolate milk can change color and at the same time be physical stable; this is seen for sample 4. Sample 4 becomes darker after its second exposure to the sun (vertical line seen in the middle of all samples)—no physical change is seen.

Structure development in the chocolate milk can be visualized by using classical image filters to generate the barcode. Marbling in samples 3 and 6 can be detected by calculating *H-domes*[6] on the original frames and summing each row up into the stability barcode, see Figure 6. H-domes are a local maximum finder and are therefor good at finding spots in chocolate milk. Calculating the *standard deviation* in each row and summing up into a barcode generates the result seen in

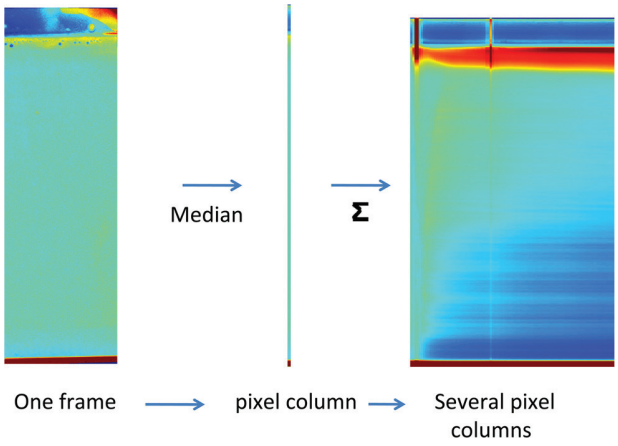

Figure 4. Procedure for generating a stability barcode. Left image is the first frame from the evaluation of sample 6. The median is calculated for pixels in each row of the picture and shown in the middle image. This is repeated for all frames, which then a summarized in the right image; the stability barcode. The x-axis in the stability barcode is a time scale, the y-axis corresponds to the height of image frames and a jet color scale is used.

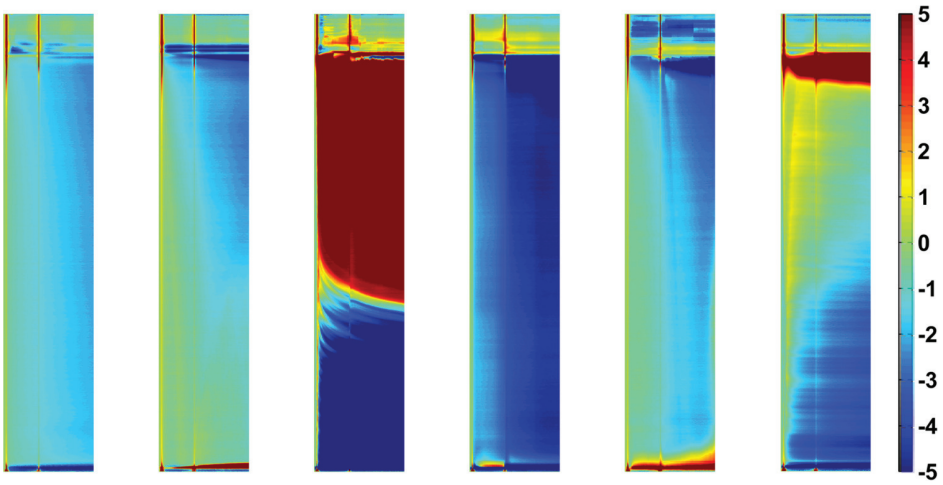

Figure 5. Median barcodes for the 6 chocolate milks. Each barcode represents 3 days of analysis at 505 nm. The x-axis represents time. Column points are calculated by a median filter of the original image rows. No change is represented by green, a darker or lighter color by blue and red, respectively.

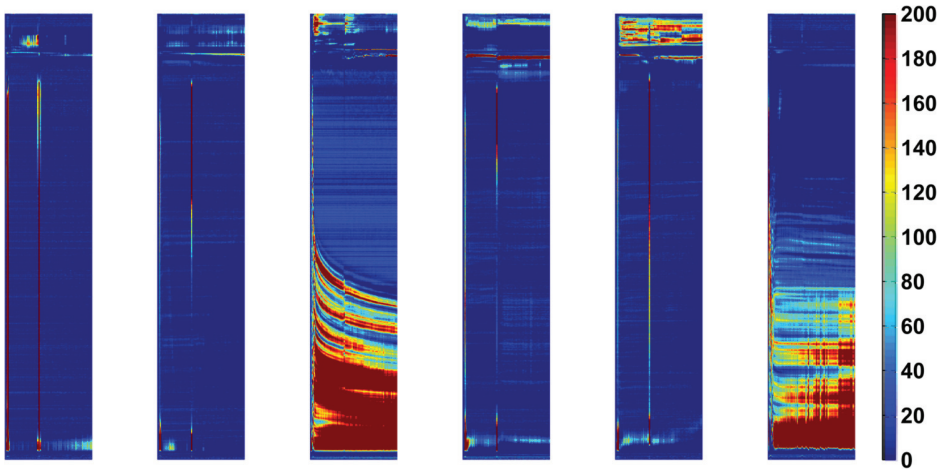

Figure 6. H-domes barcodes for the 6 chocolate milks. Each barcode represents 3 days of analysis at 505 nm. The x-axis represents time. Samples 3 and 6 show marbling developing immediately after production.

Figure 7. The standard deviation shows both marbling and the white haze associated with curdling (samples 3 + 6 and 2 + 5).

KINETIC CURVES

Graphs showing how layers or bulk defects develop as a function of time can be deduced from the barcode images. This is done by defining three regions in each sample: the top, middle, and bottom regions. Unpublished work has shown that the most robust way of quantifying a layer development is by plotting relative intensity changes in these zones. Calculating layer thickness can be difficult (setting a threshold) and gives the same conclusions as the relative method.

The three regions are defined as 15% of the top, middle, and bottom of the flask. Kinetic curves from the three regions and using the three different filters (median, H-dome, and standard deviation) are shown in Figure 8. All kinetic curves start at 0 (by subtracting the first measurement); a stable sample with no destabilization or color change will have a constant value (0) throughout the evaluation period.

Median Barcode

Layer defects are best seen using the median filter and looking at the top and bottom regions (leftmost column, top, and bottom graph). Sample 3 is very unstable and has a high level of sedimentation, which is seen as rapid decrease in reflection. Due to the severe cocoa sedimentation, sample 3 is also changing color in the top and middle parts of the flask; this is seen as increased reflection. Sample 6 shows an increased reflection in the median-top graph this is due to a fat layer forming at the top of the flask. The median-top graph also indicates less reflection from sample 4 due to a whey or water layer forming on the top of the sample. The median-middle graph is good for detecting any color changes: sample 4 becomes darker maybe as a result of

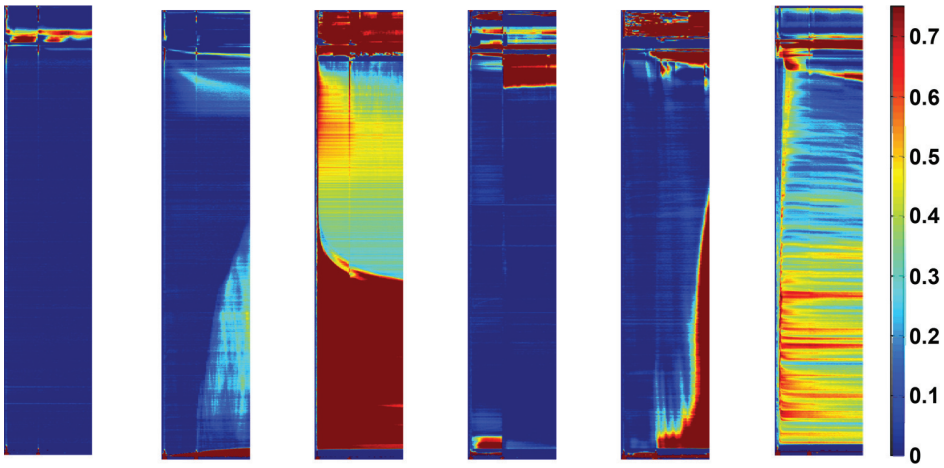

Figure 7. Standard deviation barcodes for the 6 chocolate milks. Each barcode represents days of analysis at 505 nm. Blue colors indicate a homogeneous product. A high standard deviation is seen for samples with marbling (samples 3 and 6) and for samples with curdling (samples 2 and 5).

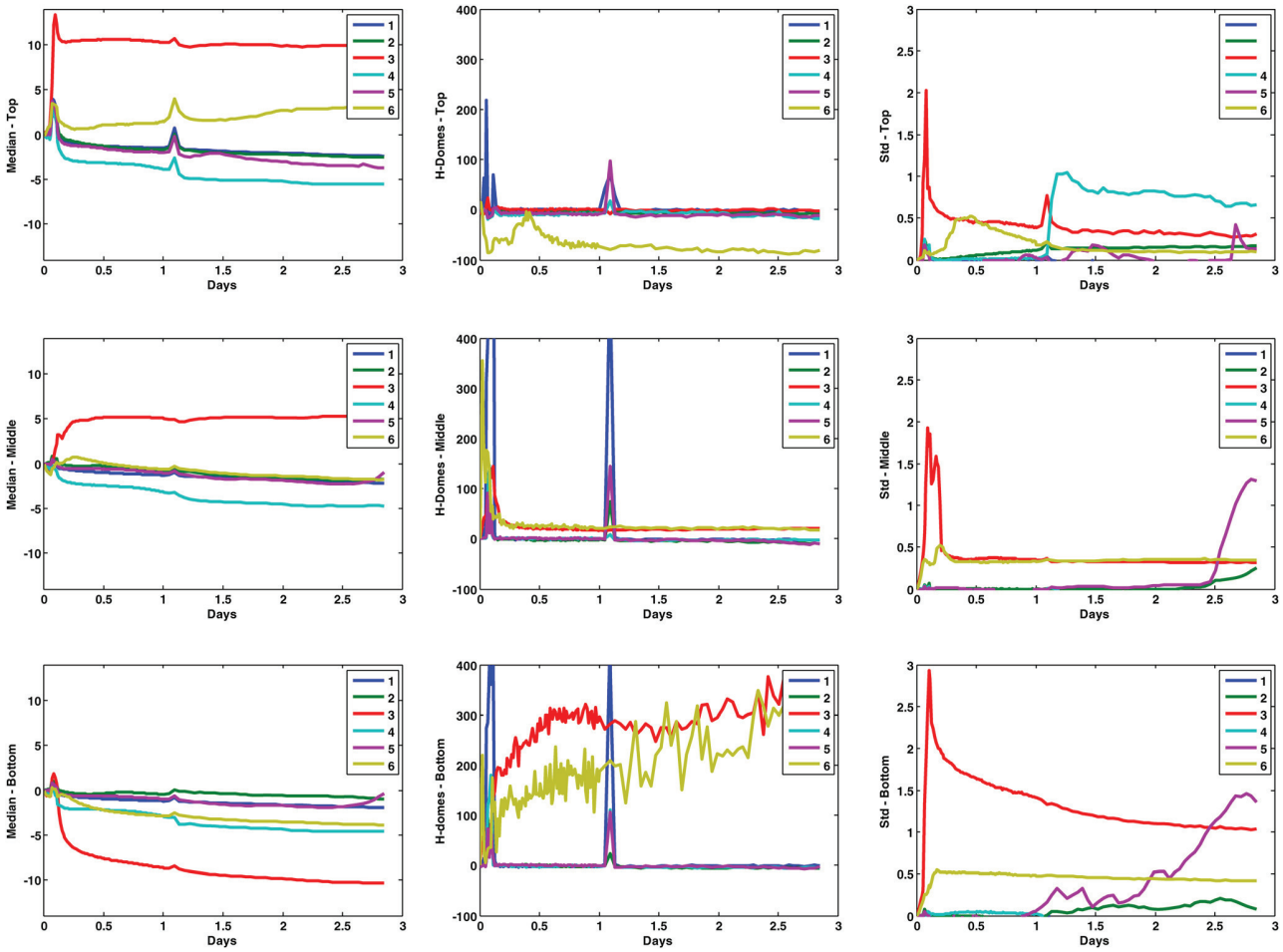

Figure 8. Kinetic curves for the 6 chocolate milks. The three rows illustrate intensity changes in the top, middle, and bottom regions. Graphs in the left column were deduced from median barcodes, graphs in the middle column were deduced from the H-dome barcodes, and the right column from the standard deviation barcodes.

aggregation or oxidation of particles (particle sizing was not performed). Sample 3 becomes light due to sedimentation of the cocoa particles.

H-domes Barcode

The H-domes' kinetic graphs are seen in the middle column. The marbling in samples 3 and 6 is detected using the H-dome filtering. The marbling is mainly seen in the bottom of the flask and only in the bottom graph. As the instrument was exposed to direct sunlight, there are two spikes which are easily seen (on day 0 and day 1).

Standard Deviation Barcode

The rightmost column in Fig. 8 shows kinetic curves generated using a standard deviation filter (top, middle, and bottom). Samples 2, 3, 5, and 6 all show a change in the kinetic curve. The H-domes showed that samples 3 and 6 developed marbling. The standard deviation in the middle or bottom part of the flask is able to detect the white haze associated with curdling (samples 2 and 5).

To find the best chocolate milk formulation, results from the different kinetics curves should be combined. Defects such as creaming, sedimentation, and marbling are highly undesired. By this measure, is samples 1, 4, and maybe 2 prove to be the best formulations.

Sample 1 is the only formulation without defects, samples 2 show curdling, and sample 4 a little whey layer and color change.

CONCLUSION

It was demonstrated how destabilization of chocolate milk could be visualized by converting a time series of images into a single image, a stability barcode. Kinetic curves quantifying different types of chocolate instability could be deduced from the stability barcodes.

By using image filters such as median, H-domes, and standard deviation it was possible to visualize and quantify defects such as sedimentation, whey separation, creaming, marbling, color change, and development of white haze associated with curdling.

Finding the optimal chocolate milk formulation should be done by combining results from the different kinetic curves. The optimal product would normally be one with no development in any of the kinetic measures.

ACKNOWLEDGMENTS

This work was partly supported by the Centre for Imaging Food Quality project, which is funded by the Danish Council for Strategic Research (Contract No. 09-067039) within the Programme Commission on Health, Food, and Welfare.

REFERENCES

[1] T. van den Boomgaard, T. van Vliet, and A. C. M. van Hooydonk, "Physical stability of chocolate milk", Int. J. Food Sci. Technol. **22**, 279–291 (1987).
[2] T. E. Grotenhuis, R. Tuinier, and C. G. de Kruif, "Phase stability of concentrated dairy products", J. Dairy Sci. **86**, 764–769 (2003).
[3] V. B. Alvarez, "Fluid milk and cream products", *The Sensory Evaluation of Dairy Products* (AVI Van Nostrand Reinhold, New York, NY, 2009), pp. 119–120.
[4] B. Saleh, *Introduction to Subsurface Imaging* (Cambridge University Press, Cambridge, United Kingdom, 2011), Chap. 6.
[5] M. White, "Jason Salavon: Emblem", Artlies, Issue 47 (2005).
[6] L. Vincent, "Morphological grayscale reconstruction in image analysis: Applications and efficient algorithms", IEEE Trans. Image Process. **2**, 176–201 (1993).

Paper III

Møller, F., Kragh, H., Laugand, D. and Carstensen, J.M. **Measuring light reflection from yoghurt surfaces: Glossiness, graininess and dullness of yoghurt.** Submitted to Food Hydrocolloids

Measuring light reflection from yoghurt surfaces: Glossiness, graininess and dullness of yoghurt

F. Møller[a], H. Kragh[a], D. Lugand[a], J. M. Carstensen[bc]

[a]DuPont Nutrition Biosciences ApS, Edwin Rahrs Vej 38, 8220 Brabrand, Denmark
[b]Videometer A/S, Lyngsø Allé 3, 2970 Hørsholm, Denmark
[c]DTU Compute, Technical University of Denmark, Richard Petersens Plads, Bldg 321, DK-2800 Kgs. Lyngby

Abstract. The effect of protein, pectin, sugar, starter culture and process shear is investigated for stirred yoghurt. The yoghurt samples are analysed with three descriptive methods, surface imaging of specular and diffuse light reflection, three rheology methods and a descriptive sensory analysis. A multivariate factor analysis shows that the imaging and rheology results are influenced differently by the production factors. Yoghurt glossiness/graininess can be predicted using surface reflection images, yoghurt thickness can be predicted using rheology.

Keywords: Yoghurt, gloss, grain, image analysis, image texture, rheology, sensory, chemometrics, 50-50 MANOVA, PLS, PCA

1 Introduction

The visual appearance is an important quality parameter for most food products. The composition and production process of fermented dairy products is controlled and optimised to ensure a constant production of high quality products. There are several analytical instruments available for chemical and physical properties. These instruments are commonly used for quality control and product development (J. A. Lucey, 2004; Tamime & Robinson, 1999). However, few instruments and little literature are available for the measurement of visual appearance of fermented dairy products. The visual appearance of the product can be very important for the consumer's expectation and liking and thereby influence the purchase (Baudet, Maire, & Pillet, 2012; J. A. Lucey, 2004; Voltz & Beckett, 1997).

The surface homogeneity of a food product will greatly influence its ability or capacity to reflect light. Gloss is not a single parameter, but a number of surface properties which together make up the light-reflecting properties of a surface. The most well-known type of gloss is specular gloss (Taylor, 2000). Specular gloss is seen with mirrors and polished metal surfaces. Specular gloss can be described mathematically and measured quantitatively, but it cannot account for all of the light-reflecting prop-

erties of a surface. Some light will be scattered due to inhomogeneity of the surface and can be measured as diffuse reflection and some light will enter the product and be scattered inside the translucent material (Jensen, Marschner, Levoy, & Hanrahan, 2001; Trezza & Krochta, 2001). There is no single method or model that can characterise all types of gloss. This article describes a method that measures specular gloss and at the same time surface structure, i.e. gloss and grains and the lack of it.

In literature, there are several analytical set-ups for measuring surface characteristics of yoghurt (Johansen, Laugesen, Janhøj, Ipsen, & Frøst, 2008; Kücükcetin, 2008; Remeuf, Mohammed, Sodini, & Tissier, 2003). Remeuf et al. used image analysis to quantify grains of diluted yoghurt. Johansen et al. used diffuse illumination to quantify graininess of yoghurt. Kücükcetin used back illumination for quantifying grains in the yoghurt and surface images for determination of surface roughness (no light geometry was specified). Specular gloss is regularly measured on flat and homogeneous surfaces such as paper and painted materials, and there are several instruments and methods for measurement of specular gloss (Serikawa & Shimomura, 1993; Trezza, et al., 2001). For fruits and vegetables, specular gloss has also been measured (Abbott, 1999; Mizrach, Lu, & Rubino, 2009). These methods measure the amount of specular reflection at a number of angles. In the computer vision literature, examples demonstrate how image gloss can be measured for images showing both specular and diffuse scattering (Landy, 2007; Motoyoshi, Nishida, Sharan, & Adelson, 2007; Toomey, et al., 2012).

In this paper we suggest a method that measures both specular and diffuse light from a yoghurt surface. The method is an imitation of how a visual inspection is typically done in the food industry, for instance when an inspector looks at the surface and records how the light is reflected (Baudet, et al., 2012; Johansen, et al., 2008; Küçükçetin, Weidendorfer, & Hinrichs, 2009; Remeuf, et al., 2003; Sodini, Lucas, Tissier, & Corrieu, 2005; Tamime, et al., 1999). The set-up comprises a ringlight with 6 LEDs and a standard greyscale camera. Figure 1 illustrates how light from one LED is reflected from a surface and detected by the camera. Smooth and very glossy yoghurt acts as a perfect mirror, resulting in a sharp image of the LED whereas grainy yoghurt is a “poor mirror” and hence results in a very diffuse image where the LED cannot be seen.

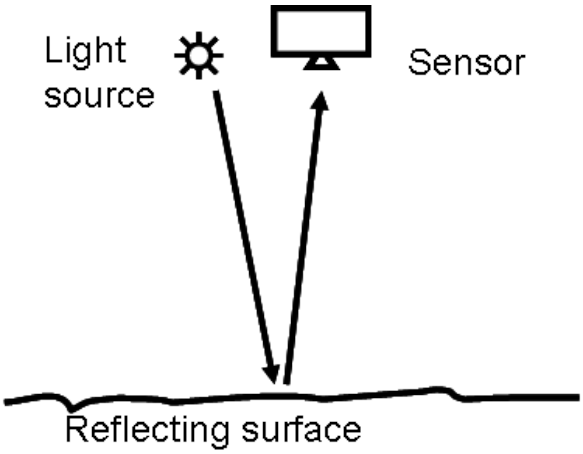

Fig. 1. A simplified set-up with one LED, reflecting surface and a camera. Specular scattering at the centre of reflection and diffuse of the scattering centre.

2 Materials and methods

2.1 Materials

Five production factors (see **Table 1**) were varied mainly with the intention to produce yoghurts with different levels grains and glossiness. The experimental plan was based on a screening design (D-Optimal design) using Modde 9.1 (Umetrics AB, Umeå, Sweden). Skimmed milk powder(BBA Lactalis, Bourgbarré, France) was used as protein source – extra protein gives higher viscosity and a less glossy product (J. Lucey & Singh, 1997), and amidated pectin, GRINDSTED® Pectin LA 410, which is a very calcium-reactive pectin. The pectin was used at the double concentration of what is normally recommended in yoghurt, a concentration known to produce grains in non-fat yoghurt (Matia-Merino, Lau, & Dickinson, 2004). Sugar (Nordzucker AG, Braunschweig, Germany)was added to alter the exopolysaccaride production (Duboc & Mollet, 2001). Three YO-MIX DuPont™ Danisco® Yogurt cultures were applied: YO-MIX™ 414 FRO which gives high viscosity and a short texture, YO-MIX™ 860 FRO which gives a high viscosity, longer texture and enhances glossiness and YO-MIX™ 511 LYO which is expected to result in lower viscosity, short texture.

Table 1. The composition of the 16 yoghurts produced. Protein, Pectin and Sugar content is listed in percentage (% w/w), Culture refers to culture number and Shear to operation speed of the YTRON pump.

Samples	Protein	Pectin	Sugar	Culture	Shear
1	3,2	0,00	1	414	5
2	5,5	0,00	1	414	5
3	3,2	0,20	1	414	5
4	5,5	0,20	1	414	5
5	3,2	0,00	8	414	5
6	5,5	0,00	8	414	5
7	3,2	0,20	8	414	5
8	5,5	0,20	8	414	5
9	4,35	0,10	4,5	414	5
10	4,35	0,10	4,5	414	5
11	3,2	0,00	1	860	5
12	5,5	0,20	1	511	5
13	3,2	0,00	1	860	15
14	5,5	0,20	1	511	15
15	3,2	0,00	1	414	15
16	5,5	0,20	1	414	15

2.2 Yoghurt production

16 yoghurt samples with different composition were produced in pilot scale, see **Table 1**. All powder ingredients were mixed and added to the standardised milk under good agitation at 45°C for 30 minutes. The milk was preheated to 70°C and homogenised at 200 bar followed by pasteurisation at 95°C for 6 minutes. Then cooled to fermentation temperature (43°C) and filled into fermentation vats. Inoculation (20 DCU / 100 liter) and fermentation to pH 4.60. The gel was broken using stainless steel bored disk, followed by a smoothing step by pumping through an YTRON-Z shear pump (YTRON, Bad Endorf, Germany). Two levels of smoothing were performed; 5% and 15% of max speed, followed by cooling to 20°C using a plate heat exchanger. The yoghurt was filled into 100 ml cups for surface characterisation, 150 ml cups for sensory evaluation and in 37 ml cups for rheology measurements and stored at 5°C in a well-ventilated fridge for one week.

2.3 Sensory evaluation

After one week of storage in a refrigerator (5°C) the samples were anonymised, randomised and evaluated by an expert judge. Sensory perceivable product attributes were measured by descriptive sensory analysis. Reference yoghurts are used to fix scale anchor points (ISO 13299, 2003; Lawless & Heymann, 2010).

The order of evaluation of the descriptors was as follows: Viscosity and grain/gloss assessed with spoon followed by evaluation in mouth. All descriptors were recorded on a 10 cm unstructured line scale anchored with appropriate terms at each end(ISO 13299, 2003), see definitions in **Table 2**.

Table 2. Sensory descriptors and their definition

	Definition	Ancor points
Thick with spoon	Viscosity measured after three stirs with spoon.	Thin–thick
Shininess	Sample on the spoon, is the surface grainy or shiny	Grain-Gloss
Thick in mouth	Perceived thickness when pressing againgst palate.	Thin–thick
Sticky in mouth	Degree of mouth coating after expectoration of the sample.	A little-a lot
Acidity	Acid taste in mouth	A little–a lot

2.4 Imaging device

The imaging set-up (SurfaceScan, (Videometer A/S, 2012)) consisted of a ringlight with six LEDs (637 nm) and a camera mounted in the centre of the ringlight (Point Grey Research, model: Dragonfly2 DR2-13S2M, 1280x960 pixels CCD). The distance from the LEDs to camera centre was 18 mm. The camera and ringlight were placed 218 mm above the evaluated object and controlled by a strobe controller. The strobe time was set to a level where no pixel saturation was detected in the most glossy products (strobe time: 1/500 [s]). The inside of the instrument can be seen in **Fig. 2**, camera and LEDs are mounted in the top facing downward, the sample is placed on the cylinder, a door (not shown) into the sample is closed during measurement.

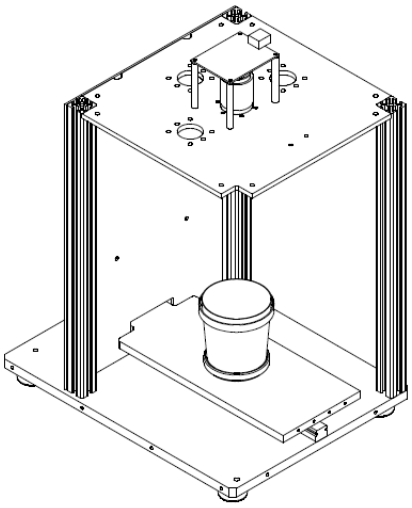

Fig. 2. Drawing of the instrument. In the centre of the top, the camera is mounted, and 6 LEDs are mounted in a ring around the camera. Distance between camera and sample is 218 mm.

Sample preparation.

A sample holder was made by placing two plates of PVC (130*100*5 mm) on top of each other. The top plate had a hole (diameter = 76mm) into which the sample was poured. The plates were shaken and tapped lightly to ensure an even sample spread. An even surface was obtained by scraping off excess sample. Two samples were prepared for each yoghurt and five pictures were taken – the sample was slightly moved and rotated between images. The scraped samples rested 120 seconds before the first image acquisition. Examples of three yoghurts are found in **Fig. 3**.

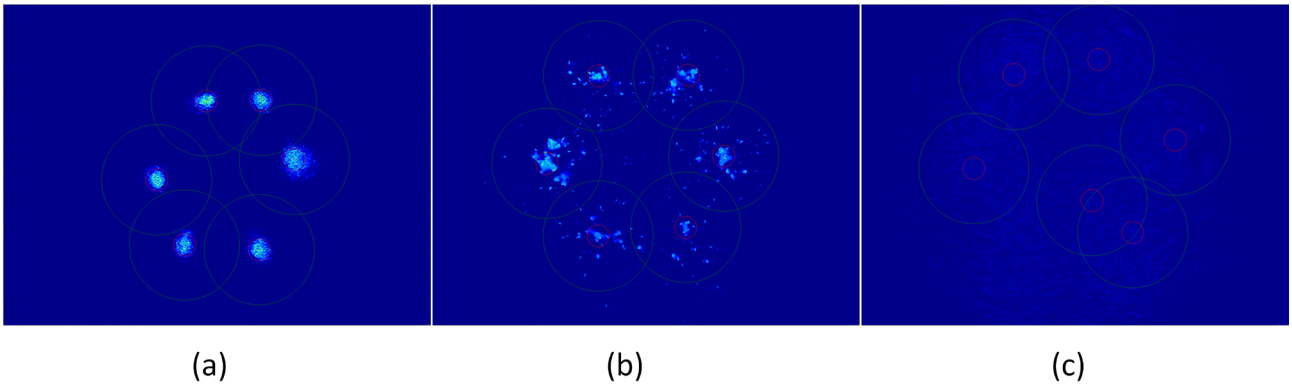

Fig. 3. Examples of reflection images of yoghurt. (a) A glossy yoghurt where most of the reflection comes from six hot spots, (b) a grainy yoghurt with a high level of glossiness, (c) a very pale and relatively smooth yoghurt.

Image analysis.
It is easy to see the difference in the different reflection images seen in **Fig. 3**, though somewhat more difficult to define a single number to describe the differences. Two types of image analysis were applied; one focusing on the six LED hot spots and a second type extracting more general image features.

Table 3. Variables calculated from the reflection images. First 8 variables from Gaussian pyramid, last 5 variables describe reflection for hot spot.

Method	Variable	Measures
Gausian Pyramid	StdDev 0	Standard deviation in base level of Gausian pyramid
	StdDev 1	Standard deviation 1 level up in Gausian pyramid diveded with StdDev 0
	StdDev 2	Standard deviation 2 level up in Gausian pyramid diveded with StdDev 0
	StdDev 3	Standard deviation 3 level up in Gausian pyramid diveded with StdDev 0
	Correlation 0	Auto correlation at base level of Gausian pyramid
	Correlation 1	Auto correlation 1 level up in Gausian pyramid
	Correlation 2	Auto correlation 2 level up in Gausian pyramid
	Correlation 3	Auto correlation 3 level up in Gausian pyramid
Hot Spot	Energy	Total amount of reflected light
	hotRatio	Relativ amount of reflected light measured in hot spot
	nearHotRatio	Relativ amount of reflected light measured close to hot spot
	GrainHot	Number of sparks measured in hot spot
	GrainNearHot	Number of sparks measured close to hot spot

The six hot spots are found by searching the image for the six brightest areas. A hot spot is then defined by the red circle as seen in **Fig. 4**, and a second, larger circle is also defined, illustrated by the green circle in **Fig. 4**. The total amount of light reflected is measured by summing all pixel values (energy), the relative amount of light from the hot spot is calculated as the relative pixel sum within the red circle relative to the total energy (hot ratio). Similarly the green circle is used to calculate the relative amount of light reflected from this area (near hot ratio). The number of small speckles inside the red and green circles were calculated using morphological reconstruction, named GrainHot and GrainNearHot (Vincent, 1993).

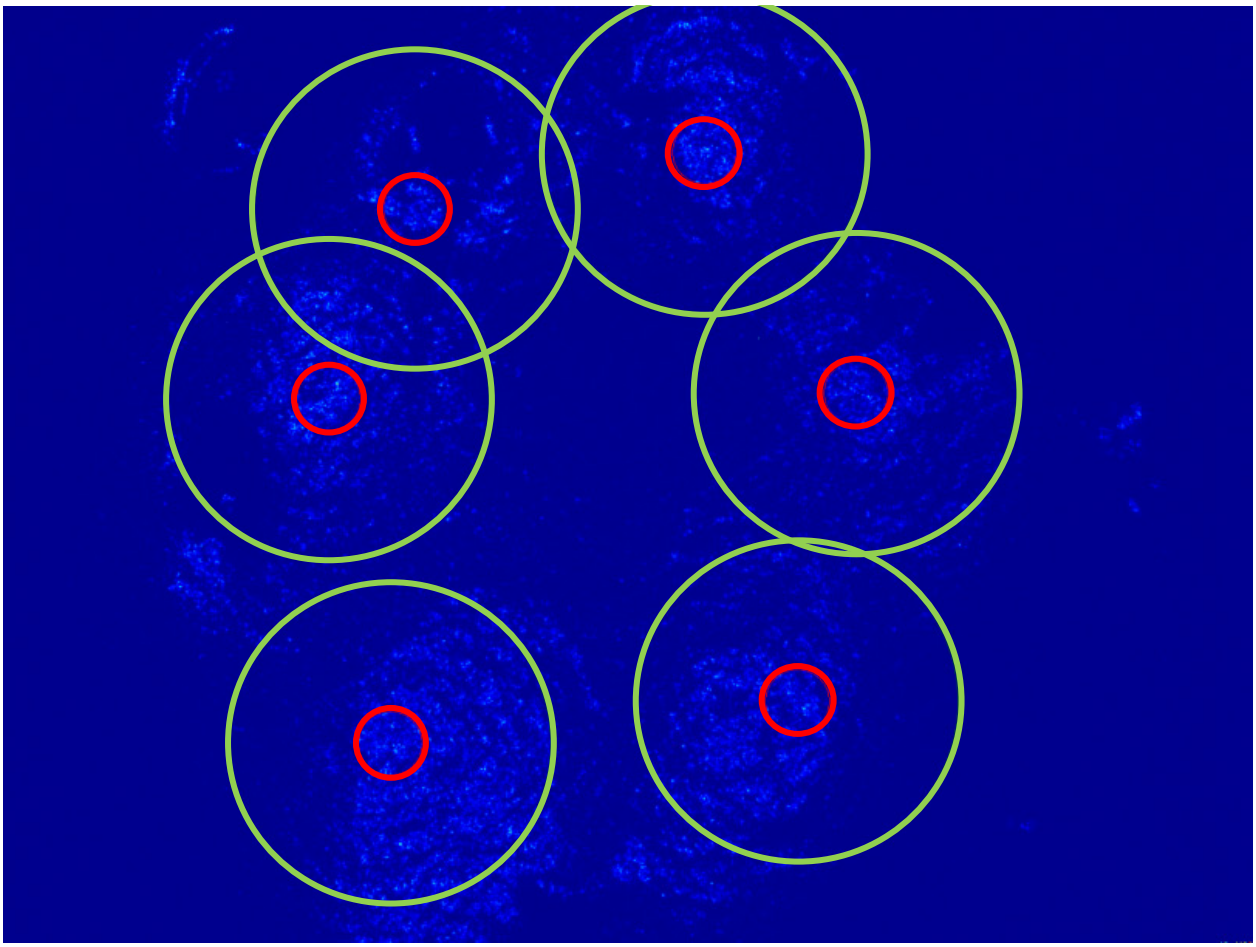

Fig. 4. Reflection image of dull yoghurt. Red and green circles define the six hot spots.

For the non-glossy products, it is often difficult to detect spots with high levels of reflection, as seen in **Fig. 3**c. For non-glossy images, general image texture features are more relevant (Gonzalez, Woods, & Eddins, 2004). Size information is also important when performing image analysis (Lindeberg, 1996). A Gaussian pyramid approach with a logarithmic scale parameter was used to calculate scale-dependent variables. A four-level Gaussian pyramid was used. The Gaussian pyramid creates a series of images which are blurred using a Gaussian filter and downscaled. This technique is used multiple times creating a stack of sequentially smaller images, with each pixel containing a local average that corresponds to a pixel neighbourhood on a lower level of the pyramid (Lindeberg, 1994). In connection with a Gaussian pyramid, several methods can be used for quantifying the image structures, e.g. first order statistics (mean, standard deviation) and second order statistics (relating two pixel values)

(Gonzalez, et al., 2004). Motoyoshi et al. have shown that for photos, skewness is positively correlated with glossy surfaces (Landy, 2007; Motoyoshi, et al., 2007; Toomey, et al., 2012). Skewness is a measure of asymmetry of a distribution, e.g. high reflecting surfaces will tend to have a positive skewness. However, in this method screening no relationship between skewness and sensory perceived glossiness was found. A method screening concluded that it was sufficient to calculate one first order (standard deviation) and one second order image feature (auto correlation) at four levels of a Gaussian pyramid. All image analyses were performed using the Videometer (www.videometer.com) image acquisition software. A total of 13 variables were calculated from the reflection images, see **Table 3**.

2.5 Rheology

The rheological properties such as shear rate dependent viscosities and strain dependent oscillatory storage and loss moduli have been measured using an Anton Paar Physica MCR 301 rheometer. The measuring system consists of a concentric cylinder-like system with the outer rim being a disposable aluminium cup (37 ml) with a diameter of 29 mm and the inner cylinder represented by a Vane geometry made of stainless steel (Barnes & Nguyen, 2001; Martin, Parker, Hort, Hollowood, & Taylor, 2005). The Vane geometry has four blades, a diameter of 22 mm and a height of 40 mm. All yoghurt samples were prefilled in the disposable cups and stored at 5°C for approximately one week before the measurements were performed. The measurements were performed at 10°C. After each disposable cup was placed in the rheometer, the Vane geometry was gently moved to its measuring position in the yoghurt after which the whole system was left to rest for 10 minutes before the measurement was started. All measurements were made in duplicate. All samples were characterised by three different methods, a viscosity profile, a strain sweep and a structure recovery profile – a fresh sample was used for each measurement. The methods are described in detail below (Barnes, 1999).

Table 4. Variables extracted from the three rheology methods.

Method	Variable	Measures
Strain sweep	G* (LVR)	G* within the Linear Viscoelastic Region (LVR)
	δ (LVR)	Phase angle within the LVR
	critical γ	Maximum strain within LVR stops
RSR	μ* (rest)	Complex viscosity before shear
	μ (shear)	Final value of shear viscosity
	μ* (recovery)	The rebuild complex viscosity after max shear
Flow curve	a	Herschel-Bulkley presumed yield stress
	b	Herschel-Bulkley viscosity (consistency value)
	p	Herschel-Bulkley exponent (flow index)
	Hysteresis	Area between two flow curves (up-shear and down-shear)

Rheology Methods.

Viscosity profile.

A standard viscosity profile was made starting at a shear rate of 0.1 s^{-1} and increasing it to 350 s^{-1} using a logarithmic ramp. The profile was then reversed decreasing the shear rate back to 0.1 s^{-1}. Selected parameters from the flow curve were then extracted and used as part of the rheological characterisation. The parameters were the hysteresis area between the two curves and the three Herschel-Bulkley (HB) parameters from the second curve (shear rates from 350 to 0.1 s^{-1}), the HB equation is seen below (1). The parameters were named the HB presumed yield stress (a), consistency value (b) and flow index (p), see equation below. τ symbolises the shear stress and $\dot{\gamma}$ the shear rate.

$$\tau = a + b(\dot{\gamma})^p \quad (1)$$

Strain Sweep.

A standard strain sweep was performed at 1 Hz starting at a strain of 0.01 % and increasing to 500 % using a logarithmic ramp. Selected parameters from the strain sweep was extracted and used as part of the rheological characterisation. The parameters were the complex modulus, G*, and the phase angle, δ, both within the Linear Viscoelastic Region (LVR) and the critical strain(γ) the point where the elastic modulus, G', has decreased to 90% of its value within LVR.

Rest, Shear and Recovery profile.

The structure recovery profile consists of combined measurements that contains both oscillatory and shear elements. The test starts with an oscillatory element performed at 8 Hz that characterises the structure before it starts being broken down. The second element is a constant shear at 200 1/s for 150 seconds made to break down the structure and the third part is an oscillatory element performed at 8 Hz that characterises the product's ability to regain its structure. Selected parameters from the Rest-Shear-Recovery (RSR) profile were extracted and used as part of the rheological characterisation. The parameters were the complex viscosity, μ*, before shear (from part 1), the final viscosity from the 2nd part and the complex viscosity after recovery (part 3).

In general all the rheological parameters have been analysed and evaluated using multivariate data analysis and correlations have been made to image features, sensory data and recipes.

2.6 Data analysis

The data was visualised, using Principal Component Analysis (PCA) (Wold, Esbensen, & Geladi, 1987). PCA is a linear data transformation or rotation, which maximises the sample variation. The rotated samples can be visualised in a score plot and variables in a loadings plot (the weight by which each variable should be multiplied to get the component score).

50-50 MANOVA (Ø. Langsrud, 2002) was applied for finding significant effects of the design factors on the response variables. The method handles the co-linearity of data by first reducing the dimensionality of the data by Principal Component Analysis into a few components and subsequently using ordinary MANOVA on these components. The method also calculates the explained variance of each factor, which is the sum of this effect's sum-of-squares for each response variable divided by the sum of the total sum-of-squares of each response variable. For each design factor, adjusted p-values or the most important variables can be found by performing a rotation test.

Partial Least Squares (PLS) models were used to express the relationship between variables and the sensory parameters (Wold, et al., 1987). All variables are usually included in the model. The influence of uninformative variables can be negative, and influence both the quality and the predictive ability of a model. Interval PLS (iPLS) (Norgaard, et al., 2000) was used to remove non-informative variables and hence build better models. iPLS objectively finds subsets of variables that contain relevant information and eliminates those variables that are clearly uninformative. The best model was selected based on leave-one-out cross validation and by selecting the predictive model with the smallest root-mean-square error estimated by cross-validation (RMSEP).

The PCA and PLS were performed using Evince 2.5.5 (Umbio AB, Umeaa, Sweden). 50-50 Manova was performed in the free software package from MATFORSK (Øyvind Langsrud, 2008). iPLS was performed using the PLS_Toolbox 7.0 (Eigenvector Research, Inc) and Matlab 8.0 (The Mathworks Inc.).

3 Results and discussion

Score plots only focusing on sensory, image or rheology data can be seen in **Fig. 5**. The composition of the samples can be seen in **Table 1**. The first principal component (PC1) gives similar sample distributions for all three methods, e.g. PC1 axis for the sensory data ranges from high viscosity to high gloss. The PC1 axis for the image data ranges from grainy+dull to high gloss. For the Rheology data the PC1 range from high to low viscous products.

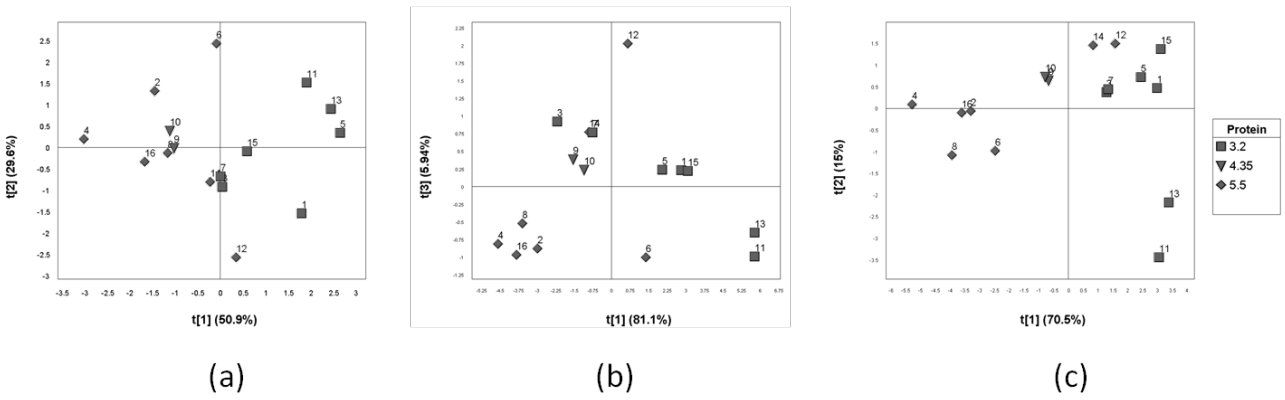

Fig. 5. Score plots for sensory data (PC1-PC2) (a), image data(PC1-PC3)(b) and rheology data(PC1-PC2)(c). Symbols indicate protein concentration. The numbers refer to sample numbers, which can be seen in **Table 1**.

The influence of production factors on yoghurt was evaluated using 50-50 MANOVA, see **Table 5**. Both PCA and 50–50 MANOVA show effects of the experimental design on measured variables. The PCA can visually show sample groups and effect of the design parameters, which can be related to and explained by the measured variables. 50–50 MANOVA, which is based on PCA scores, gives an indication of significant design effects and can show some relationships that are not easily seen using PCA.

The sensory evaluation could detect a significant effect of all factors except Shear, see **Table 5**. All factors except Sugar had a significant influence on the yoghurt rheology. All factors except Shear had a

significant influence on SurfaceScan images. The global model with all variables was significantly influenced by all factors except Sugar and Shear. That the global model using all variables had less discrimination ability than the individual models is an example of the fact that significant information can 'drown' in big models. The shearing of the yoghurt was applied in an attempt to produce yoghurt with a smooth surface, but the shearing did not have any significant effect on surface reflection. The rheology methods could detect a significant viscosity changed due to shearing – but this viscosity change could not be found by the sensory analysis. The added sugar had a detectable influence on the sensory profile and Surface reflection. A rotation test (Øyvind Langsrud, 2008) indicated that the sugar added mainly resulted in a more acidic yoghurt (sensory) and a higher total light reflection (Energy) from the yoghurt surface.

Table 5. Summary of the factor analysis using 50-50 MANOVA. All factors were continuous, except Culture.

	Sensory		Rheology		SurfaceScan		All variables	
Factor	Exp. Var (%)	p-value	Exp. Var (%)	p-value	Exp. Var (%)	p-value	Exp. Var (%)	p-value
Protein	24,2	0,0141	45,1	0,0000	14,5	0,0001	28,4	0,0000
Pectin	12,7	0,0017	3,8	0,0025	19,9	0,0014	12,3	0,0016
Sugar	9,3	0,0019	0,9	0,5048	4,0	0,0025	3,6	0,1203
Culture	23,7	0,0025	34,3	0,0000	26,4	0,0005	29,1	0,0000
Shear	3,2	0,5493	3,6	0,0337	0,5	0,7981	2,2	0,2797
Total model	73,1		87,7		65,4		75,6	

3.1 Reflection images

The score plot of image data forms a triangle with corners defined by samples 11 – 12 – 4; see **Fig. 5**a-b-c. Lower right corner: a glossy surface, lower left corner: a grainy surface, upper corner: a dull and smooth surface.

The X-axis (PC1) ranges from random scatter to very ordered reflection (glossy). The loading for PC1 is very influenced by all of the pyramid variables and reflection from the hot spot. The Y-axis (PC3) has a positive loading for Near Hot Ratio and a negative for Energy; e.g. typically a rough surface with reflecting light from larger lumps. Samples in the lower right corner have six very reflecting points (reflection from the six LEDs), i.e. a glossy surface (samples low in protein and pectin; samples 11 and 13). Samples in the lower left corner have little light reflection from many small points, i.e. dull and non-grainy yoghurt (high protein samples). The top point of the triangle reflects light from six larger points, i.e. reduced gloss and a surface with some structure. 50-50 MANOVA indicated a significant effect of

protein, pectin, sugar and culture. The glossiest yoghurt was obtained using; a low protein concentration, no pectin[1], a high sugar content and YO-MIX™ culture 511 or 860.

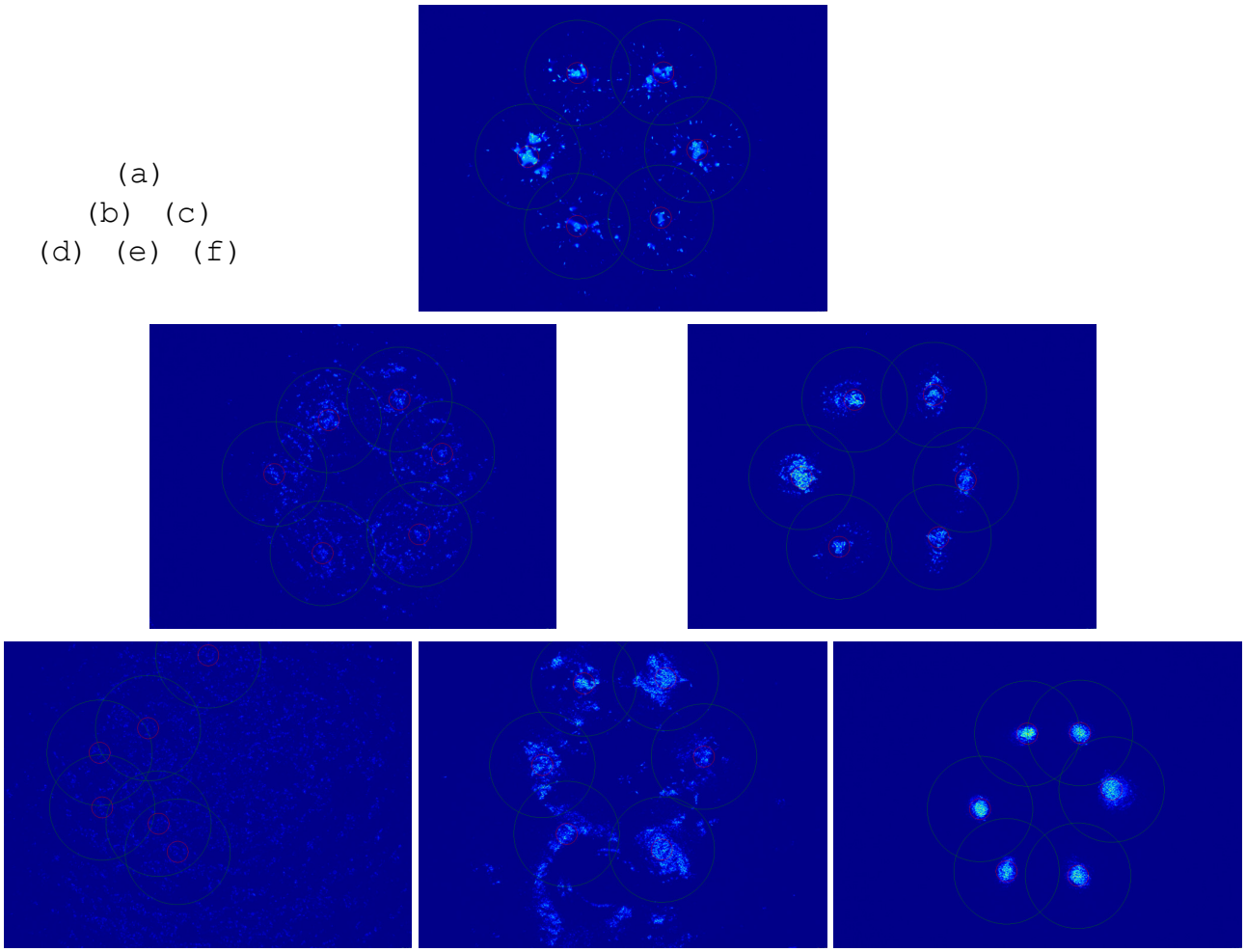

Fig. 6. Corner and edge images representing corner and edge samples in the score plot. Pictures a-f corresponds to samples: 12, 3, 15, 4, 6 and 13.

3.2 Rheology

The score plot of the variables extracted from the three rheology methods are seen in **Fig. 5**c. Variables from all three methods influence PC1, i.e. samples with a high protein content have a high vis-

[1] Extra high pectin concentration used to enhance grain formation.

cosity. PC2 is mainly influenced by variables from the strain sweep and flow curve. 50-50 MANOVA revealed a positive and significant effect of extra protein and pectin on the viscosity. Extra shear during cooling had a small but significant effect on the viscosity.

3.3 Sensory

50-50 MANOVA showed a significant effect of protein content, i.e. higher protein content results in a higher viscosity. The pectin added formed grains. Sugar gave a more glossy yoghurt. The three cultures resulted in different texture.

3.4 Relating sensory and instrumental data

PLS was used to relate instrumental data to sensory values. iPLS was used to find the best subspace of variables, while searching for a high linear relationship between measured and predicted Y (high r^2) and low RMSEP, see summary in **Table** .

Table 6. Summary of sensory parameters predicted based on rheology or SurfaceScan data. iPLS was used to select the best subspace of variables.

	Rheology					SurfaceScan				
	Thick with spoon	Thick in mouth	Sticky in mouth	Acidity	Gloss	Thick with spoon	Thick in mouth	Sticky in mouth	Acidity	Gloss
r^2	0,70	0,76	0,43	0,33	0,52	0,61	0,60	0,35	0,37	0,80
RMSEP	1,65	1,15	0,86	2,03	1,70	1,89	1,48	0,92	1,98	1,10
iPLS selected	b	G* (LVE) μ(shear)	δ (LVE) δ at critical γ μ* (rest) Hysteresis	δ (LVE) critical γ	δ at critical γ a p	StdDev 0 Energy GrainNearHot	StdDev 0 Energy	GrainHot	StdDev 0 Correlation 0	Correlation 3 GrainHot

The rheology data made good predictive models for two sensory parameters; thickness measured with a spoon and in the mouth. iPLS was used to find the best subset of variables, Thickness measured with a spoon was best predicted with a one variable model using the consistency value (b) from the flow curve. Thickness measured in the mouth could best be described using two values; G* within Linear Viscoelastic Region and the viscosity (μ shear) from the RSR measurement. The last three sensory variables were not related to thickness and are not expected to be described using rheological parameters. A summary of how the two analytical methods could predict the five sensory variables can be seen in **Table** , iPLS was used to select the best subset of variables.

The image data could only make satisfactory prediction of the sensory variable; glossiness. iPLS selected two image variables for the PLS modelling of sensory glossiness/graininess, with an r^2=0,80 and RMSEP=1,10. Two variables from the image analysis of the SurfaceScan images were selected by iPLS

in the iPLS modelling of Glossiness/graininess: correlation at 3rd level of the Gaussian pyramid and number of sparks measured in the LED hot spots (GrainHot).

Prediction of glossiness from the other sensory variables was not possible (not shown), this indicates that yoghurt thickness and glossiness are two different phenomena.

4 Conclusion

The specular gloss and diffuse light reflection could be measured on yoghurt surfaces. The light reflection could predict glossiness/graininess of yoghurt. Rheology could predict yoghurt thickness (with a spoon and in the mouth).

A multivariate factor analysis confirmed different discrimination effect of three evaluated methods, i.e. sensory, reflection images and rheology. It could be concluded that the extra shear during the yoghurt cooling did reduce viscosity, did not affect surface grains/gloss and could not be detected in the sensory profile. The addition of extra sugar had a significant effect on the sensory profile and surface reflection, but could not be measured using rheology.

The reflection images (**Fig. 6**) and the score plot triangle (**Fig. 5**b) showed that the reflection images can predict three sensory parameters: glossiness, graininess and dullness. Further work especially with focus on sensory vocabulary development and training is suggested.

To our knowledge, this is the first dedicated instrument that can measure specular gloss, graininess and dullness of foods.

5 ACKNOWLEDGMENTS

This work was partly supported by the Centre for Imaging Food Quality project, which is funded by the Danish Council for Strategic Research (Contract No. 09-067039) within the Programme Commission on Health, Food, and Welfare.

6 REFERENCES

Abbott, J. A. (1999). Quality measurement of fruits and vegetables. *Postharvest Biology and Technology, 15*(3), 207-225.

Barnes, H. A. (1999). The yield stress—a review or 'παντα ρει'—everything flows? *Journal of Non-Newtonian Fluid Mechanics, 81*(1), 133-178.

Barnes, H. A., & Nguyen, Q. D. (2001). Rotating vane rheometry—a review. *Journal of Non-Newtonian Fluid Mechanics, 98*(1), 1-14.

Baudet, N., Maire, J. L., & Pillet, M. (2012). The visual inspection of product surfaces. *Food Quality and Preference*(Articles in Press).

Duboc, P., & Mollet, B. (2001). Applications of exopolysaccharides in the dairy industry. *International Dairy Journal, 11*(9), 759-768.

Gonzalez, R. C., Woods, R. E., & Eddins, S. L. (2004). *Digital Image processing using MATLAB*. Upper Saddle River, NJ: Pearson/Prentice Hall.

ISO 13299. (2003). Sensory analysis — Methodology — General guidance for establishing a sensory profile. In *ISO 13299*.

Jensen, H. W., Marschner, S. R., Levoy, M., & Hanrahan, P. (2001). A practical model for subsurface light transport. In *Proceedings of the 28th annual conference on Computer graphics and interactive techniques* (pp. 511-518): ACM.

Johansen, S. M. B., Laugesen, J. L., Janhøj, T., Ipsen, R., & Frøst, M. B. (2008). Prediction of sensory properties of low-fat yoghurt and cream cheese from surface images. *Food Quality and Preference, 19*(2), 232-246.

Kücükcetin, A. (2008). Effect of heat treatment and casein to whey protein ratio of skim milk on graininess and roughness of stirred yoghurt. *Food Research International, 41*(2), 165-171.

Küçükçetin, A., Weidendorfer, K., & Hinrichs, J. (2009). Graininess and roughness of stirred yoghurt as influenced by processing. *International Dairy Journal, 19*(1), 50-55.

Landy, M. S. (2007). Visual perception: A gloss on surface properties. *Nature, 447*(7141), 158-159.

Langsrud, Ø. (2002). 50–50 multivariate analysis of variance for collinear responses. *Journal of the Royal Statistical Society: Series D (The Statistician), 51*(3), 305-317.

Langsrud, Ø. (2008). 50-50 MANOVA. In (1.74 ed.). http://www.matforsk.no/ola/program: MATFORSK

Lawless, H. T., & Heymann, H. (2010). *Sensory evaluation of food: principles and practices*: Springer.

Lindeberg, T. (1994). Scale-space theory: A basic tool for analyzing structures at different scales. *Journal of applied statistics, 21*(1-2), 225-270.

Lindeberg, T. (1996). Scale-space: A framework for handling image structures at multiple scales. *CERN EUROPEAN ORGANIZATION FOR NUCLEAR RESEARCH-REPORTS-CERN*, 27-38.

Lucey, J., & Singh, H. (1997). Formation and physical properties of acid milk gels: a review. *Food Research International, 30*(7), 529-542.

Lucey, J. A. (2004). Cultured dairy products: an overview of their gelation and texture properties. *International Journal of Dairy Technology, 57*(2-3), 77-84.

Martin, F. L., Parker, A., Hort, J., Hollowood, T. A., & Taylor, A. J. (2005). Using vane geometry for measuring the texture of stirred yogurt. *Journal of texture studies, 36*(4), 421-438.

Matia-Merino, L., Lau, K., & Dickinson, E. (2004). Effects of low-methoxyl amidated pectin and ionic calcium on rheology and microstructure of acid-induced sodium caseinate gels. *Food Hydrocolloids, 18*(2), 271-281.

Mizrach, A., Lu, R., & Rubino, M. (2009). Gloss evaluation of curved-surface fruits and vegetables. *Food and Bioprocess Technology, 2*(3), 300-307.

Motoyoshi, I., Nishida, S. y., Sharan, L., & Adelson, E. H. (2007). Image statistics and the perception of surface qualities. *Nature, 447*(7141), 206-209.

Norgaard, L., Saudland, A., Wagner, J., Nielsen, J. P., Munck, L., & Engelsen, S. (2000). Interval partial least-squares regression (iPLS): a comparative chemometric study with an example from near-infrared spectroscopy. *Applied Spectroscopy, 54*(3), 413-419.

Remeuf, F., Mohammed, S., Sodini, I., & Tissier, J. (2003). Preliminary observations on the effects of milk fortification and heating on microstructure and physical properties of stirred yogurt. *International Dairy Journal, 13*(9), 773-782.

Serikawa, S., & Shimomura, T. (1993). Method for measuring glossiness of plane surfaces based on psychological sensory scale. *IEICE TRANSACTIONS on Fundamentals of Electronics, Communications and Computer Sciences, 76*(3), 439-446.

Sodini, I., Lucas, A., Tissier, J. P., & Corrieu, G. (2005). Physical properties and microstructure of yoghurts supplemented with milk protein hydrolysates. *International Dairy Journal, 15*(1), 29-35.

Tamime, A. Y., & Robinson, R. K. (1999). *Yoghurt: science and technology*: Woodhead Publishing.

Taylor, A. E. F. (2000). Illumination fundamentals. *Lighting Research Center, Rensselaer Polytechnic Institute*.

Toomey, M. B., Butler, M. W., Meadows, M. G., Taylor, L. A., Fokidis, H. B., McGraw, K. J., & Archives, T. P. S. U. C. (2012). Behav Ecol Sociobiol DOI 10.1007/s00265-010-0926-z METHODS A novel method for quantifying the glossiness of animals.

Trezza, T., & Krochta, J. (2001). Specular reflection, gloss, roughness and surface heterogeneity of biopolymer coatings. *Journal of applied polymer science, 79*(12), 2221-2229.

Videometer A/S. (2012). www.videometer.com. In (pp. Hørsholm, Denmark).

Vincent, L. (1993). Morphological grayscale reconstruction in image analysis: Applications and efficient algorithms. *Image Processing, IEEE Transactions on, 2*(2), 176-201.

Voltz, M., & Beckett, S. (1997). Sensory of chocolate. *Manufacturing Confectioner, 77*, 49-53.

Wold, S., Esbensen, K., & Geladi, P. (1987). Principal component analysis. *Chemometrics and Intelligent Laboratory Systems, 2*(1), 37-52.

Paper IV

Møller, F., Vogel, C. and Carstensen, J.M. **Spectral imaging for monitoring structure and colour development of dry fermented sausages.** Submitted to Meat Science

Spectral imaging for monitoring structure and colour development of dry fermented sausages

Flemming Møller, DuPont Nutrition & Biosciences ApS

Christian Vogel, DuPont Nutrition & Biosciences ApS

Jens Michael Carstensen, DTU Informatics, Technical University of Denmark

Abstract. During ripening of fermented sausages a colour, texture and structure development is occurring. Multispectral images are used to evaluated meat colour and homogeneity of sliced salami. Normalised Canonical Discriminant Analysis (nCDA), a supervised classification method, is used to segment between meat and fat. nCDA is also used to define a new linear colour scale, ranging between fresh and mature salami meat. The homogeneity of sliced salami is evaluated at 850 nm by calculated the autocorrelation at 6 levels of a Gaussian Pyramid. Six fermented salamis were evaluated for 20 days of ripening. Data clearly shows meat colour is not correlated to hardness and surface homogeneity. Reference samples and salamis containing lactose have a slow development of all parameters. Salamis containing dextrose and saccharin are developing hardness and colour very fast.

Keywords: Sausages, colour, multispectral, image analysis, nCDA, segmentation, Gaussian pyramid, texture, PCA

1 Introduction

The colour and visual texture of meat products are two of the most important factors influencing consumers' purchase decision [Steenkamp and van Trijp, 1996]. The perceived colour of meat is a function of its chemical composition and viewing conditions, and it is changing with age and lighting conditions. Visual structure includes the surface roughness, and the size and distribution of fat regions; the latter feature being particularly important in certain markets [Steenkamp and van Trijp, 1996; Grunert et al., 2004].

The storage conditions of dried sausages play an important role in the structure and taste development of the finished product. Several chemical reactions take place affecting the colour of the meat product [Campbell Platt and Cook, 1994; Feiner, 2006; Leroy et al., 2006; Marianski and Mariański, 2009]. The most important chemical reactions that take place are lipid oxidations which affect the oxidation of haem pigments whose red colour turns into

brown, see the salami to the right in Figure 1. These chemical reactions inducing discoloration of the meat products depend on various factors, e.g. temperature, addition of antioxidants (in the occurrence of spices), if smoke applied, haem pigment concentration, and others [Mancini and Hunt, 2005; Møller and Skibsted, 2006].

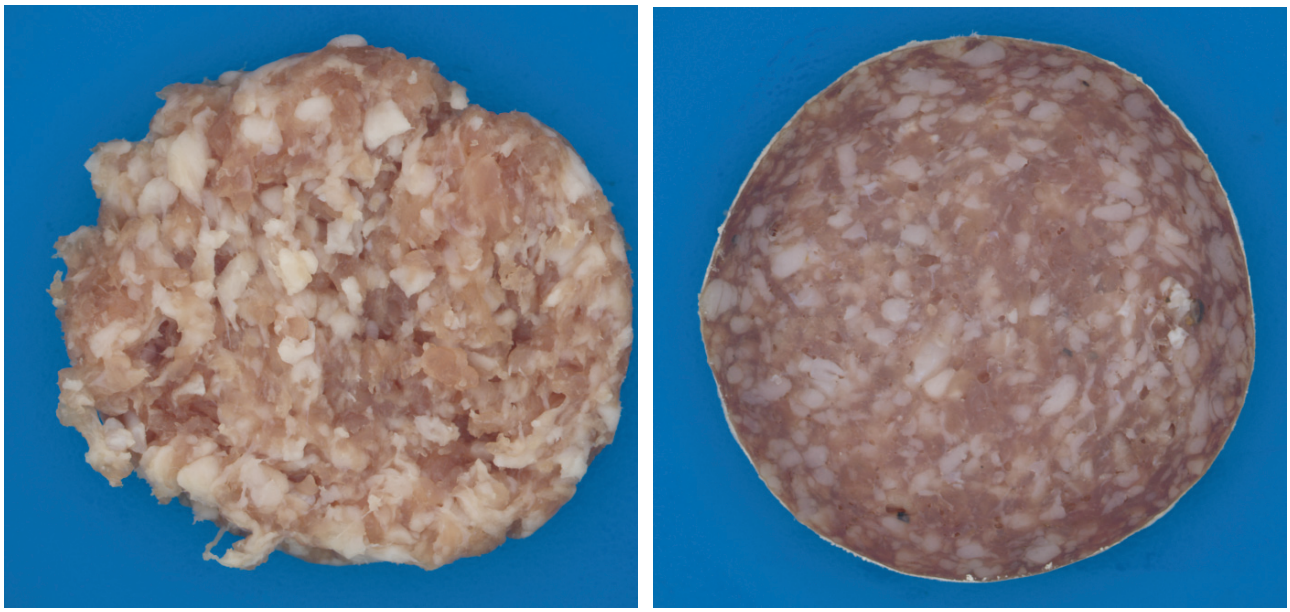

Figure 1 Salami slices illustrating how structure and colour changes during 20 days of fermentation. 1 and 20 days after manufacture left and right respectively.

For a successful and standardised dry fermented sausage production, the use of starter cultures is essential [Feiner, 2006; Ammor and Mayo, 2007]. Modern starter cultures consist of three types of active ingredients:

- Bacteria with acidifying and inhibiting activities
- Bacteria with reducing and flavouring activities
- Yeasts with neutralising and flavouring activities

1.1 Bacteria with acidifying and inhibiting activities

This group mainly consists of lactic acid bacteria of the genera *Lactobacillus* and *Pediococcus*. Their main functionality is the acidification of the dry fermented sausage by converting car-

bohydrates into lactic acid [Ammor and Mayo, 2007]. These starter cultures allow the meat processor to [Feiner, 2006]:

• control maturation to generate the appropriate drying and texture in line with regional product characteristics
• reach optimal pH for the chemical fixation of nitrite oxide (NO) with myoglobin to improve colour development and indirectly reduce NO availability for nitrosamine formation
• control the growth of undesirable microorganisms (intrinsic spoilage flora as well as pathogenic flora)

1.2 Bacteria with reducing and flavouring activities

The second group mainly consists of bacteria from the *Micrococcaceae* family, more specifically of the genera *Kocuria* and *Staphylococcus*. Their primary functionality is to initiate colour development by reducing nitrate into nitrite through their nitrate reductase enzymatic activity [Montel et al., 1996; Feiner, 2006]. The initial reduction of nitrate provides substrate (nitrite) for subsequent chemical conversion to nitrite oxide, which then binds to myoglobin to generate the typical red colour of fermented dry meat [Arneth, 1998]. The catalase activity of bacteria is essential for the degradation of peroxide produced by intrinsic spoilage flora, thus preventing off-flavour development as well as greening and rancidity. Certain strains have the ability to inhibit undesirable microorganisms through specific inhibitory systems (including bacteriocins and competitive exclusion), thus further improving the microbial quality of finished products. The proteolytic and lipolytic enzymatic activities of yeast also contribute actively to the development of flavour and aroma in the meat product.

1.3 Yeasts with neutralising and flavouring activities

The third group consists of yeast. Yeast may be added to a starter culture, such as lactic acid starter cultures, to take advantage of their ability to utilise lactic acid as a carbon source after the bacteria has depleted the fermentable sugar source towards the end of the ripening period [Campbell Platt and Cook, 1994]. Their assimilation of lactic acid can results in a pH increase towards the end of the ripening period, similar to that which occurs when a surface mould culture is used. The proteolytic and lipolytic enzymatic activities of yeast also have an active contribution to the development of flavour and aroma in the meat product [Campbell Platt and Cook, 1994; Leroy et al., 2006]. As a result, the final product has a mild, less acidic taste.

1.4 Sugar

The type and quantity of sugar used can influence the pH drop. In addition, each microorganism has its own characteristics with regard to the type of sugar they can ferment, types they cannot ferment at all, and types that they can adapt to and will consume once preferred sugars are used up [Campbell Platt and Cook, 1994; Leroy and De Vuyst, 2004; Feiner, 2006]. In general, dextrose is the easiest one for most types of microorganism to transfer into lactic acid and, consequently, catalyses the fastest pH drop. Lactose, on the other hand, can only be used by specific strains, which can sometimes only consume part of the total quantity [Acton et al., 1977; Marianski and Mariański, 2009]. The amount of dextrose, or sugar in general, added to dry fermented sausage depends of course on the cultures used, the initial pH and the buffering capacity of the raw materials, and how far and fast the pH should drop. Typically 4-5g of dextrose/kg is the right amount of sugar to achieve a sufficient pH drop, as well as colour and flavour development. For special types of dry fermented sausage, for example slow-ripened types as are produced in France, other types of sugar can be added, e.g. 10g lactose/kg [Campbell Platt and Cook, 1994; Feiner, 2006; Danisco A/S, 2011].

1.5 Objective

The heterogeneous structure of fermented sausages combined different kinetics of the colour changes in separate layers of the sausage [Møller and Skibsted, 2006] makes it difficult to measure and evaluate these changes using reflectance spectrophotometers. Therefore image analysis and especially spectral images are desirable technologies for quantifying the colour and structural changes taking place throughout the salami fermentation. Figure 1 shows how the colour and structure of the salami change during the fermentation period; after 20 days of fermentation the salami is darker and more homogeneous. The salami can have a darker edge than the centre after end ripening [Arneth, 1998; Møller and Skibsted, 2006].

The primary purpose of this paper is to develop a method for quantifying the meat colour distribution and meat colour in the salami centre. Secondly, a method is developed for quantifying the visual structure changing from loose raw meat into sliceable salami. A method is proposed for measuring the structure and colour changes in fermented salami based on spectral imaging and image analysis. The image analysis uses normalised Canonical Discriminant Analysis (nCDA) for image segmentations (background/salami followed by

fat/muscle), and the nCDA approach is also used to define a meat colour scale, ranging from fresh till mature meat. The structure development is measured using an auto-correlation (AC) function derived at different levels of a Gaussian pyramid.

2 Materials and methods

One type of Italian sausages with different sugars and fermented with TEXEL® meat cultures was studied.

2.1 Manufacture of dry fermented salami

Six salami batches were produced, 10kg each. The formulation is seen in Table 1, the meat and fat was cut in cubes with a size of approx. 5 x 5 cm and stored for 12h at -2°C (meat) an -18°C (fat).

Table 1 Composition of the salamis produced

Ingredient Name	Unit	Ref	Ref2	Dex 0.5	Lac 0.5	Sac 0.5	Dex + Salt
Pork Shoulder 3% - 6% Fat	%	76.79	76.79	77.39	77.39	77.39	77.34
Pork Back Fat	%	19.00	19.00	19.00	19.00	19.00	19.00
Nitrite Salt 0.6%	%	2.80	2.80	2.80	2.80	2.80	
NaCl	%						2.80
Sodium Nitrate	%						0.05
Dextrose	%			0.50			0.50
Lactose	%				0.50		
Saccharose	%					0.50	
Completmix for Salami	%	1.40	1.40				
Sodium Ascorbate	%			0.05	0.05	0.05	0.05
Pepper, White, Ground	%			0.20	0.20	0.20	0.20
Garlic Powder	%			0.05	0.05	0.05	0.05
TEXEL SA-241	%		0.01				
TEXEL PLM	%	0.01					
TEXEL Prism 1	%			0.01	0.01	0.01	0.01
Total	%	100.0	100.0	100.0	100.0	100.0	100.0

The production took place in a 30l bowl chopper - 5000 Express 30 Liter (Kilia, Neumuenster). In a first step, the fat was added into the bowl chopper, then the meat followed by the pre-solubilised starter cultures and a dry blend of all other ingredients except salt. After 30 rounds of cutting, the salt was added, cut for 5 rounds, after which the meat batter was mixed for another 65 rounds. Immediately afterwards the meat batter was stuffed with a vacuum stuffer – VF 50 (Handtmann, Biberach) in cellulose casings Naturin R2 (Naturin Viscofan GmbH Weinheim) caliber 60. The fermentation and ripening was done according to the figures shown in Figure 2. Before the sausages were placed into the fermentation chamber, they were left for 5h at a temperature of approx. 12-14°C for acclimatisation. Immediately before putting them into the fermentation chamber they were dipped in a solution with surface cultures.

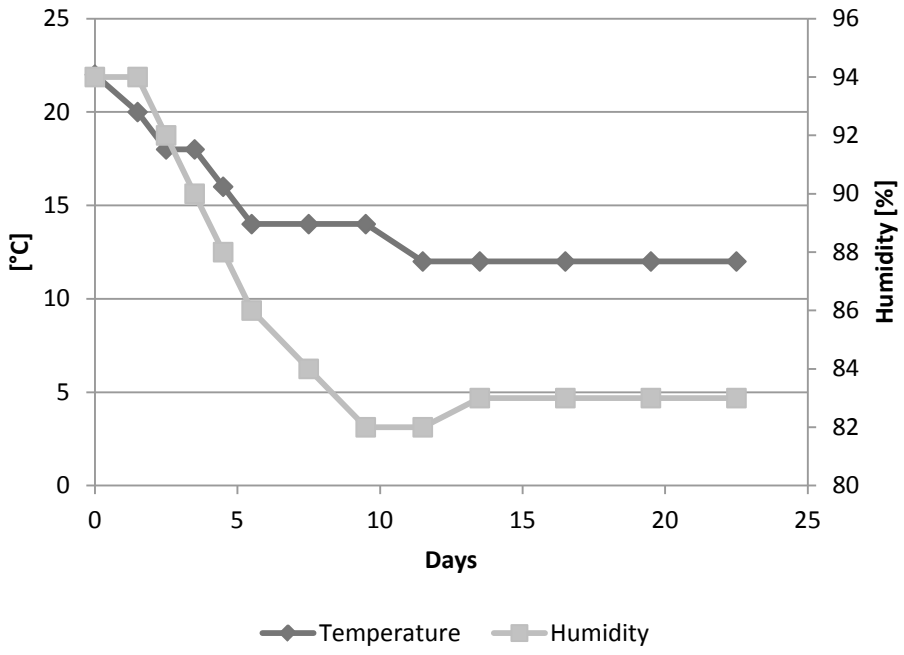

Figure 2 Programmed fermentation and ripening temperature and humidity.

2.2 Start cultures and sugars

Three starter cultures were used: TEXEL® SA-241, TEXEL® PLM and TEXEL® Prism-1. The three starter cultures were commercial blends of *Lactobacillus sakei* and *Pediococcus pento-*

saceus (acidifying and inhibiting) and *Staphylococcus carnosus* and *S. Xylosus* (reducing and flavouring). TEXEL® SA-241 and TEXEL® PLM are slow fermenting starter cultures which result in a slow texture development. The slow fermentation is also expected to give more time to develop an intense red colour development. TEXEL® Prism-1 starter cultures are fast fermenting, therefore results in a fast texture development and less colour development. Two fast fermenting sugars were used: Dextrose, and Saccharose, and one slow fermenting sugar: Lactose, which can only be fermented by some starters. The fast fermenting sugars are expected to have a fast texture and colour development. The slow fermenting lactose will have a slower texture development and more time to develop colour. The two reference salamis were fermented using a salami mix, containing fast fermenting sugars: dextrose and maltodextrin.

2.3 Imaging system

The spectral imaging system [Videometer A/S, 2012] used in this research consists of a 5 mega pixel CCD camera, mounted inside the top of an integrating sphere. Illumination is carried out by strobing LEDs with 18 different wavelengths, ranging from 375 to 970 nm – one wavelength at a time. The sample is placed at the bottom of the integrating sphere. The instrument design ensures diffuse and reflection-free illumination. The power of the LEDs is set independently at each wavelength to ensure an optimal signal to noise ratio. The instrument is NIST-calibrated using a bright and dark reference object, and spectral-aligned using a dotted plate.

Meat colour can be estimated either in CieLAB coordinates, or as a meat colour index. CieLAB values are spectrally reconstructed from the raw image spectra, and the meat colour index is calculated using a normalised canonical discriminant analysis.

All sausages were manually cut with the aim to obtain sliced samples with a thickness of ~10 mm. The slices were imaged within 10 minutes after slicing.

Image analysis.

A flowchart for the steps involved in the image analysis deriving meat colour in the centre and at the edge, mm dark meat and structure parameters is shown in Figure 3.

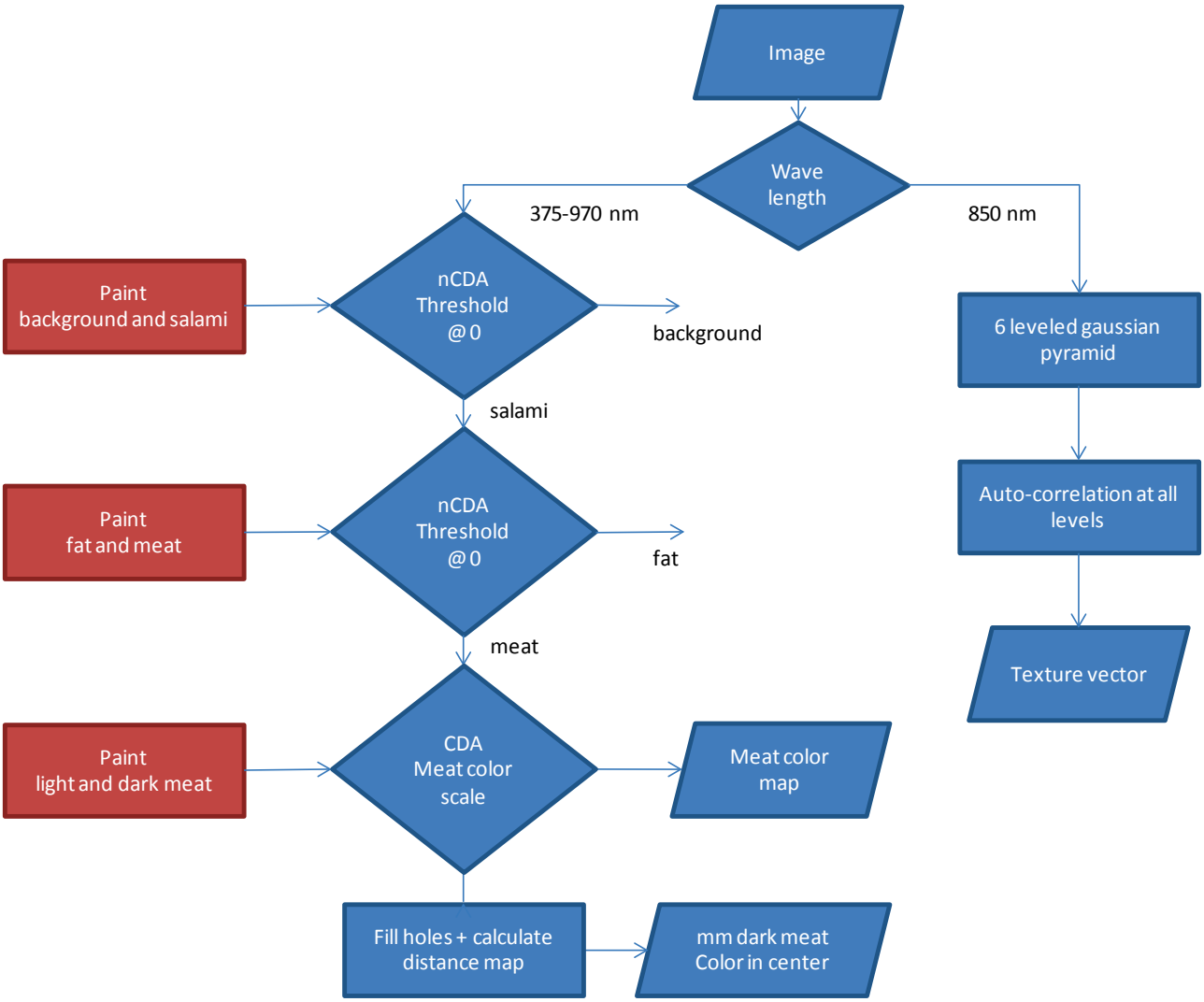

Figure 3 Flowchart illustrating the steps involved in finding and measuring meat colour and salami structure. Left column illustrates the steps involved in measuring colour development, the right column the structure quantification.

Structure analysis.

Human visual perception is very good at detecting colour and size changes [Koenderink, 1984; Westland and Ripamonti, 2004]. Human beings look at images at several levels of resolution simultaneously, and it is therefore natural to do the same when analysing images

mathematically. In this paper, we use the Gaussian pyramid approach where the logarithmic scale parameter is intuitively in good agreement with human perception [Koenderink, 1984; Lindeberg, 1994; 1998]. There are several methods for quantifying image structures, e.g., size, shape, first order statistics (mean, standard deviation) and second order statistics (relating two pixel values) [Gonzalez et al., 2004]. After a method screening, it was decided only to calculate the Auto Correlation feature (AC) with a displacement of one pixel at all levels in the image pyramid. The Gaussian pyramid creates a series of images which are blurred using a Gaussian filter and downscaled. This is repeated multiple times, which creates a stack of sequentially smaller images, with each pixel containing a local average that corresponds to a pixel neighborhood on a lower level of the pyramid, see Figure 4a[Lindeberg, 1994].

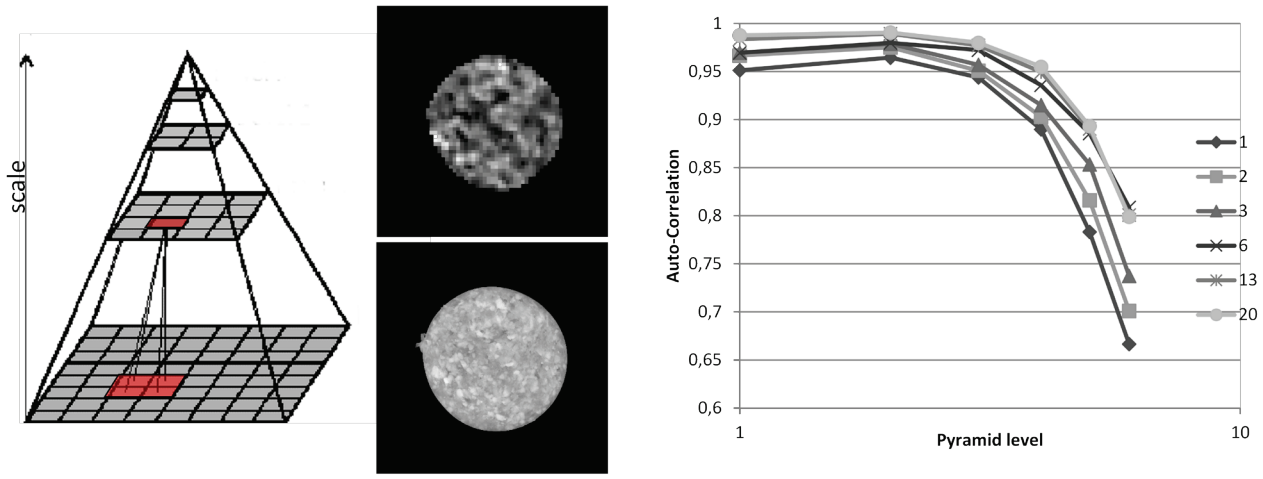

Figure 4 Gaussian pyramid (left), two salami images; bottom image is the original, top image is at the 6th pyramid level (middle). Auto-correlation as a function of pyramid level for salamies aged 1 to 20 days (right).

Normalised Canonical Discriminant Analysis.

Principal Component Analysis (PCA) is probably the most common method for unmixing spectral images [Sun, 2010]. In this paper, we have used a modified version classical Canonical Discriminant Analysis (CDA) also known as fisher discriminant analysis [Guang and Maclean, 2000]. Unlike the PCA, the CDA is a supervised method where some training sam-

ples (pixels in images) are designated as belonging to different classes. The CDA finds directions along which points within a group are clustered as tightly as possibly while maximising the between group separation. Despite the fact that PCA and CDA is much alike, a single PCA cannot discriminate better than the first canonical component; the CDA derives canonical variables that summarise between-class variation while a PCA summarises total image variation [Guang and Maclean, 2000; Franc and Hlavác, 2004].

CDA is a supervised method where the discriminating model is built based on some training samples. The training samples are pure samples selected during the model building. In Figure 5a, it can be seen how a user have annotated meat and fat pixels, this is done dark/light/fresh/old pixels. After the model has been build can it be used on subsequent images.

In this paper, we use a modified version of CDA called normalised Canonical Discriminant Analysis (nCDA). nCDA is more suited separating classes of different size and for thresholding between groups. With nCDA the zero level is set to the mean of class means instead of the overall pixel mean, and the loadings are scaled so that the maximum and minimum class mean numerical deviation is one and negative one. Thresholding between two classes can be difficult and subjective [Tajima and Kato, 2011], but as nCDA is defined the optimal threshold for class separation will always be zero, see Figure 5b+c. The segmentation of salami/background and meat/fat was performed using nCDA, the steps involved in the segmentations are seen in the left column of Figure 3.

Spectral pre-treatment.

It was found that a spectral normalisation significantly removed the darkening seen toward the edge of the salami. The edge darkening was seen for both meat and fat and was notable at all wavelengths. The normalisation was done by dividing all wavelengths with 435 nm.

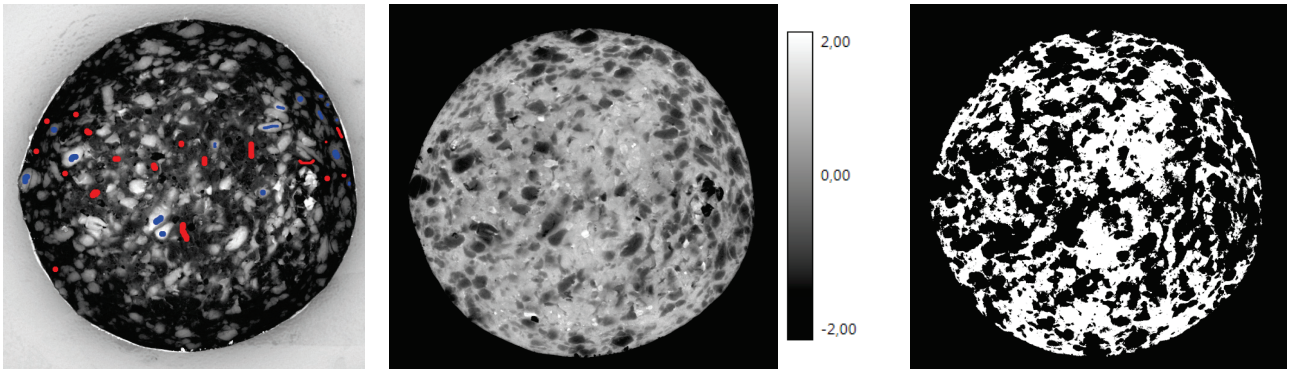

Figure 5 Segmentation of meat and fat, (a) blue and red labelling for nCDA model, (b) nCDA applied to image, (c) meat segmentation.

Meat colour scale.

Meat colours are often described by sensory analysis as purple-red, cherry-red, pink, brown, light or dark red etc. In literature several objective methods are used to describe meat colour, e.g. CieLab, RGB, XYZ [Mancini and Hunt, 2005; Wu and Sun, 2012]. Correlating the measured colour data to the sensory data can be done with multivariate methods [Lu et al., 2000]. In this paper we chose to use nCDA to define the most relevant meat colour scale, i.e. done by defining a fresh meat class and a dark meat class. The fresh meat was selected from salami one day after production (set to -1 on the nCDA scale) the dark meat was selected at the edge of salami 20 days after production (set to +1 on the nCDA scale). Only wavelengths visible for humans were used to define the salami colour scale (375-700 nm).

2.4 Hardness

A texture profile obtained using a texture analyser (TA.XT2i, Stable Micro Systems Ltd, Surrey, England). A 10 mm slice was made from each dry fermented salami. A single compression cycle test was performed up to 50% compression of the original portion height with an aluminium cylinder probe P/25. Force-time deformation curves were obtained with a 25 kg load cell applied at a cross-head speed of 2 mm/s. From the deformation, curves one parameter was derived; hardness (N) as maximum force required to compress the sample [Herrero et al., 2007].

2.5 Data analysis

The data were visualised, using Principal Component Analysis (PCA)[Wold et al., 1987]. PCA is a linear data transformation or rotation, which maximises the sample variation. The rotated samples can be visualised in a score plot and variables in a loadings plot. PCA estimates the correlation structure of the variables, this can be used to find the variables that express most of the information in the data set. The corresponding scores plot can be used to visualise groups of samples and common trends [Wold et al., 1987; Martens et al., 1989]. All variables were autoscaled (mean subtraction and division by the standard deviation).

All image analysis was performed using the image acquisition software (Videometer A/S, Hørsholm, Denmark). The PCA was performed using Evince 2.5.5 (Umbio AB, Umeå, Sweden).

3 Results and discussion

3.1 Salami structure

The change in salami structure (sliceability) could be detected at all available wavelengths. It was therefore decided only to measure the structure at 850 nm, which had the least difference between meat and fat. Figure 4c shows the change in AC as a function of scale for one salami type during 20 days of fermentation. A homogeneous salami (nice smooth cut) had a high AC value – an increase in AC as a function of ripening time was seen at all pyramid levels. Especially pyramid levels of 4-6 seemed suitable for monitoring the structural changes taking place in salamis during fermentation.

3.2 Colour

The loadings for the nCDA colour scale are seen in Figure 6 and in Figure 7 applied to a salami at different ages. The loading vector has three main peeks, i.e. a positive blue and yellow peek and a negative red peek. This means that the salami meat is red right after production (low nCDA value) and during the fermentation the meat becomes more blue and yellow and less red.

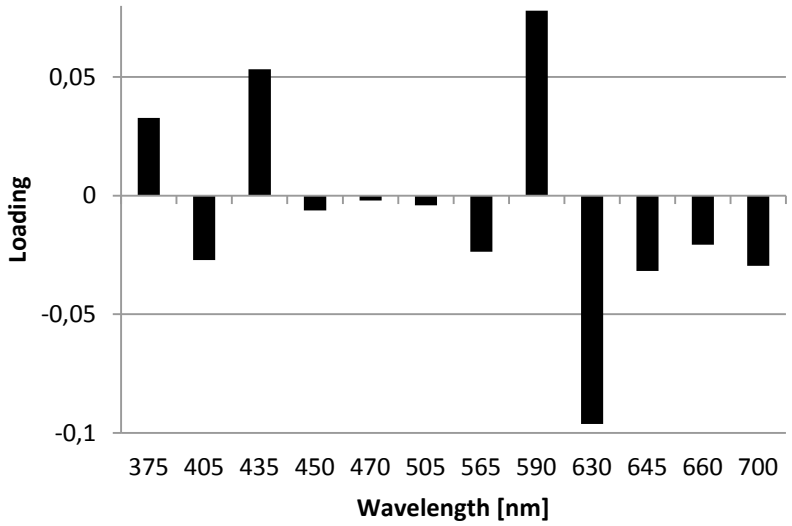

Figure 6 Loading values for the meat nCDA scale.

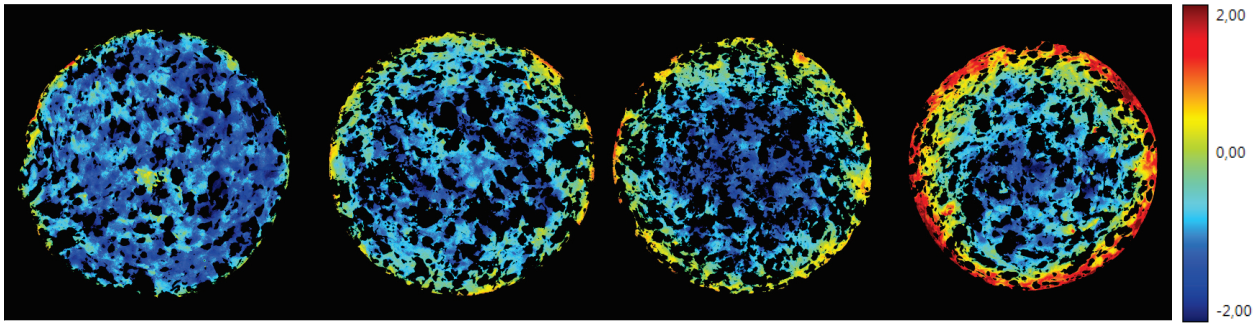

Figure 7 nCDA meat colour scale applied to salamis with different ages; left to right: 1, 3, 6 an 13 days of manufacture.

Three colour measures were calculated; (1) colour in the salami centre, (2) colour 2 millimetre from the edge, (3) millimetre dark meat ring calculated at nCDA=0, see Figure 8. Three values were derived as indicators of salami ripening:

- Colour in salami centre (radius of 5 mm)
- Colour at 2 mm from the surface.
- Millimetre dark ring

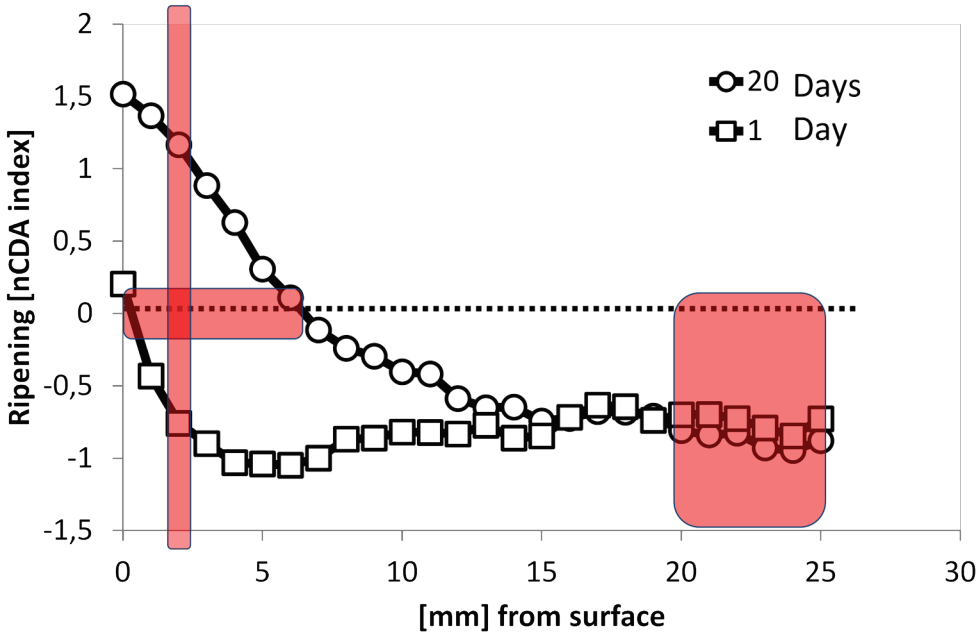

Figure 8 Colour index as a function of distance to the salami surface. Three values were extracted: millimetre dark ring (measured at 0), colour in the centre (5 central mm) and the colour 2 mm from the surface.

3.3 Data evaluation

The six different salamis were followed for 20 days (days 1, 3, 6, 9, 13 and 20). Five variables were measured: one image structure parameter (AC at level 4), 3 colour parameters and one hardness. The PCA loading plot for the five variables is seen in Figure 9. The first two

principal components (PC1 and PC2) explain 94.2% of the variation in the data set. The first principal component (x-axis) primarily reflects salami hardness and three-image-derived variables (mm dark ring, colour at 2 mm and AC4). The second principal component is primarily defined by colour in the centre of the salamis.

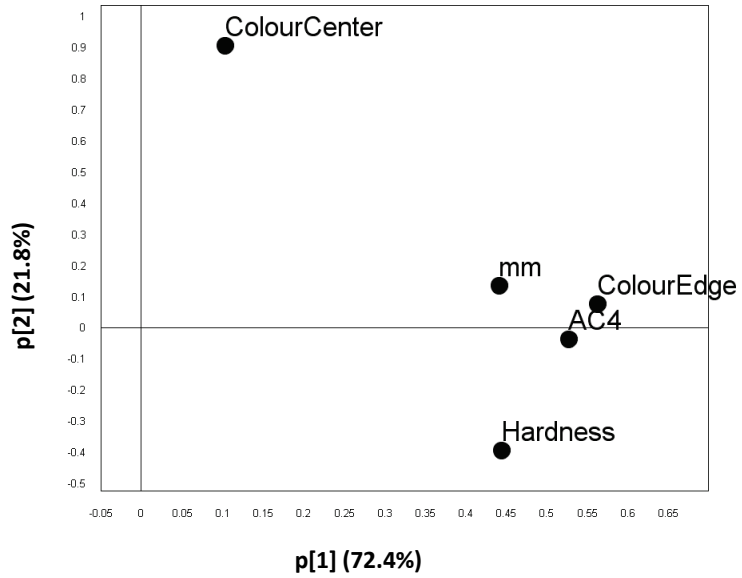

Figure 9 Loading plot for the five extracted parameters.

The PCA scores plot is seen in Figure 10. The different salami formulations are indicated with symbols and their sizes reflect age at measurement (from small to large), see formulation in Table 1. In the score plot, most samples during ripening go through an U-shaped development curve, e.g. at day one the samples are soft and with a rough structure. During ripening the product changes colour, becomes lighter (down) and then darker, hardness increases while the samples become more homogeneous (move right in PCA score plot).

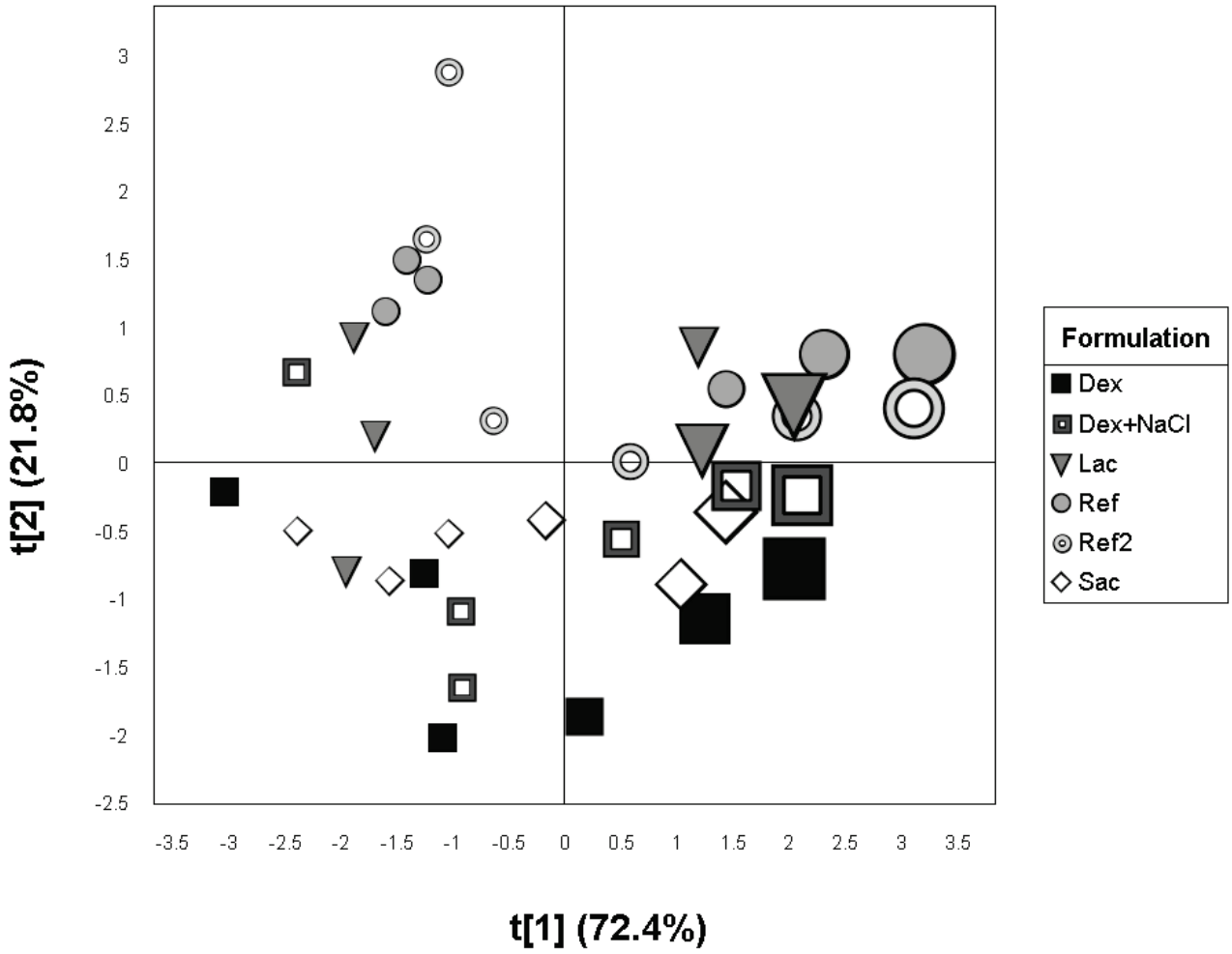

Figure 10 Score plot from PCA performed on five variables. The symbols relates to the salami formulation and the size of the symbols increase with number of storage days (1, 2, 3, 6, 13 and 20 days). Refer to Table 1 for product abbreviations.

The PCA loading plot was used to select variables expressing different information. Hardness vs. salami centre colour and hardness vs. surface homogeneity (AC4) is seen in Figure 11a+b. The scatter plot of colour vs. hardness show that the two reference samples continue developing colour and hardness throughout the fermentation period. The two reference samples end up as the hardest and darkest of all the evaluated formulations, seen in Figure 11a. Like the reference samples had the fast starter culture (TEXEL® Prism-1) in combination with

the slow fermentable lactose, a slow hardness development, and it never achieved the same dark colour as with reference cultures. The final hardness was reached two days after production for the fast starter culture when combined with the easy fermentable sugars, seen in Figure 11a.

The PCA loading plot (Figure 9) had grouped hardness and AC4 (surface homogeneity), which indicates a high degree of co-variation. Figure 11b shows a plot of hardness vs. AC4, this plot shows that surface homogeneity (AC4) *continues* developing after final hardness has been achieved. Dextrose gave the hardest products of the four sugar samples. Extra sodium chloride added to dextrose resulted in a product with a more mature colour and no change in hardness. Products made with saccharose and lactose resulted in similar hardness, which was softer than if made with dextrose – the lactose sample had a more mature meat colour than saccharose.

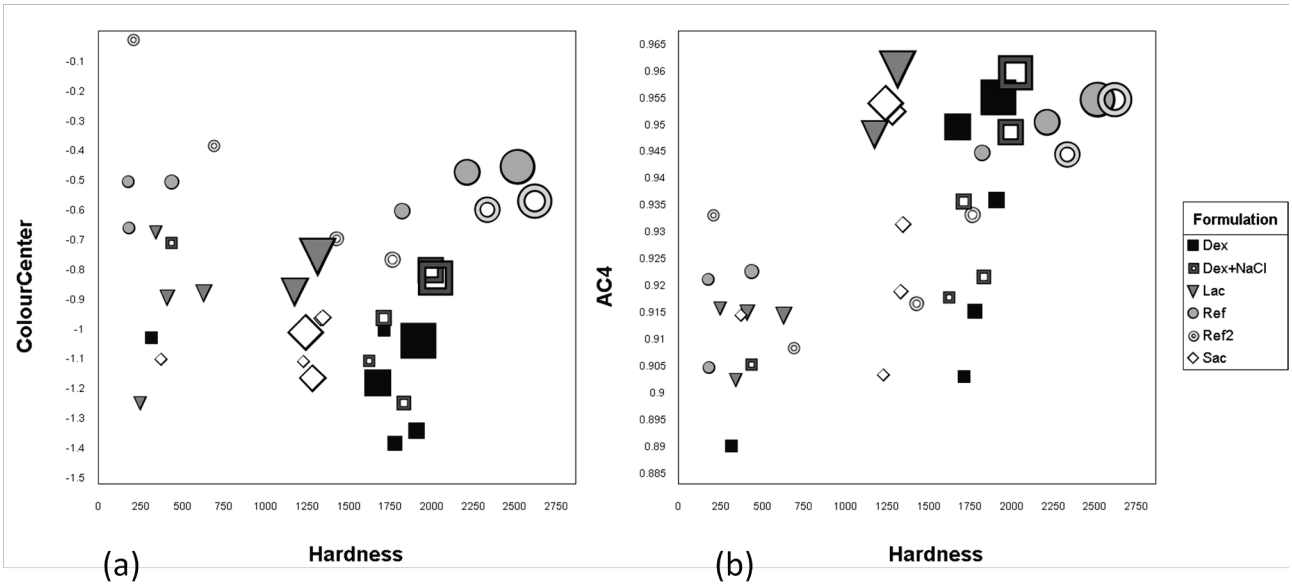

Figure 11 Scatter plots of (a) Salami colour vs. Hardness and (b) Image structure (AC4) vs. Hardness. The symbols relate to the salami formulation, and the size of the symbols increases with number of storage days (1, 2, 3, 6, 13 and 20 days). Refer to Table 1 for product abbreviations.

4 Conclusion

Based on multispectral images, a method for objective measures of meat colour and surface homogeneity of dry fermented sausages was developed. The separation of meat and fat was achieved in a multistep approach where multiple normalised Canonical Discriminant Analysis segmentations were combined. Spectral normalization was used to reduce the colour gradient from edge towards the salami middle. A meat maturates colour scale was developed using normalized Canonical Discriminant Analysis. The approach for quantifying surface homogeneity of sliced salami is based on Auto-Correlation calculation of an image at 850 nm.

In combination with hardness measures, the two methods were used to monitor how starter cultures and sugars influenced structure development of dry fermented sausages. The results showed that rate of colour development and final colour were starter culture dependent – sugar type and salt had a minor influence on the colour. The development of surface homogeneity was time dependent. The hardness development was culture and sugar type dependent.

4.1 Further work

To investigate how well the methods can predict human perception.

5 ACKNOWLEDGMENTS

This work was partly supported by the Centre for Imaging Food Quality project, which is funded by the Danish Council for Strategic Research (Contract No. 09-067039) within the Programme Commission on Health, Food, and Welfare.

6 REFERENCES

Acton J, Dick R, Norris E (1977). Utilization of various carbohydrates in fermented sausage. *Journal of Food Science* 42: 174-178.

Ammor MS, Mayo B (2007). Selection criteria for lactic acid bacteria to be used as functional starter cultures in dry sausage production: An update. *Meat science* 76: 138-146.

Arneth W (1998). Chemische grundlagen der umrötung. *Fleischwirtschaft* 78: 868-874.

Campbell Platt G, Cook P (1994). *Fermented meats*, London (UK), Blackie Academic, 1994.

Danisco A/S (2011). Texel ® meat cultures – maturation starters. In *Technical Memorandum*, p 8. Danisco A/S.

Feiner G (2006). Meat products handbook. *Practical Science*.

Franc V, Hlavác V (2004). Statistical pattern recognition toolbox for matlab. *Prague, Czech: Center for Machine Perception, Czech Technical University*.

Gonzalez RC, Woods RE, Eddins SL (2004). *Digital image processing using matlab*. Upper Saddle River, NJ, Pearson/Prentice Hall.

Grunert KG, Bredahl L, Brunsø K (2004). Consumer perception of meat quality and implications for product development in the meat sector—a review. *Meat science* 66: 259-272.

Guang Z, Maclean AL (2000). A comparison of canonical discriminant analysis and principal component analysis for spectral transformation. *PE&RS, Photogrammetric Engineering & Remote Sensing* 66: 841-847.

Herrero A, Ordóñez J, de Avila R, Herranz B, de la Hoz L, Cambero M (2007). Breaking strength of dry fermented sausages and their correlation with texture profile analysis (tpa) and physico-chemical characteristics. *Meat science* 77: 331-338.

Koenderink JJ (1984). The structure of images. *Biological cybernetics* 50: 363-370.

Leroy F, De Vuyst L (2004). Lactic acid bacteria as functional starter cultures for the food fermentation industry. *Trends in Food Science & Technology* 15: 67-78.

Leroy F, Verluyten J, De Vuyst L (2006). Functional meat starter cultures for improved sausage fermentation. *International journal of food microbiology* 106: 270-285.

Lindeberg T (1994). Scale-space theory: A basic tool for analyzing structures at different scales. *Journal of applied statistics* 21: 225-270.

Lindeberg T (1998). Feature detection with automatic scale selection. *International journal of computer vision* 30: 79-116.

Lu J, Tan J, Shatadal P, Gerrard D (2000). Evaluation of pork color by using computer vision. *Meat science* 56: 57-60.

Mancini R, Hunt MC (2005). Current research in meat color. *Meat science* 71: 100-121.

Marianski S, Mariański A (2009). *The art of making fermented sausages*, Bookmagic Llc.

Martens H, Næs T, Naes T (1989). *Multivariate calibration*. Chichester, Wiley.

Montel MC, Reitz J, Talon R, Berdagué JL, Rousset-Akrim S (1996). Biochemical activities of micrococcaceae and their effects on the aromatic profiles and odours of a dry sausage model. *Food Microbiology* 13: 489-499.

Møller JKS, Skibsted LH (2006). Myoglobins: The link between discoloration and lipid oxidation in muscle and meat. *Química Nova* 29: 1270-1278.

Steenkamp JBEM, van Trijp HCM (1996). Quality guidance: A consumer-based approach to food quality improvement using partial least squares. *European Review of Agricultural Economics* 23: 195-215.

Sun DW (2010). *Hyperspectral imaging for food quality analysis and control*, Academic Press.

Tajima R, Kato Y (2011). Comparison of threshold algorithms for automatic image processing of rice roots using freeware imagej. *Field Crops Research* 121: 460-463.

Videometer A/S (2012). Www.Videometer.Com. pp Hørsholm, Denmark.

Westland S, Ripamonti C (2004). *Computational colour science using matlab*. Hoboken, NJ, J. Wiley.

Wold S, Esbensen K, Geladi P (1987). Principal component analysis. *Chemometrics and Intelligent Laboratory Systems* 2: 37-52.

Wu D, Sun DW (2012). Colour measurements by computer vision for food quality control–a review. *Trends in Food Science & Technology*.